MASTER IN BIOCHEMISTRY AND MOLECULAR AND CELLULAR BIOLOGY

Autophagic alterations associated with proximal tubule lipotoxicity

Delmotte, Valentine

Award date:
2024

Awarding institution:
University of Namur

Faculté des Sciences

Study of autophagic alterations associated with proximal tubules lipotoxicity

Mémoire présenté pour l'obtention

du grade académique de master 120 en biochimie et biologie moléculaire et cellulaire

Valentine DELMOTTE

Août 2024

Université de Namur
FACULTE DES SCIENCES
Secrétariat du Département de Biologie
Rue de Bruxelles 61 - 5000 NAMUR
Téléphone: + 32(0)81.72.44.18 - Téléfax: + 32(0)81.72.44.20
E-mail: celia.defoin@unamur.be - http://www.unamur.be

Study of autophagic and lysosomal alterations associated with proximal tubules lipotoxicity

DELMOTTE Valentine

Résumé

L'obésité est associée à un dysfonctionnement du tissu adipeux blanc conduisant à des maladies associées à l'obésité telles que la maladie rénale chronique. Dans cette maladie, les cellules épithéliales tubulaires proximales rénales (PTECs) accumulent des gouttelettes de lipides et sont sensibles à la lipotoxicité. Ce phénotype est associé à un stress oxydatif, un stress du réticulum endoplasmique et des altérations autophagiques et lysosomales. En effet, notre groupe de recherche a montré que les cellules murines (mPTECs) exposées au palmitate (PA) présentent une accumulation d'autophagosomes. Ce travail vise à déterminer le contenu de ces autophagosomes accumulés et l'effet putatif de la lipotoxicité sur le phénotype des mPTECs. Bien que les données protéomiques nous aient orientés vers la ER-phagie, nous n'avons pas pu confirmer que cette voie était affectée par la lipotoxicité induite par le PA. En outre, nous n'avons pas pu montrer d'activation de la lipophagie, de la mitophagie ni de la lysophagie dans les mPTECs soumises à un stress lipidique induit par le PA pendant 24 heures. Ces cellules traitées au PA présentent une accumulation de lysosomes perméabilisés après 24 heures, qui ne déclenche pas la lysophagie. De plus, nous avons montré que des agrégats de protéines marquées à l'ubiquitine se forment et sont dirigés vers l'autophagie dans les cellules et ce, dès 6 heures après le traitement au PA. Enfin, nous montrons que la lipotoxicité induite par le PA altère les caractéristiques structurales et fonctionnelles des mPTECs. Nous avons montré que les mPTECs présentent une diminution de la réabsorption des protéines médiée par l'endocytose dépendante des récepteurs dès 6 heures après le traitement au PA, ainsi qu'une diminution des marqueurs épithéliaux et une augmentation des marqueurs mésenchymateux après 24 heures de traitement. Dans l'ensemble, ce travail permet de mieux comprendre comment la lipotoxicité altère la fonction lysosomale par la perméabilisation de la membrane lysosomale, ce qui conduit à l'accumulation d'autophagosomes contenant des agrégats de protéines et à la dédifférenciation des mPTECs.

Mémoire de master 120 en biochimie et biologie moléculaire et cellulaire

Août 2024

Promoteur: Thierry Arnould

Co-promotrice: Anne-Emilie Declèves

FACULTE DES SCIENCES
Secrétariat du Département de Biologie
Rue de Bruxelles 61 - 5000 NAMUR
Téléphone: + 32(0)81.72.44.18 - Téléfax: + 32(0)81.72.44.20
E-mail: celia.defoin@unamur.be - http://www.unamur.be

Study of autophagic and lysosomal alterations associated with proximal tubules lipotoxicity

DELMOTTE Valentine

Abstract

Obesity is associated with white adipose tissue dysfunction leading to obesity-associated diseases such as chronic kidney disease. In this disease, renal proximal tubular epithelial cells (PTECs) accumulate lipid droplets and are thus sensitive to lipotoxicity. This phenotype is associated with oxidative stress, endoplasmic reticulum stress and autophagic and lysosomal alterations. Indeed, our research group showed that murine PTECs (mPTECs) exposed to palmitate (PA) display autophagosomes accumulation. In view of these considerations, this work aims to determine the content of these accumulated autophagosomes and the putative effect of lipotoxicity on mPTECs phenotype. Although proetomics data directed us towards ER-phagy, we could not confirm that this pathway was affected by PA-induced lipotoxicity. In addition, we did not find any evidence of activation of lipophagy, mitophagy nor lysophagy in mPTECs under PA-induced lipid stress for 24 h. However, mPTECs displayed an accumulation of Gal3-positive lysosomes representative of permeabilised lysosomes without activation of lysophagy. Finally, we observed that ubiquitin-tagged protein aggregates were formed and delivered to autophagy already at 6 h after treatment with PA. We also asked whether PA-induced lipotoxicity might alter mPTECs structural and functional features. We demonstrated that mPTECs display a decrease in receptor-dependent endocytosis as soon as 6 h after PA-treatment, a decrease in the abundance of epithelial markers and an increase in mesenchymal markers after 24 h of treatment. Taken altogether, this work provides deeper insights on how lipotoxicity impairs lysosomal function through lysosomal membrane permeabilization leading to accumulation of autophagosomes containing protein aggregates and mPTEC dedifferentiation.

Master thesis of the master 120 in biochemistry and cellular and molecular biology

August 2024

Thesis supervisor: Thierry Arnould

Thesis co-supervisor: Anne-Emilie Declèves

Acknowledgments

All along this master thesis, I was lucky to be well surrounded, guided and supported. I would like to start by thanking my supervisor, Mr Arnould, for his supervision throughout my thesis, his help with the writing and his numerous pieces of advice, as well as my co-supervisor, Mrs Declèves, for her help and her encouragement.

A special thank you to the different members of my jury for taking the time to read and evaluate my thesis.

I would also thank the different members of the URBC laboratory for their help, especially the technicians Antoine, Catherine, Sophie, Marc and Caroline, as well as colleagues from other UNamur infrastructures. Among these, I would like to thank URPHYM laboratory and especially Benjamin, Kaoutar, Axelle, Alexis, Lucie and Dominique for their help, collaboration and kindness when I came to work in the laboratory. Many thanks also to PTSV and especially Amélie, Marie-Line and Roxane for their great help with the mice.

I've learnt and progressed a lot thanks to the ORBI team, and in particular to Pasty's good advice and kindness. I've also benefited from the support of ORBI team members Louise, Giacomo, Sebastien, Debakshee and Lorris, as well as the other teams SAGE, TumHyp, HomER and DoME.

I'm grateful to have shared these moments with friends and made new friends alongside Laurie, Alex, Marie, Eloïse, Dorian, Ilario, Maria and Randy. These moments could not have been what they are without my incredible friends at my side. I can't thank Alesia, Chloé, Emma and Marie-Eugénie, as well as Marine and Louise, enough. We laughed, we cried, we doubted, but we always had each other's backs. I can't wait to get back to our chatty moments and our laughs between two PCR plates loads. We'll always remember our time in URBC.

The people around me have been my greatest support. The biggest thank you goes to my family, my sister and my friends who heard too often about my cell treatments or my impatience to find out whether my micrographs would be good. Thank you for supporting me and helping me through the difficult times, but above all for all the moments of joy that followed.

This work would not have been possible without Louise and her constant support. Thank you so much for your patience (you needed a lot of it), your kindness and the motivation you gave me. Thank you for pushing me to surpass myself, for always being there to help me with the experiments and with the writing. I'm happy and grateful to have learnt so much from you and can now move on to the next stage of my career with confidence. I wish you all the best for the future.

Table of contents

List of abbreviations

acetyl-CoA	Acetyl Coenzyme A
ADP	Adenosine Diphosphate
ALA	α linoleic-acid
α-SMA	A-Smooth Muscle Actin
AMN	Amnionless
AMP	Adenosine Monophosphate
AMPK	AMP-Activated Protein Kinase
ANOVA	Analysis of Variance
apoB48	Apolipoprotein B-48
APOL1	Apolipoprotein L1
AQP-1	Aquaporin-1
AT	Adipose tissue
ATF4	Activating Transcription Factor 4
ATF6α	Activating Transcription Factor 6 α
ATG14	Autophagy-Related Gene 14
ATGL	Adipose Triglyceride Lipase
ATL3	Atlastin GTPase 3
ATP	Adenosine Triphosphate
AUP1	Ancient Ubiquitous Protein 1
Baf A1	Bafilomycin A1
BAT	Brown Adipose Tissue
BCA	bicinchoninic acid
BMI	Body Mass Index
BMP	Bone Morphogenetic Protein
BNIPL3	BCL2/adenovirus E1B 19 kDa interacting protein 3-like
BSA	Bovine Serum Albumin
CACT	Carnitine-AcylCarnitine Translocase
CAKUT	Congenital Anomalies of the Kidney and Urinary Tract
CaMKKβ	Calcium/Calmodulin-dependent Protein Kinase Kinase β
CCPG1	Cell-Cycle Progression Gene 1
CD44	Cluster of differentiation 44
CDH16	Cadherin-16
CHOP	C/EBP Homologous Protein
ChREBP	Carbohydrate-Responsive Element-Binding Protein
CKD	Chronic Kidney Disease
CMA	Chaperone-Mediated Autophagy
CoA	Coenzyme A
CP	Core particle
CPT	Carnitine Palmitoyltransferase
CT	Computed Tomography
CUBN	Cubilin
CWE	Column Wash Solution
DAPI	4′,6-diamidino-2-phenylindole

DBP	D-binding Protein
DFCP1	Double FYVE-containing Protein 1
DGAT	Diacylglycerol O-Acyltransferase
DMEM/F12	Dulbecco's Modified Eagles Medium/Nutrient Mixture F12
DNA	Deoxyribonucleic acid
DNL	De Novo Lipogenesis
DPK1	3-Phosphoinositide Dependent Protein Kinase-1
DRAM	Damage-Regulated Autophagy Modifier
DS	Dissection buffered solution
DSP	Desmoplakin
DTT	Dithiothreitol
Ebp41L5	Erythrocyte Membrane Protein Band 4.1 Like 5
E-CDH	E-Cadherin
EDTA	EthyleneDiamineTetraacetic Acid
EGTA	Ethylene Glycol-bis(β-aminoethyl ether)-N,N,N′,N′-Tetraacetic Acid
ER	Endoplasmic Reticulum
ERAD	Endoplasmic Reticulum-Associated Degradation
ESCRT	Endosomal Sorting Complex Required for Transport
ESRD	End-Stage Renal Disease
ETC	Electron Transport Chain
FA	Fatty acid
FABP	Fatty Acid Binding Protein
FADH2	Flavin Adenine Dinucleotide (reduced)
FAM134B/RETREG1	Family with Sequence Similarity 134, Member B-2a/reticulophagy regulator 1
FAO	Fatty Acid Oxidation
FAS1	Fatty Acid Synthase 1
FAT	Fatty Acid Translocase (CD36)
FATP	Fatty Acid Transport Protein
FBXO27	F-box Protein 27
FCCP	Carbonyl Cyanide-p-TrifluoromethoxyPhenylhydrazone
FIP200	AK Family Interacting Protein of 200 kDa
FOXM1	Forkhead Box M1
FOXO1	Forkhead Box O1
FXR	Farnesoid X Receptor
Gal3	Galectin-3
GBM	Glomerular Basal Membrane
GFR	Glomerular Filtration Rate
HBSS	Hanks Balanced Salt Solution
HDAC6	Histone Deacetylase 6
HDL	High-Density Lipoprotein
hEGF	human Epidermal Growth Factor
HEPES	4-(2-hydroxyethyl)-1-piperazineethanesulfonic acid
HFD	High-Fat Diet

HIFBS	Heat-Inactivated Fetal Bovine Serum
HOPS	Hepatocyte Odd Protein Shuttling
HSL	Hormone-Sensitive Lipase
Hsp70	Heat Shock Protein 70
IL	Interleukin
IMM	Inner Mitochondrial Membrane
IRE1α	Inositol-Requiring Enzyme 1 α
kDa	kiloDalton
LA	Lipoic Acid
LAL	Lysosomal Acid Lipase
LAMP1	Lysosomal-Associated Membrane Protein 1
LAMP2A	Lysosomal-Associated Membrane Protein 2A
L-arg	L-arginine
LCHAD	Long-Chain 3-Hydroxyacyl-CoA Dehydrogenase
LDL	Low-Density Lipoprotein
LIR	LC3-Interacting Region
LKB1	Liver Kinase B1
LLOMe	L-Leucyl-L-Leucine Methyl Ester
LMP	Lysosomal Membrane Permeabilization
LMW	Low Molecular Weight
LP	Lipoprotein
LPL	Lipoprotein Lipase
LPN2	Lethal Protein N2
LR	Lethal Resistance
Lrc2	Leucine-Rich Repeat Containing 2
Lrp2	Low-Density Lipoprotein Receptor-Related Protein 2
MAG	Monoacylglycerol
MAP1LC3	Microtubule-Associated Protein 1 Light Chain 3
MCC	Methylcrotonyl-CoA Carboxylase
MCP1	Monocyte Chemoattractant Protein-1
MES	2-(N-morpholino)-ethanesulfonic acid
MFN	Mitofusin
MG132	N-Benzyloxycarbonyl-L-leucyl-L-leucyl-L-leucinal
MGL	MonoacylGlycerol Lipase
MHO	Metabolic Healthy Obesity
MLI	Major Lipid Involvement
MOA	Mechanism Of Action
mPTEC	murine Proximal Tubule Epithelial Cells
MS	Mass Spectrometry
MTOC	Microtubule-Organizing Center
mTORC1	Mechanistic Target of Rapamycin Complex 1
MUFA	Monounsaturated Fatty Acid

MUO	Metabolic Unhealthy Obesity
MW	Molecular Weight
NADH	Nicotinamide Adenine Dinucleotide
NBIP3	BCL2/adenovirus E1B 19 kDa protein-interacting protein 3
NBR1	Neighbor of BRCA1 Gene 1
NCD	Nuclear Chain Damage
NEFA	Non-Esterified Fatty Acids
NH4Cl	Ammonium Chloride
NHE	Sodium Hydrogen Exchanger
NIX	Nip3-like protein X
NRK-52E	Normal Rat Kidney-52E Cells
OA	Octanoic Acid
OCR	Oxygen Consumption Rate
OMM	Outer Mitochondrial Membrane
OXPHOS	Oxidative Phosphorylation
p53	Tumor Protein p53
p62/SQSTM1	Sequestosome 1
PA	Phosphatidic Acid
PBS	Phosphate buffered saline
PE	Phosphatidylethanolamine
PEA	Phenylethylamine
PERK	Protein Kinase RNA-like Endoplasmic Reticulum Kinase
PFA	Paraformaldehyde
PGC-1α	Peroxisome Proliferator-Activated Receptor Γ Coactivator 1-α
PINK	PTEN-Induced Putative Kinase 1
PKR	Protein Kinase R
PLIN2	Perilipin 2
POA	Palmitoleic Acid
PPARγ	Peroxisome Proliferator-Activated Receptor Γ
PPARGC1A	Peroxisome Proliferator-Activated Receptor Γ Coactivator 1-α
PT	Proximal Tubule
PTEN	Phosphatase and Tensin Homolog
PUFA	Polyunsaturated Fatty Acid
PVDF	Polyvinylidene Fluoride
RAP	Ribosome-Associated Protein
RER	Rough Endoplasmic Reticulum
RETREG1	Reticulon 3
RNA	Ribonucleic Acid
ROS	Reactive Oxygen Species
RP	Ribosomal Protein
RPM	Revolution Per Minute
RT	Reverse Transcription
RWA	Right Wavelength Angle
SBTI	Soybean Trypsin Inhibitor
SEC62	Preprotein Translocation Factor
SEM	Standard Error of the Mean

SER	Smooth Endoplasmic Reticulum
SFA	Saturated Fatty Acid
SGLT	Sodium-Glucose Linked Transporter
SHH	Sonic Hedgehog
Slc5A2	Solute Carrier Family 3 Member 1
SNARE	Soluble N-ethylmaleimide-sensitive factor Attachment protein Receptor
SREBP1	Sterol Regulatory Element-Binding Protein 1
STX17	Syntaxin 17
TAG	TriAcylGlycerol
TBS	Tris-Buffered Saline
TEX264	TEX264 (DNA/RNA Helicase TEX264)
TFEB	Transcription Factor EB
TGFβ	Transforming Growth Factor B
TM	TransMembrane
TNFα	Tumor Necrosis Factor A
TNL3	Toll-Like Receptor 3
TOM	Translocase of Outer Mitochondrial Membrane
TRIM16	Tripartite Motif-Containing 16
t-SNARE	Target-SNARE
Ub	Ubiquitin
UBA5	Ubiquitin-Activating Enzyme 5
UFC1	Ubiquitin-Fold Modifier Conjugating Enzyme 1
UFL1	UFM1 specific ligase 1
UFM1	Ubiquitin-Fold Modifier 1
UFSP	UFM1 Specific Peptidase 1
ULK1	Unc-51 Like Autophagy Activating Kinase 1
UPR	Unfolded Protein Response
UPS	Ubiquitin-Proteasome System
VCP	Vasopressin-Induced Channel Protein
VDAC	Voltage-Dependent Anion Channel
VIM	Vimentin
VLCAD	Very Long-Chain Acyl-CoA Dehydrogenase
VLDL	Very Low-Density Lipoprotein
Vps34	Vacuolar Protein Sorting 34
v-SNARE	Vesicle-Associated Membrane Protein-Associated Protein B
V-type H+-ATPase	V-Type Proton ATPase
WAT	White Adipose Tissue
WHO	World Health Organization
WIPI	WD Repeat Domain Phosphoinositide-Interacting Protein

I. INTRODUCTION

A. Obesity

Obesity is a complex multifactorial disease defined by the World Health Organization (WHO) as an "*abnormal or excessive fat accumulation that may impair physical and/or mental health*"[1,2]. Its worldwide scope makes it a clinical and public health burden. In 2020, estimations showed that 14 % of the world population was concerned by obesity[3]. Indeed, it is estimated that 24 % of world population will be obese in 2035[3,4]. This increase in the prevalence of obesity is observed regardless of age, gender, ethnicity, changes in diet inhabits over the last 30 years, or socioeconomic status[1,3]. However, obesity prevalence rates fluctuate considerably between regions and countries leading to a difference of nearly 30 % between Bangladesh (3.5 %) and the USA (32 %)[5]. In addition, rates of obesity increase in richer countries across Europe, North America and Oceania and has finally attained an "epidemic" expanse in Europe[2]. At the moment, recent reports estimated that 59 % of the European adult population are overweight and 23 % are obese[2]. It is guessed that obesity prevalence in adults rose by 21 % from 2006 to 2016 and by 138 % since 1975[2]. Among children and adolescents, obesity is one of the most common pediatric chronic diseases and has major relevance in their life because of its tendency to remain in adulthood[2,6]. In 2020, worldwide, 11,6 % of children aged of 5 to 9 years and approximately 7 % of children aged of 10 to 19 years suffered from obesity. Since 1975, obesity levels rose rapidly by nearly 500 % among children and adolescents[2].

Obesity occurs also when there is a long-term energy imbalance between an excessive caloric intake and its poor consumption leading to body weight gain[1,2,4,7]. Energy intake is defined as energy produced from food and drinks while energy expenditure is the use of energy in the form of adenosine triphosphate (ATP), to ensure biological functions, physical exercise and maintain body homeostasis, including basal metabolism (consuming, in average 1300-1600 kcal out of 2000-2400 kcal ingested daily)[8]. Historically, humans evolved to survive periods of famine. This led to the selection of traits promoting energy storage, low energy expenditure and low activity. This could explain why these early adaptations are involved in today's obesity epidemic in high-income countries[7]. The socioeconomic aspect has been a shift in the fast expansion of obesity during the last century. Indeed, especially in high-income countries, the availability to cheaper and unhealthy (junk) transformed food, the increased urbanization and the obesogenic environment (including endocrine disruptors and low physical activity) have a decisive role to play in this increase[2,4,7].

Obesity can be diagnosed through a non-invasive anthropometric method based on the Body Mass Index (BMI)[1,2,4,7]. It is the body weight in kg divided by the height in meters squared (kg/m^2). This measurement is sex- and age- independent for adults. Values range from underweight ($< 18.5\ kg/m^2$) to morbid obesity ($\geq 40\ kg/m^2$). More specifically, a person is classified as overweight when its BMI varies between $\geq 25\ kg/m^2$ and $< 30\ kg/m^2$ and obese when the BMI is higher or equal to $30\ kg/m^2$[1,2,4,7]. However, the BMI does neither discriminate between subcutaneous and visceral nor intra-abdominal fat which is at the origin of greater health issues in obese individuals. Therefore, the measurement of waist circumference has been suggested to provide information on the amount of visceral fat[1,2,4]. It has been decided that the combination of both analyses will provide deeper information and be a better predictor of secondary health problems[1,2,4]. Finally, imaging techniques such as computed tomography (CT) or magnetic resonance imaging (MRI) are the most accurate tools to determine the spatial distribution of WATs and body composition components to discriminate lean mass and fat mass[9].

Obesity is (very often but not always) strongly associated with increasing risks of noncommunicable diseases (NCDs) such as metabolic diseases (diabetes mellitus, chronic kidney disease or non-alcoholic fatty liver disease), cardiovascular diseases, mental health problems, musculoskeletal complications, apnea, and some types of cancers (mainly : melanoma, uterus, thyroid, breast, colorectal, kidney, and liver cancers)[2,7]. More broadly, obesity is usually associated with the metabolic syndrome (MS) that affects the metabolic fitness. It is characterized by a large waist circumference, hypertriglyceridemia, high blood pressure, resistance to insulin and hyperglycemia. People are classified as suffering from a MS when they fulfil at least three of these features[10–12]. Right now, two different types of obesity are recognized: metabolically healthy obesity (MHO) and metabolically unhealthy obesity (MUO)[13–15]. MHO is defined by the absence of metabolic dysfunctions such as insulin resistance or dyslipidemia[13]. In MHO, the positive energy balance leads to a healthy expansion of the adipose tissue (AT) (mainly white adipose tissues). It is characterized by an increased adipogenesis (hyperplasia), adipocyte hypertrophy with anti-inflammatory molecule secretion profile (such as IL-10 or TGFβ[16]) and a still high insulin sensitivity allowing a sharpest regulation of glucose and lipid homeostasis[13,14]. Nevertheless, depending on the WAT locations affected, microbiota composition, and/or pro-inflammatory status, obesity is often associated with WAT metabolic "maladaptations" to energy imbalance. Unhealthy expansion of WAT is associated with hypertrophy, hyperplasia and hypoxia as well as pro-inflammatory profile, fibrosis, dyslipidemia, and insulin resistance[17]. Obesity is thus mainly associated, initially, with changes in the adipose tissues and among them, more specifically in the WAT. We will now rapidly describe the different types of adipose tissues.

1. Adipose tissues

The adipose tissue (AT) is the main energy storage depot and has a heterogenous disposition in the body[13,18]. Different types of adipose tissues are found: the White Adipose Tissue (WAT), the Brown Adipose Tissue (BAT), the BRITE (BRown-In-whiTE) and the pink AT. These tissues contain adipocytes which differ by their function, size, shape or their intra-cellular organelle structure and composition[18,19]. BAT plays a particularly important role in maintaining thermal homeostasis, especially in newborns for the body fat oxidation and non-shivering adaptive thermogenesis[18]. While less abundant, this tissue is still present and can be activated in adults (but in variable amounts between individuals) and is found in supraclavicular, cervical, mediastinal, paraspinal and abdominal regions[18,20]. Brown adipocytes display an ellipsoidal-shape, cytosolic multilocular lipid droplets (LDs) and cristae-dense mitochondria required for the high oxidative phosphorylation (OXPHOS) activity, especially of FA[18,20]. However, these cells express the gene encoding UCP-1 (uncoupling protein-1) that disconnects the respiration from the phosphorylation of ADP in ATP, representing a futile system that dissipates energy in the form of heat. Conditions to activate BAT are, for example but not exhaustively, excess of calorie intake or cold exposure[21].

As its name suggests, BRITE AT comes from a combination of WAT and BAT and is located subcutaneously. Some proportion of the WAT can turn BRITE by the direct differentiation of precursors such as myf5 negative cell lineage[22] or trans-differentiation of adipocytes (in response to β-adrenergic stimulation like in cold-exposure[23]) and may be protective against metabolic dysfunctions and obesity as cells of this tissue do also express the gene encoding UCP-1. On the other hand, pink AT is involved in the formation of lactiferous

alveoli[18]. WAT are however the main tissues affected in obesity[24] and will be further characterized in the following section.

a) Healthy WAT

The WAT displays three major functions : the energy storage in the form of triacylglycerols (TAGs), a secretory function through the secretion of many adipokines (over 800 identified) and the function of regulation of glucose and lipid metabolism through its sensitivity to insulin for glucose uptake and control of lipolysis[14,18]. WAT deposition can be concentrated to the abdominal region as visceral fat or is mainly subcutaneously[14,19]. Unlike brown adipocytes, white adipocytes have a sphere shape and a large unilocular LDs covering almost the entire cell volume and pushing the organelles to the periphery of the cell[18,25]. Adipocytes mainly compose the WAT even if other cell types are present such mesenchymal stem cells, preadipocytes, macrophages and immune cells, fibroblasts, endothelial cells and nerve fibres (Figure 1A)[26].

In physiological conditions, the balance between lipogenesis (FA synthesis from acetyl-CoA and their esterification on glycerol to form TAGs) and lipolysis (mobilisation of FA from TAGs) allows the WAT to maintain energy homeostasis and insulin sensitivity. Indeed, in a fed state, energy is stored in adipocytes as TAGs while this energy is released as free fatty acids (FFAs) during starvation or fasting[13,18]. When a meal is taken, lipids from the diet end up in the bloodstream, carried by lipoproteins (LPs). These circulating TAGs are hydrolysed by lipoprotein lipase (LPL) to release FFAs in the blood that are taken up by adipocytes and esterified in TAGs[18]. Meanwhile, a *de novo* lipogenesis (DNL) can occur when acetyl-CoA concentrations are elevated due to a high substrate oxidation (glucose, ketogenic amino acids, ...). Excess of acetyl-CoA is used to form FFAs that are next esterified on glycerol backbones[18]. On the contrary, during a physical activity or periods of fasting, glycerol and FFAs are delivered through lipolysis of TAGs stores[18]. FFAs are released sequentially by the action of adipose triglyceride lipase (ATGL), the hormone sensitive lipase (HSL), an enzyme highly regulated by energy-demanding neuronal and hormonal process[27], and the monoacylglycerol lipase (MGL)[18]. In pathological conditions, the balance between lipogenesis, lipolysis and lipophagy is impaired starring to a massive release of FFAs in the circulation, and finally, in non-adipose organs, a process at the basis of lipotoxicity for many cell types such as hepatocytes, pancreatic β-cells or proximal tubular cells[28].

WAT are also secretory tissues. Its action is endocrine, paracrine and autocrine[18,29]. In physiological conditions, three major hormones are secreted by the white adipocytes: adiponectin in high concentrations when compared to leptin or resistin (for which the role is still misunderstood in human), as well as several pro-inflammatory cytokines such as TNFα and IL-6[30]. Adipokines represent a set of molecules (hormones, peptides, cytokines, chemokines,…) by which adipocytes communicate with other tissues and organs[31]. For example, adiponectin targets skeletal muscles, heart, liver, bones or AT[18,30] and reduces glucogenesis and lipogenesis, increases insulin sensitivity in the skeletal muscles and stimulates fatty acid oxidation in mitochondria through the activation of AMP-activated protein kinase (AMPK). Clear evidence show a decrease in the expression and secretion of adiponectin in the onset of obesity[18,30]. Leptin is a hormone mainly involved in the control of appetite (phagic behaviour affecting the orexigenic and anorexigenic pathways) and energy homeostasis. In combination with the regulation of lipid and glucose metabolism, leptin also controls angiogenesis, bone homeostasis, immune function and haematopoiesis. However, during

obesity, an increase in leptin expression and concentration is observed as its expression is directly proportional to the amount of WAT but its anorexigenic effect is inhibited as a result of leptin resistance[18,30]. Human resistin, has a strong effect on glucose levels, insulin resistance and contribution to inflammation through direct action on immune cells and pro-inflammatory cytokines (TNFα, IL-6, IL-12, Monocyte Chemoattractant Protein-1 (MCP1)) secretion[32]. Moreover, its action on liver, heart and AT leads to the inhibition of glucogenesis and adipogenesis, along with a stimulation of pro-inflammatory responses and vascular dysfunctions[18,30]. WAT also contain immune cells such as M2 macrophages. These cells secrete anti-inflammatory cytokines such as interleukine-10 (IL-10), IL-13 or TGF-β[33].

In case of chronic energy imbalance in favour of the storage, the WAT expand. This expansion may be healthy, in this case it is achieved by adipogenesis, a process in chich preadipocytes differentiate in mature adipocytes[24].

b) Unhealthy WAT

Unlike MHO, MUO is determined by metabolic dysfunctions arising from the onset of obesity[15]. At that stage, WAT are considered as pathological. This unhealthy expansion of WAT is characterized by a defective adipogenesis, adipocyte hypertrophy and hyperplasia, insulin resistance, a low-grade inflammation (metabolic endotoxemia), and a phenotypic shift between M2 anti-inflammatory macrophages, and activated M1 pro-inflammatory macrophages (Figure 1B)[14,17].

In MHO, adipogenesis is promoted by the release of paracrine and autocrine signals by adipocytes. On the contrary, in MUO, the persistent caloric imbalance promotes the secretion of factors such as gremlin1, a bone morphogenetic protein (BMP) antagonist, accounting for the inhibition of adipogenesis by a mechanism that involves BMP4 inhibition[14,34,35]. Moreover, in unhealthy WAT, hypertrophic adipocytes promote episodes of hypoxia, fibrosis and cell death in which pro-inflammatory mediators such as leptin, IL-6, IL-8, MCP-1 and TNF-α are secreted, either by the adipocytes themselves or infiltrated and/or resident immune cells[14]. In addition, the abundance of anti-inflammatory proteins such as adiponectin is reduced. This results in local and systemic inflammation along with a conversion from M2-polarized macrophages to M1-polarized macrophages[12,14,34,36–39]. Then, these M1 macrophages also secrete pro-inflammatory molecules leading to a positive feedback that reinforce the inflammatory profile[37]. Besides, insulin-mediated lipolysis is impaired in MUO leading to the excess accumulation of TAGs in adipocytes. Insulin resistance along with hypertrophic adipocytes and altered adipogenesis result in rising the concentration of unesterified FFAs and cholesterol in the bloodstream[40].

In obese people, the imbalance between the consumption and the storage of lipids leads to dysfunction of adipocytes along with an increase in the breakdown of lipids into FFAs. This may result in dyslipidaemia characterised by an increase in triacylglycerols and FFAs in the plasma and is accompanied by a decrease in HDL (High Density Lipoproteins) and an increase in LDL (Low Density Lipoproteins)[41]. However, the excess of FFAs found in obesity are oxidized, causing an accumulation of unused glucose, hyperglycemia, glucotoxicity and insulin resistance[42]. This pathological increase in FAO (Fatty Acid Oxidation) results in incomplete lipid oxidation as well as an increased oxidative stress due to overload of this mechanism[39]. The release of FFAs by unhealthy WAT drives and enhances dyslipidaemia and abnormal accumulation of lipids in non-adipose cells such as β-cells[43], hepatocytes[44] or renal cells as

tubular epithelial cells and podocytes[45] which results in lipotoxicity. Lipotoxicity, associated with glucotoxicity as well as pro-inflammatory and pro-fibrotic environments, lead to the development of obesity-associated diseases such as diabetes and/or chronic kidney disease (CKD)[10,14,15]. More information about CKD will be presented in section Introduction D.

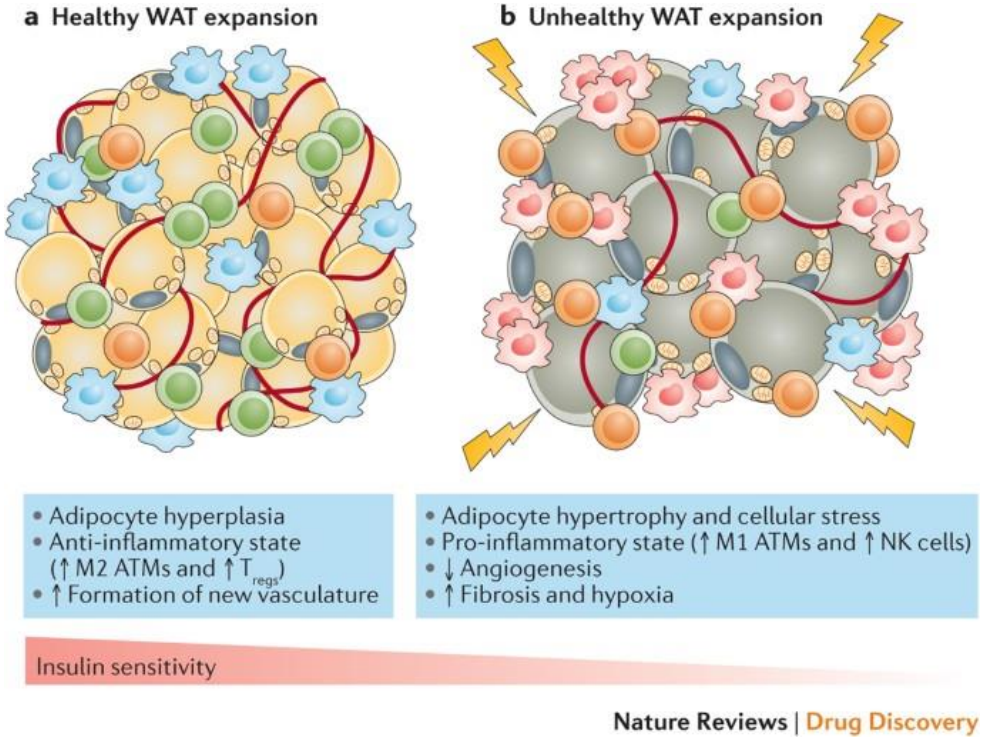

Figure 1: Representation of healthy and unhealthy expansion in WAT. *(A) Healthy WAT expansion is characterised by an increased anti-inflammatory environment, a sufficient vasculature leading to adipocytes hyperplasia. (B) On the opposite, unhealthy WAT harbours enlarged hypertrophic adipocytes increasing cellular stress, associated with a pro-inflammatory environment, a decrease of angiogenesis and thus increased fibrosis and hypoxia.*[46]

2. Type of lipids and fatty acids and their role in lipotoxicity

Lipids are an important part of organic compounds found in food, along with carbohydrates, proteins and vitamins[47,48]. These are the richest source of energy provided by nutrients. The diversity of lipids is huge (over 100 000 different molecules) and these molecules are characterized by their immiscibility in water and physical characteristics[49]. These are classified as simple lipids, or carbonamides, and complex lipids, called esters, such as glycolipids, phospholipids, sphingolipids or polycyclic lipids named sterols[48,50].

In mammals, FAs are stored under the form of TAGs in LDs found in adipocytes to maintain an energy supply even if all cell types contain LDs but smaller[48]. FAs, build up lipid membranes under the form of phospholipids and sphingolipids which enables biological processes like cell division, intracellular trafficking, or the assembly of proteins on lipid rafts[51,52]. In addition, FAs can be oxidized by several types of oxidation (peroxisomal or mitochondrial) and some of them such as eicosanoids interact with and acts as ligands of transcription factors (FT) such as peroxisome proliferator-activated receptor γ (PPARγ) (a master TF that regulates adipogenesis) to regulate the expression of numerous genes[51,53]. FAs

have also been shown to participate to post-translation modifications of proteins/enzymes such as protein acylation including S-palmitoylation or N-myristoylation[54,55].

FAs contained in food provide an important source of energy (9 kcal/g). They can be saturated FAs (SFAs, meaning that their carbon chain is saturated in hydrogen), monounsaturated FAs (MUFAs) or polyunsaturated FAs (PUFAs) when they contain one or several double bonds in their hydrocarbon chain, respectively. They also vary in the number of carbon atoms in their hydrocarbon chains: short (up to 6 atoms of carbon), medium (6 up to 10 atoms of carbon), long-chain (12 up to 18 atoms of carbons) or very long chain (more than 20 atoms of carbon) FFAs. Among these, we can distinguish between essential fatty acids as PUFA omega-3 and omega-6 provided by food and that cannot be synthetised in the body, and non-essential fatty acids such as SFAs[56].

FFAs vary according to their carbon number, the degree of saturation and the position of the double bonds in the hydrocarbon chain[57–60]. Food may contain saturated fatty acids in the form of palmitic acid (PA, C16:0) and stearic acid (SA, C18:0). MUFAs are found in olive oil and animal fats in the form of oleic acid (OA, C18:1), myristoleic acid (MOA) and palmitoleic acid (POA). Finally, some PUFAs are not synthesised by humans and are known as essential fatty acids, such as linoleic acid (LA, C18:2) or α-linoleic acid (ALA, C18:3)[57]. PA is involved in maintaining membrane physical properties, protein palmitoylation, palmitoylethanolamide (PEA) biosynthesis and lung surfactant production. It is one of the most common SFAs found in diet[61]. As SFAs are largely correlated to the development of obesity and associated diseases, SFAs such as PA are widely used in research to induce fat accumulation[62]. Indeed, *in vivo* models are exposed to PA-containing HFD (High Fat Diet : 60 % of energy comes from TAGs) while *in vitro* different types of cells such as hepatocytes of proximal tubular epithelial cells (PTECs) are often treated/incubated with various concentrations of PA[62,63].

Nowadays, SFAs, notably PA, are consumed in excess amounts in the diet (20-30 g/day). Indeed, it has been established that people suffering from obesity have high levels of circulating free fatty acids, particularly saturated fatty acids such as PA[57,61,64]. This increase is not only due to the consumption of PA via the diet but also to the deregulation of DNL, whose role is to counterbalance the excessive intake of PA by the synthesis of other FAs[61,62]. However, it has been shown that OA is protective against PA-induced dyslipidaemia because it promotes the storage of the SFA in the LDs[63,65,66].

When energy is needed in peripheral organs, FFAs are released by adipocytes into the circulation and transported to the muscles, heart or renal cortex. These circulating FAs, attached to albumin, are taken up by the cells by fatty acid transporters (FATs). To produce energy in the form of ATP, FAs undergo mitochondrial (or peroxisomal for long FA) OXPHOS[48,67]. As our experimental work studied the lipotoxicty of PA in murine PTECs (mPTECs), we will now introduce the role and functions of these cells in kidneys.

B. Kidneys

1. Generalities

Kidneys control the body fluid homeostasis, endocrine function and metabolic activities such as removal of metabolic wastes such as urea and xenobiotics. To achieve this, the kidneys are irrigated with 200 litres of fluid per day at a flow rate of 120 mL/min. The blood is filtered by the functional and structural unit of the kidney, the nephron, and processed through secretion

or reabsorption of water and electrolytes such as sodium, chloride or calcium to produce the final urine. Kidneys thus allow the removal of metabolic waste products, toxins, ions while keeping nutrients[68–70]. These organs also ensures the regulation of plasma osmolarity and acid-base balance[68,70,71]. Kidneys are endocrine organs engaged in the production and secretion of 3 key hormones: erythropoietin involved in the haematopoiesis, 1,25-dihydroxycholecalciferol (calcitriol) and renin (part of the renin-angiotensin-aldosterone system), an inter-related endocrine system important in volume and blood pressure control[70].

Kidneys are bean-shaped excretory organs located on both side of the spinal column in the retroperitoneum. They are protected by a fibrous capsule and are made up of two main parts: cortex and medulla (Figure 2). Cortex is the peripheral portion of kidneys [68,70,71] while medulla, at the centre of kidneys, can be divided in outer and inner medulla and is composed of medullary pyramids, also called pyramids of Malpighi, separated from each other by renal columns. Urine continues to be processed in the medulla before being delivered to the ureter followed by the rest of the excretory system[71]. PTECs, the cells we work on in this Master thesis, are characterized by a well-developed endolysosomal system needed for secretion and reabsorption process that requires a high density of mitochondria, mostly found at the basolateral membrane[72].

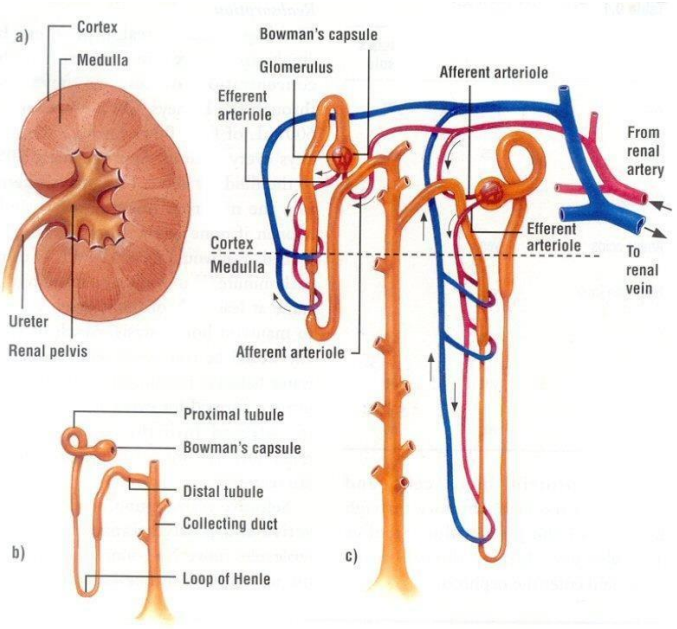

Figure 2: Schematic illustration of the anatomy of the kidney and the nephron (A) Illustration of the kidneys and their vascularization (B) Kidneys are composed of a cortex with glomeruli, as well as the proximal and distal convoluted tubules of the nephron, a medulla that contains the straight section of the proximal tubule, Henle's loop, and part of the collecting system. (C) An illustration of the various segments of the nephron and (D) their relationship with the network of peritubular capillaries.[73]

There are approximatively 1,000,000 nephrons per kidney. Nephrons contain a glomerulus followed by a tubular network[70,74]. This complex structure is built around the renal vasculature, where their proximity enables the exchange of water and electrolytes between plasma and urine[74] (Figure 2). A nephron begins with the glomerulus, composed of a convoluted fenestrated capillary surrounded by the Bowman's capsule. Blood is delivered by the afferent arteriole and a fraction is filtrated through the porous endothelium, the podocytes foot processes and a thick extracellular membrane which, altogether, define the glomerular basement

membrane (GBM) which delivers primary urine in the Bowman's space[68,71,74]. This filtration barrier filters 20 % of the cardiac output. Primary filtrate is mainly composed of metabolic waste products such as ammonia, uric acid, urea, toxins, ions and proteins smaller than 90 kilodaltons (kDa). On the opposite, larger proteins such as albumin or immunoglobulins remain in the bloodstream[68,69,71]. Then, primary urine passed successively through renal tubules: proximal tubule, thin descending and ascending and thick ascending limbs of loop of Henle and distal tubules (Figure 2C) in which it is modified through reabsorption of glucose, amino acids, water, as well as sodium, potassium, calcium and chlorides and secretion processes of urea and uric acids, drugs, protons and other metabolites as creatinine or ammonia[69,71]. Each segment has specific characteristics and functions. In this regard, each segment of the nephron expresses specific receptors, channels and transporters [70]. Finally, definitive urine is excreted[69].

2. Proximal tubules

a) Physiology

Proximal tubules (PT) are divided into three interconnecting segments: S1 including most of the convoluted PT, S2 including the late convoluted PT and the beginning of the straight PT and S3 which represents the end of the straight PT. These segments are composed of PTECs. These are polarized cuboidal epithelial cells that display microvilli to increase contact size with the tubular lumen. These cells also display a primary cilium and an apical brush border containing peptidases responsible for protein degradation before reabsorption[75]. In addition, epithelial cells such as PTECs express adherent junctions, desmosomes and tight junctions. This allows a tight interconnection between them as well as a sealed epithelium to maintain apico-basal polarity and directional transport[76].

PTs display most of reabsorption and secretion capacity of the nephron. Indeed, PTECs, especially in the S1 segment, have a great capacity for reabsorption (70 % of all resorptive activity), allowing the uptake of almost all of ions Na^+, K^+, Ca^{2+}, magnesium, bicarbonate, phosphate, sulfate, vitamins as well as 100 % of the glucose[69,70,77]. For instance, sodium is reabsorbed under the form of sodium chloride (NaCl) by a primary active transport requiring Na^+/K^+-ATPase pumps at the basolateral membrane of PTECs. The Na^+ transport needs a high amount of energy expenditure and allows the passive transport of water by osmosis back to the bloodstream[69,70]. Other transporters such as sodium-glucose transporters (SGLTs), Na^+/H^+ exchangers (NHEs), Na^+/Ca^{2+} exchangers of Na^+/HCO_3^- co-transporters are expressed in PTECs to regulate fluids electrolyte composition and volume[77]. After their passage across PTECs, these nutrients go back to the bloodstream by vasa recta capillaries[70]. To ensure these functions are fulfilled, PTECs require a high energy metabolism[78].

PTECs are responsible for protein reabsorption through receptor-mediated endocytosis and display a well-developed endo-lysosomal trafficking system (Figure 3). This process allows the filtration of amino acids and low molecular weight proteins (MW $\leq$ 60 kDa) such as transferrin or insulin[79]. Two multiligand endocytic receptors, megalin and cubilin, are of particular importance for tubular reabsorption of proteins[80]. Megalin is a big 600 kDa transmembrane protein encoded by the *Lrp2* gene and expressed at the apical membrane of PT. At its cytoplasmic domain, megalin presents two NPXY motifs that interact with protein complexes involved in coated pit formation for clathrin-dependent endocytosis. Thanks to its ligand binding clusters, this receptor ensures the internalization of nearly all filtered plasma proteins [79]. Cubilin is a 400 kDa receptor highly expressed in PTs. This multiligand binding

receptor has no transmembrane domain since it is a peripheral membrane protein, meaning that cubilin requires transmembrane proteins such as megalin or amionless (AMN) for its association with the membrane. In addition, its interaction is reinforced by their shared ligands including vitamin D binding protein (DBP), albumin, hemoglobin or receptor-associated protein (RAP)[80,81]. AMN is a 38- to 50-kDa transmembrane receptor at the apical surface of PTECs. The latter has been shown to interact with cubilin and mediate endocytosis through its intracytoplasmic NPXY domain[79,81].

The clathrin-dependent endocytic process begins with the recognition of the ligand by specific receptors leading to its internalization in clathrin-coated pits. The release of the clathrin coat results in fusion of apical vesicles one with each other or with acidic early endosomes. Dissociation of ligands from megalin or cubilin is a pH-dependent process. Membrane receptors such as megalin and cubilin are then recycled to the apical membrane. Mature endosomes can fuse with lysosomes to deliver its soluble content for degradation by acidic hydrolases. Then, recycled free amino acids, vitamins and nutrients are released into the circulation by transcytosis[79,81]. The dysregulation of the endocytic process may result from genetic and acquired disorders often associated with tubular proteinuria leading to tubular and interstitial injuries, inflammation and fibrosis[80].

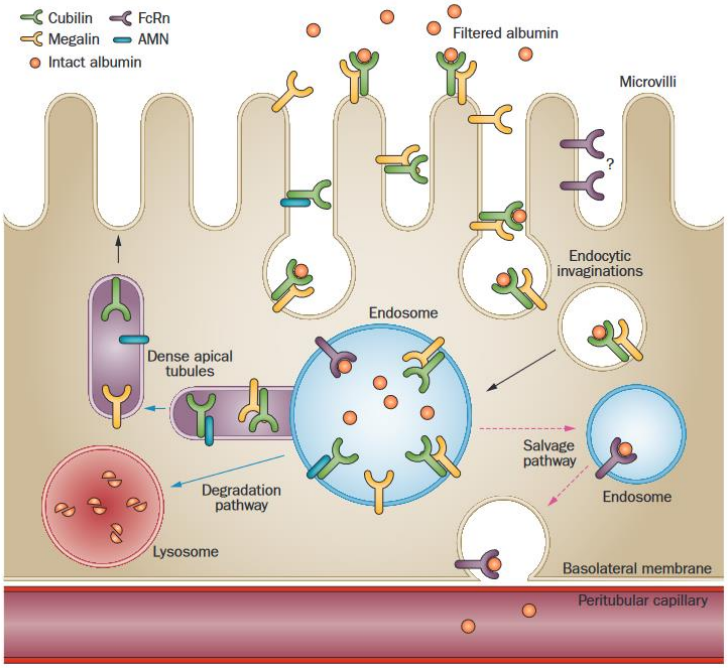

Figure 3: Protein-mediated endocytosis of albumin in renal proximal tubules. Filtered plasma proteins bind primarily to cubilin, associated with the transmembrane receptor proteins megalin and AMN to mediate internalization by apical clathrin-coated pits into coated vesicles and then into endosomes. Then, albumin dissociates from the receptors and is transported to lysosomes for degradation, after dissociation from megalin-cubilin, albumin may bind to neonatal Fc receptor (FcRn) and go through transcytosis[82].

b) Energy metabolism

As PTECs ensure important reabsorption and secretion processes, kidneys are high energy-demanding organs. To generate a lot of ATP, PTECs thus display a high density of mitochondria with an elevated oxidative metabolic rate at their basolateral side. For example,

mitochondrial energy production is required for the active transport of electrolytes generated by the Na^{+}-K^{+}-ATPase[83]. Even if PTECs can use a variety of substrates as energy sources, the major carbon source for renal ATP production is generated by the mitochondrial β-oxidation of FFAs[84].

FAs can be delivered to PTECs in a free or albumin-bound form and internalised passively or actively. On the one hand, PTECs express various transporters at their basolateral side to allow active transport of FFAs[84,85]. For instance, the fatty translocase CD36 is a multifunctional receptor involved in the uptake of FFAs, oxidized LDL and oxidized phospholipids. Other transporters such as FA transport proteins (FATPs) or FA binding proteins (FABP) also facilitate FFA cellular uptake[86]. On the other hand, FAs bound to albumin present in the first filtrate are internalised by protein-mediated endocytosis, as described below (Figure 4)[85].

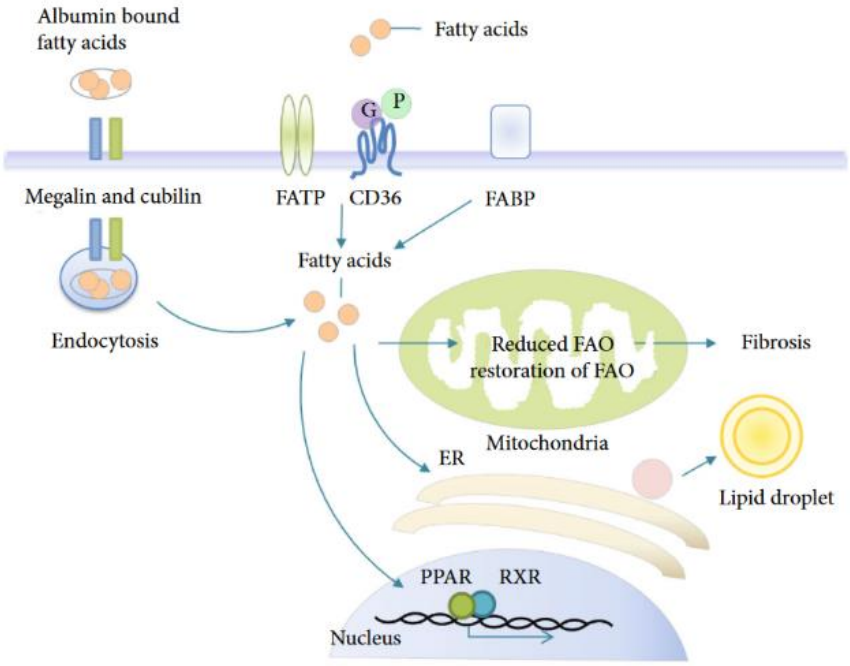

Figure 4: Schematic representation of kidney cellular uptake of fatty acids. FA is first transported across the plasma membrane by receptor-mediated endocytosis or protein-mediated mechanisms. Depending on their subcellular localization, FAs in cells bind to different FABPs and are used in membrane synthesis, energy production and storage, and nuclear transcription factor activation (PPAR/RXR, for example)[85,87].

In conclusion, FFAs may be either internalised, derived from DNL or from the catabolism of LDs by lipolysis or lipophagy. Then, they are used for mitochondrial ATP production (Figure 5)[84]. FFAs are first activated by the formation of a thioester bond with coenzyme A (CoA) by acetyl-CoA synthase to generate fatty acyl-CoA. While small FAs can diffuse across the mitochondrial membrane, long-chain hydrocarbon FAs require carnitine palmitoyltransferase I (CPT I) to catalyse the transesterification of acyl-CoA to acylcarnitine which cross the inner mitochondrial membrane (IMM) and the outer mitochondrial membrane (OMM), while CPT II converts acylcarnitine in acyl-CoA in mitochondria[88,89]. Then, fatty acyl-CoA enter the β-oxidation, a biochemical pathway that involves four enzymes (acyl-CoA dehydrogenase, enoyl-CoA hydratase, (S)-3-hydroxyacyl-CoA dehydrogenase and 3-ketoacyl-CoA thiolase) that oxidizes the fatty acyl-CoA in acetyl-CoA (Ac-CoA) to enter the

tricarboxylic acid (TCA) cycle. Each round of oxidation generates electron carriers/reducing equivalent, including flavin adenine dinucleotide ($FADH_2$) and nicotinamide adenine dinucleotide (NADH) which are then used to produce ATP by the mitochondrial OXPHOS[87,88]. Each molecule of PA produces at the end 106 molecules of ATP[88,90].

This process is first regulated by CPT I that acts as the rate-limiting enzyme of FAO as it allows the entry of the FA in the mitochondria and is allosterically and negatively regulated by malonyl-CoA[89]. In addition, the peroxisome proliferator-activated receptors (PPARs) and PPARγ coactivator-1a (PPARGC1A) have been shown to regulated FA uptake and FAO[91].

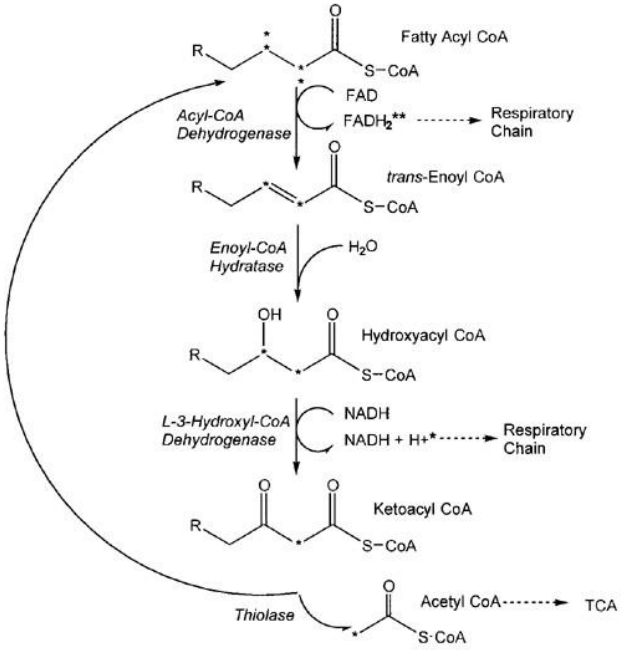

Figure 5: Diagram of the different reactions and enzymes involved in the FA β-oxidation[92].

Several studies demonstrated that, in kidneys, lipids accumulate predominantly in renal PTECs[91,93,94] and that these cells are very sensitive to lipotoxicity. It will be discussed in section Introduction C.3. [95,96]. In physiological conditions, FFAs delivered to PT are stored under the form of TAGs in LDs. This process has the advantage to store energy resources that could be rapidly mobilized in periods of starvation. In addition, it has been shown, in rats, that FFAs are transported bidirectionally between the kidney cells and the blood, suggesting that lipid export may be a protective mechanism against lipid overload[84].

C. Obesity-induced CKD

1. What is CKD?

According to the UK Kidney Association, CKD, a non-communicable disease, is described as a condition in which kidneys present functional and/or structural abnormalities for more than 3 months. These alterations include a glomerular filtration rate (GFR) less than 60 mL/min/1.72m² and albuminuria higher than 30 mg per 24 h as abnormal, abnormal urine sediment or kidney histology, renal tubular disorders as well as a kidney transplantation

history[97,98]. CKD is poorly diagnosed because less than 5 % of patients report awareness of their disease.

As we have seen, obesity is not only associated with WAT dysfunctions but also perturbations of intrarenal hemodynamics, mostly leading to CKD[97]. Besides, CKD may arise from multiple aetiologies such as hypertension, diabetes mellitus, autoimmune disease, chronic infections, as well as environmental factors. Evidence suggest that genetic risk factors may also lead to CKD. Patients may experience complications of the disease, resulting in hyperkalemia, metabolic acidosis, hyperphosphatemia, vitamin D deficiency, hyperparathyroidism and anemia[97].

2. Does obesity lead to CKD?

There is a strong correlation between obesity and risk of developing CKD and end-stage renal disease (ESRD). Indeed, this risk increases significantly for people with a BMI of 25 kg/m² or higher. This may be explained by changes in intrarenal hemodynamics, oxidative stress, lipotoxicity and/or inflammatory factors. In addition, obesity dysregulate the renin-angiotensin-aldosterone system (RAAS), and is associated with insulin resistance and adipokine secretion perturbations such as leptin, visfatin and adiponectin[99,100].

So far, the accumulation of lipids in kidney cells (podocytes, PTECs, …) is known to trigger lipotoxicity and drive CKD[101]. Pieces of evidence show that cellular dysfunctions triggered by lipotoxicity are associated with glomerular and tubular alterations observed in obesity-mediated CKD[102]. These glomerular and tubular alterations involve endothelial and podocyte dysfunction, glomerular basement membrane thickening and mesangial expression as well as low-grade tubulo-interstitial fibrosis and inflammation[10,72].

3. Lipotoxicity in PTECs

Lipotoxicity refers to the ectopic redistribution of lipids and their accumulation in excess in non-adipose tissues leading to a pathological phenotype. In this work, we set up an in vitro cellular model of murine primary PTECs exposed to PA to mimic the lipotoxic phenotype that could be observed in obesity-associated CKD[103]. Indeed, the effects of lipotoxicity are mainly studied in *in vivo* models of HFD-fed mice or *in vitro* in cell lines such as human (HK-2) or rat (NRK-52E) PTEC treated with PA[63,104–106]. Isolated primary mPTECs have thus the advantage (over cell lines) to represent a more relevant model for studying the impact of lipotoxicity on PTEC functions and metabolism. The lipotoxic phenotype has also been reported in obese patients as well as mouse models of obesity[45,107]. Even though PTECs are affected by an imbalance in lipid metabolism, other renal cell types such as podocytes and mesangial cells also display signs of lipotoxicity[10,45].

Lipotoxicity is reported to trigger cellular dysfunctions such as mitochondrial damages, reactive oxygen species (ROS) production and oxidative stress, as well as dysfunctions of cellular degradation pathways. Lipotoxicity results from an imbalance between FA uptake, oxidation and synthesis. Excessive intracellular accumulation of FAs leading to the formation of toxic metabolites such as ceramides, diacylglycerol or fatty acyl-CoA, which in turn activates inflammatory pathways[84].

Increase amount of non-esterified FAs (NEFAs) in renal cells provokes mitochondrial respiration perturbations and peroxide-mediated apoptosis[85]. Due to the importance of lipid oxidation for energy metabolism, the increasing flux of FAs leads to exhaustion of oxidative

capacity of mitochondria and FAs storage in LDs. Indeed, PTEC lipotoxicity is associated with mitochondrial alterations and an increase in the production of ROS leading to oxidative and organelle stress[45].

Lipid overaccumulation also triggers deregulations of the endoplasmic reticulum (ER) functions through modifications of its membrane lipid composition, inhibition of calcium signalling, reduction of protein translation and activation of inflammatory kinases such as IL-1 and TNFα[45,63,108,109].

Finally, renal lipotoxicity results in lipid metabolism dysregulations, release of proinflammatory and profibrotic factors, insulin resistance and perturbations of RAAS axis in kidneys[84,110]. These events globally contribute to PTEC dysfunction characterized by the loss of the brush border, polarity alterations as well as defects in the reabsorption of filtered proteins. Finally, the severity of these dysfunctions could end in lipid-induced apoptosis, called lipoapoptosis[10,84].

In addition, it has been shown that the excess of intracellular FAs results in dysfunctions of the autophagic flux through lysosomal deficiency[108]. Indeed, HFD-mice display changes in lysosomal and autophagic markers in proximal tubules as in obese patients[103,108]. However, there are still many unknowns regarding the mechanisms by which lipotoxicity disrupts degradative pathways in mPTECs.

D. Cellular degradation pathways

1. Ubiquitin-proteasome pathway

To ensure their homeostasis, cells require dynamic and self-regulating cellular quality control processes to adapt to new environmental conditions and protect against prolonged damages. These quality-control mechanisms include degradation and recycling through the ubiquitin-proteasome system (UPS) and the autophagic pathway[111,112]. While UPS ensures the degradation of short-lived, misfolded or damaged proteins in a structure called the proteasome, autophagy allows the degradation of larger cargos such as protein aggregates, cellular components and/or organelles[111].

UPS is a selective proteolytic system in which altered proteins are tagged with ubiquitin (Ub) chains and delivered to the proteasome for degradation. Misfolded, unfolded, degraded or unfunctional proteins/enzymes are tagged by the ubiquitination system. It allows the addition of Ub chains to a substrate through the cooperative action of three ubiquitination enzymes : the Ub-activating enzyme (E1), the Ub-transferring enzyme (E2), and the Ub ligase (E3) (Figure 6)[113].

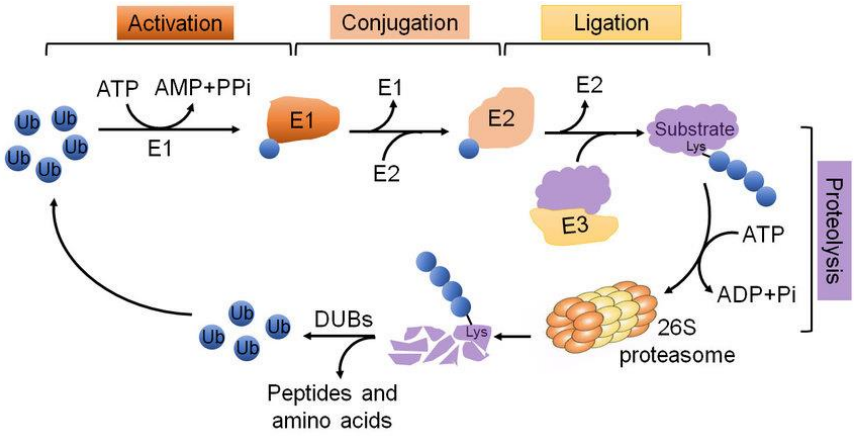

Figure 6: Ubiquitin-proteasome system*. Free Ub is activated by E1 Ub-activating enzyme through ATP hydrolysis. Activated Ub is transferred by E2 Ub-conjugating enzyme to the substrate to degrade and attached by E3 Ub-ligase enzyme. Polyubiquitinated substrates are then recognized by the regulatory particle (RP) of the proteasome before being digested in peptides and amino acids by the core particle (CP) of the proteasome*[114].

The proteasome emphasizes two subunits: a barrel-shaped core particle (CP, also called 20S proteasome) and a regulatory particle (RP, also called 19S proteasome). The RP recognizes poly-ubiquitinated substrates and after the Ub removal by deubiquitinases, substrates to be degraded are sent to proteolysis in the CP. The latter has caspase-like, trypsin-like and chymotrypsin-like activities to ensure protein digestion in peptides and amino acids. Degradation by the UPS is regulated by the abundance and the activity of the proteasome[111].

2. Autophagy

a) Generalities

Autophagy is a self-degradative process required for balancing sources of energy and recycling building blocks to compensate for lack of nutrients and/or energy[115]. It also has a housekeeping role in the degradation of misfolded or aggregated proteins, damaged organelles, such as mitochondria (mitophagy), ER (reticulophagy), lysosomes (lysophagy) and peroxisomes (pexophagy) (among others), as well as intracellular pathogens (xenophagy)[116,117]. Finally, autophagy can also promote cell senescence and cell surface antigen presentation, protect against genome instability and prevent necrosis[118].

There are three defined autophagic pathways: macro-autophagy (hereafter referred to as “autophagy”), micro-autophagy and chaperone-mediated autophagy (CMA). Those three autophagic pathways share a proteolytic degradation of cytoplasmic components in lysosomes. However, the mechanisms of delivery to lysosomes are different. Autophagy enables the degradation and recycling of larger cytoplasmic cargos, sequestered/engulfed in a double-membrane vesicle, the autophagosome. In contrast, micro-autophagy refers to the direct uptake of cytoplasmic elements by the lysosome through invagination of the lysosomal membrane. Finally, CMA is an autophagic route that targets cytosolic proteins exposing the KFERQ motif. These are recognized by heat shock 70 kDa protein 8 (HSC70) which binds LAMP2A to allow proteins unfolding, translocation and degradation[111,115].

It is now clear that the autophagic process can be divided into 2 major pathways: a non-selective or a selective pathway. Non-selective autophagy is characterized by the sequestration and degradation of bulk portions of cytoplasm. In contrast, selective autophagy specifically targets cellular structures such as organelles, nuclear components, the proteasome, protein aggregates, stress granules or invasive pathogens[119].

b) Canonical pathway

Although autophagy is a continuous process, it can be virtually divided into 5 main steps: initiation, membrane nucleation (initiated by the omegasome formation: a PI3P rich region in the ER to which DFCP1 localizes, and which goes through the cycle of expansion, maturation,…) and phagophore formation, phagophore expansion, fusion with lysosomes and lysosomal degradation[115]. This multistep process is regulated by metabolic sensors such as Mechanistic Target of Rapamycin Complex 1 (mTORC1) and AMPK, as well as several autophagy-related proteins (ATGs) assembled into complexes : Unc-51-like kinase 1 (ULK1) initiation complex, class III PI3K nucleation complex and phosphatidylinositol 3-phosphate (PI3P)-binding complex (Figure 7)[120].

First, the autophagic process is initiated by the formation of an isolation membrane, also called the phagophore. In mammalian cells, phagophore membranes originate from the lipid bilayer of the ER forming the omegasome, but also from the trans-Golgi, endosomes and nucleus under specific conditions such as presentation of endogenous viral peptides[121]. A stress initiates the autophagic process through AMPK activation (mainly sensitive to bioenergetic stress affecting and increasing the AMP/ATP ratio) and mTORC1 inhibition (mainly sensitive to a nutrient stress, especially a lack of certain amino acids such as glutamine, leucine, arginine or methionine)[122], leading to the formation of ULK1 complex comprising the serine/threonine kinases ULK1 and ULK2, ATG13, FAK family kinase-interacting protein of 200 kDA (FIP200) and ATG101[115,123]. It results in phosphoinositide 3-kinase (PI3K) III nucleation complex phosphorylation and vesicular protein sorting 34 (Vps34) interaction with beclin 1 as well as beclin 1-regulated autophagy-related key regulator (ATG14) to promote PI3P production at the omegasome and the phagophore nucleation from the ER lipid bilayer[115,120]. Then, PI3P-binding proteins are recruited for phagophore expansion to finally form a double membrane organelle: the autophagosome. Additional membranes from ER, Golgi, mitochondria or endosomes with the support of PI3P-binding proteins WD repeat domain phosphoinositide-interacting proteins (WIPIs) and zinc-finger FYVE domain-containing protein 1 (DFCP1) are delivered to phagophore in ATG9-containing vesicles[120,123]. This process requires two Ub-like systems: the ATG12-ATG5-ATG16L1 conjugation complex and the microtubule-associated protein light chain 3/γ-aminobutyric acid receptor-associated proteins (MAP1LC3, hereafter called LC3/GABARAPs) conjugation complex. In the first system, ATG17 acts like an E1 ubiquitin activating enzyme to activate ATG12. ATG10 acts as the E2 Ub conjugating enzyme to bind ATG12 to ATG5 which are both attached to ATG16L1. The ATG12-ATG5-ATG16L1 complex facilitates membrane curvature of the growing phagophore and promotes LC3 conjugation with its E3 Ub ligase activity[115,120]. In parallel, the second Ub-like system is processed. LC3B is subjected to a proteolytic cleavage by ATG4 in the cytosolic form LC3B-I. LC3B-I is activated and conjugated with phosphatidylethanolamine (PE) by ATG7 and ATG3, respectively, and added by the ATG12-ATG5-ATG16L1 conjugation complex in pre-autophagosome and autophagosome membranes, under the membrane bound LC3B-II form. Then, LC3B-II participates in cargo recognition and recruitment to the autophagosome through

the binding of LC3-interacting regions (LIRs) host by cargo adaptors such as p62 for poly-ubiquitinated poly-aggregates or specific organelles adaptors [115,123].

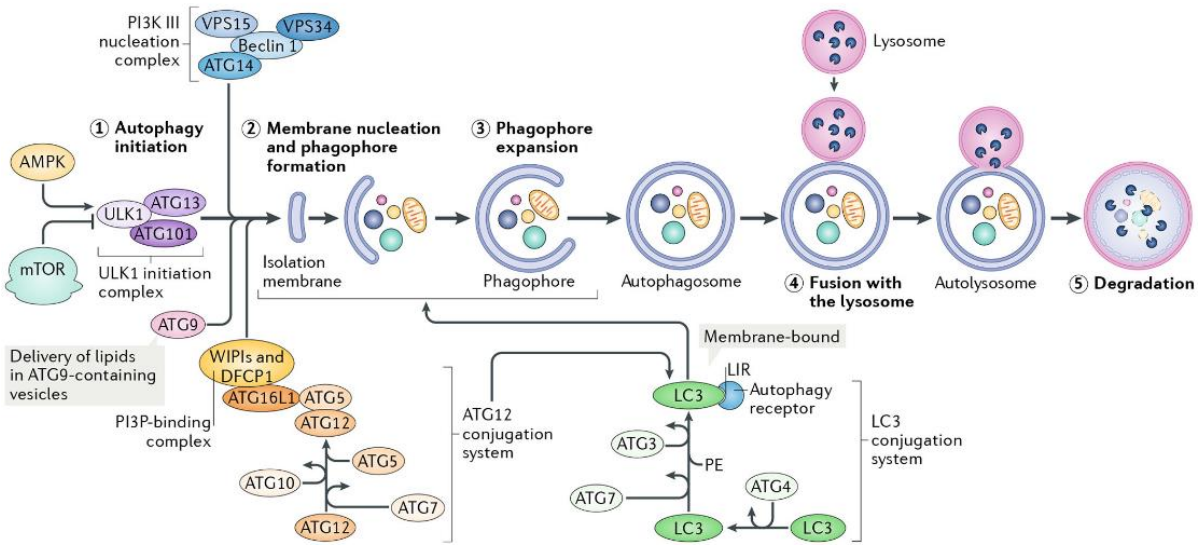

Figure 7: Representation of autophagic pathway. *Autophagy consists of 5 steps: initiation, membrane nucleation, phagophore formation, phagophore expansion, fusion with the lysosome, and degradation, each controlled by numerous autophagy-related proteins (ATGs). ATG complexes include ULK1 initiation complex, PI3K III nucleation complex, and PI3P-binding complex, facilitating phagophore formation with ATG12 and LC3/GABARAPs conjugation systems. In the ATG12 conjugation complex, ATG12 binds to ATG5 and ATG16L1, followed by dimerization and interaction with the PI3P-binding complex (composed of WIPIs and DFCP1). ATG12-ATG5-ATG16L1 complex helps binding to LC3 (or GABARAP, another family of autophagic receptors) by ATG4 protease cleaving LC3 to generate LC3B-I, which then associates with phosphatidylethanolamine (PE) to form LC3B-II. LC3 is found in pre-autophagosomal and autophagosomal membranes, where it interacts with cargo receptors that contain LC3-interacting motifs (LIRs)*[120].

When autophagosome formation and cargo recognition are completed, autophagosomes and their content are delivered to lytic compartments such as lysosomes. Autophagosomes can first fuse with early and late endosomes prior to fusion with lysosomes to reduce the vesicle pH and to provide elements of the membrane fusion machinery to lysosomes[115,124]. Autophagosomes are transported from the peripheral region along microtubules to the perinuclear region where lysosomes are already located. This process requires cytoskeleton components such as microtubules and motor proteins such as dynein and kinesin. This fusion process is also regulated by tethering factors like homotypic fusion and vacuole protein sorting (HOPS) complex, RAB GTPases and specific soluble N-ethylmaleimide-sensitive factor attachment protein receptor (SNARE) complexes resulting in the formation of autolysosomes[123,124].

After the fusion, lysosomal hydrolytic enzymes are responsible for the breakdown of proteins, polysaccharides and complex lipids in building blocks such as amino acids, monosaccharides and FFAs, respectively, which are exported for energy homeostasis or recycled in anabolic pathways. Lysosomes display a large variety (about 60 enzymes)[125] of hydrolases such as proteases, glycosidases and lipases. These enzymes require an acidic environment for their optimal activity[126]. In this regard, lysosomes ensure the maintenance of ionic homeostasis and membrane potential by ion channels and transporters. To provide

lysosomal acidification (pH ~ 4.6), H^+ are pumped in the lumen by the vacuolar-ATPase (V-ATPase). Lysosomal degradation is an adaptative process well-regulated through nutrient status and cell signaling. For example, upon change in nutrient concentration, lysosome morphology abundance (involving the balance between biogenesis and lysophagy) and distribution change from small numerous lysosomes in fed cells to fewer and larger lysosomes in starved ones[126].

c) Autophagy regulation

Although autophagy is an active process at basal level to maintain cellular homeostasis, this mechanism is highly regulated and can be activated by different signals such as oxidative stress and ER stress, pathogen invasion, deoxyribonucleic acid (DNA) damage, starvation or hypoxia[124].

An important signal that activates autophagy is nutrient deprivation. Indeed, it modulates the energy-sensing serine/threonine kinases mTORC1 and AMPK, as well. mTORC1 inhibits autophagy in nutrient-rich conditions and AMPK displays the opposite effect[115]. Activated mTORC1 phosphorylates the ULK1 complex and blocks autophagy initiation. In addition, it promotes ribosome biogenesis and mRNA translation to achieve protein synthesis. On the contrary, in nutrient starvation situations, mTORC1 is inhibited and dissociates from ULK1 complex resulting in autophagy initiation[127]. In addition, in these conditions, AMPK promotes and reinforce the activation of autophagy by directly activating ULK1 and by inhibiting mTORC1[123].

AMPK is a cellular energy sensor complex composed of a catalytic α-subunit, a scaffolding β-subunit and a regulatory γ-subunit[128]. AMPK is activated in response to increase in cellular AMP/ATP (but also ADP/ATP) ratio through allosteric binding of AMP leading to the increase in phosphorylation of the catalytic subunit on Thr-172, mainly mediated by the inhibition of a phosphatase: PP2A[129]. Indeed, the phosphorylation of AMPK is regulated by upstream kinases such as the liver kinase B1 (LKB1, previously called AMPKK) and Ca^{2+}/calmodulin-dependent protein kinase β (CaMKKβ)[130,131]. AMPK is thus a central metabolic regulator and energy sensor which activates catabolic pathways such as glucose uptake, glycolysis, FAO and autophagy while inhibiting anabolic processes, consuming ATP, such as lipogenesis, glycogenolysis and protein synthesis[132,133]. In addition, the activation of AMPK appears to reduce tumour proliferation[112,131].

Under conditions of nutrient deprivation, autophagy is increased, a consequence of mTORC1 inhibition. This response is accompanied by the translocation of transcription factor EB (TFEB) which promotes lysosomal biogenesis, function and trafficking[134]. Indeed, transcription factors such as TFEB, transcription factor E3 (TFE3) or forkhead box O1 (FOXO1) promote lipophagy under nutrient deprivation conditions[135]. On the opposite, feeding-induced transcription factors (FXR) inhibits the autophagic pathway[126].

3. Crosstalk between UPS and autophagy

UPS and autophagy were first thought to be independent mechanisms, now it becomes clear that both act as an interconnected network of regulation. Regulation of the crosstalk between these two pathways is specific and occurs through selective enzyme reactions and expression of specific receptors to deliver cellular content to proteasome or lysosomes respectively. Cargo delivery to the proteasome or lysosomal degradation system is mainly

mediated by the avidity of a complex of proteins, not just the affinity of receptors for Ub[136]. One of the processes contributing to this crosstalk is the N-terminal arginylation of the N-end rule pathway. This conjugation of L-arginine (L-Arg) to N-terminal aspartate (Asp), glutamate (Glu), glutamine (Gln), asparagine (Asn) and cysteine (Cys) with or without post-translational modifications to modulate the autophagic proteolysis. It redirects undegraded cargos to lysosomal degradation through the recognition of p62 and sequestration in the autophagosomes[137].

Another crosstalk pathway occurs in the UPS-ER-autophagy circuit, when misfolded proteins accumulate in the ER lumen, leading to ER stress and the initiation of the unfolded protein response (UPR) pathway. In this case, the molecular chaperone BiP dissociates from ER membrane receptors Activating Transcription Factor 6α (ATF6α), Inositol-Requiring Enzyme 1α (IRE1α) and Protein Kinase R (PKR)-like Endoplasmic Reticulum Kinase (PERK), which alleviate their inhibition[138] (Figure 8). Each of these receptors promotes the downstream autophagic pathway. For instance, ATF6 acts as a transcription factor to promote 3-Phosphoinositide Dependent Protein Kinase-1 (DPK1) expression and subsequent beclin-1 phosphorylation. IRE1α facilitates the formation of autophagosomes through expression of autophagic core genes and Bcl-2 phosphorylation. In parallel, ER molecular chaperones are synthesised to facilitate ER protein folding or misfolded proteins degradation by the ERAD pathway. Finally, PERK indirectly regulates ATG gene expression, ATF4 and C/EBP Homologous Protein (CHOP-10) synthesis, LC3 lipidation and autophagosome biogenesis. A third mechanism that links UPR and the autophagic pathway is p53-induced autophagic degradation throughout proteasome inhibition. In this case, inhibition of the proteasome promotes p53 nuclear stabilisation and accumulation, leading to the transcription of autophagy housekeeping genes such as damage-regulated autophagy modifier (DRAM)[139].

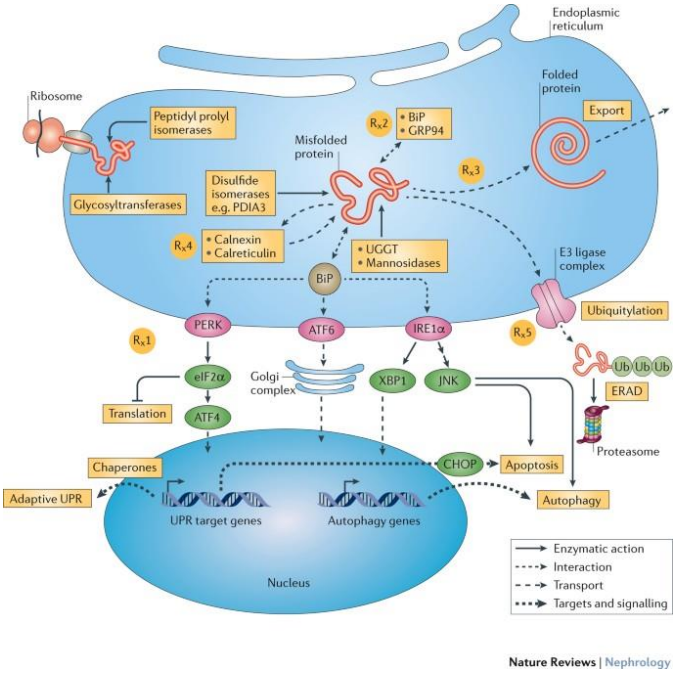

Figure 8: Schematic representation of the crosstalk between UPR and autophagic pathway. *UPR activation by misfolded proteins initiates 3 different pathways through ER stress sensors PERK, ATF6 and IRE1α which regulate UPR target genes as well as autophagy-related genes modulating the autophagic response during ER stress*[140].

4. Selective autophagy

As mentioned before, autophagy may be selective. Three conditions must be met for this machinery to function properly: a specific cargo recognition, an effective cargo sequestration in autophagosomes and exclusion of non-cargo material from the autophagosome[119].

Specific cargo receptors, and their adaptors, provide the selectivity for this mechanism. They enable the tethering of cargos to the nascent autophagosome when binding both the cargo and LC3B-II on the inner autophagosomal membrane. Cargo adaptors can either be attached directly to the cargo or attach poly-Ub chains to the surface of the cargo molecules. Indeed, the human cargo adaptor p62 can bind Ub on aggregated proteins as well as other organelles such as mitochondria, LDs, ER fragments or lysosomes. Then, these cargos trapped in the autophagosomes undergo the degradation process as described for the canonical pathway[119]. Among the numerous selective pathways of autophagy, five are detailed in the following sections as related to the results generated during this Master thesis: lipophagy, mitophagy, lysophagy, ER-phagy and aggrephagy.

a) Lipophagy

In starved conditions, FFAs are derived from LDs either by lipolysis or lipophagy of TAGs to serve as energy sources (Figure 9) [141,142]. Intracellular lipolysis requires the interaction between neutral cytosolic lipases and structural proteins at the surface of LDs such as perilipins (PLINs)[143]. In contrast, lipophagy is defined by the engulfment and sequestration of parts of LDs through LC3B-II recognition of cargo receptors. A prerequisite for the lipophagic pathway is the lysosomal degradation of LDs structural proteins PLIN2-3 by CMA[144]. It has been shown that AMPK phosphorylates PLIN2, leading to its degradation by CMA and promotes lipophagy in L2A KO mouse embryonic fibroblast cells treated with AMPK inhibitor[141,145]. These are recognized by Hsp70 by the KFERQ motif and internalized by LAMP2 in the lysosomal lumen for degradation. PLINs influence LD catabolism by controlling lipids recognition by neutral lipases or autophagic machinery. Indeed, PLIN inhibition promote the catabolism of LD and TAG breakdown[141,146].

The lipophagy may also be promoted by the cytosolic lipase ATGL when it binds to LC3B-II. Other mechanisms such as poly-ubiquitination of apolipoprotein B induces autophagic initiation at the LD surface. It has also been shown that the ancient ubiquitous protein 1 (AUP1) integration at LD surface seems necessary for lipophagy[141,142]. In addition, lipophagy may be transcriptionally regulated like autophagy by TFEB, TFE3, FOXO1 or PPAR-γ coactivator 1 α (PGC-1α)[141].

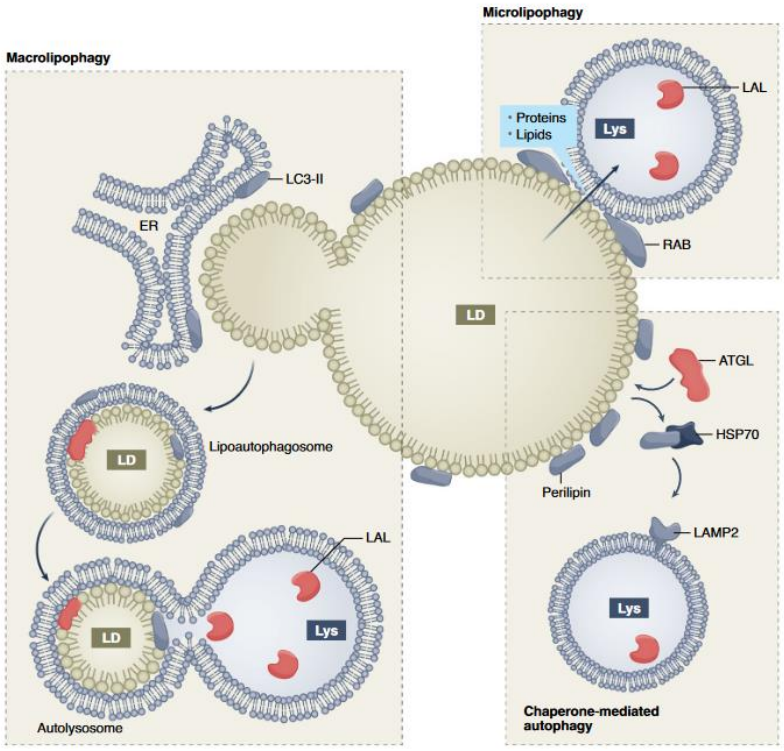

Figure 9: Schematic view of lipophagic pathways. *The 3 lipophagy degradation pathways enable lysosomal lipolysis of TAGs contained in LDs. This requires the degradation of LD structural proteins. CMA also enables the degradation of LD structural proteins by chaperones. Thereafter, microlipophagy enables direct interactions between LDs and lysosomes, so that lysosomal associated lipases (LALs) degrade lipids. Macrolipophagy allows the sequestration of budding part of the LDs, engulfed in the autophagosome before being targeted to the lysosome*[146].

b) Mitophagy

Mitochondria, among their numerous functions, contribute to ATP production and ROS production[147–149]. Besides, these are particularly sensitive to oxidative stress which may lead to mitochondria damages[147]. To maintain proper cellular functions, damaged mitochondria can be removed by the selective autophagic turnover of mitochondria, called mitophagy. This process regulates the abundance of mitochondria and their fitness in basal conditions. Mitophagy thus acts as mechanism that control both quality and quantity of mitochondria in cells[147,148].

Mitophagy is initiated by the recognition of specific OMM receptors or ubiquitinated proteins[149]. Mitochondria recognition may be mediated by several different mechanisms such as either parkin-dependent (using the phosphatase and tensin Homolog (PTEN)-induced kinase 1 (PINK1)-Parkin interaction) or parkin-independent (using mitophagic adaptors like Bcl2-interacting protein 3 (BNIP3) and NIX, also called BNIP3 like (BNIP3L)) (Figure 10)[147]. Mitophagy is initiated by diverse cellular stress such as a decrease (depolarisation by perturbations of OXPHOS, ROS or calcium influx, leading to a hypopolarisation) in mitochondrial membrane potential[150]. In this situation, PINK1, a mitochondrial serine/threonine kinase, is recruited and stabilized to OMM by the translocase of the outer membrane (TOM). This allows the recruitment of the cytosolic Parkin (an E3-Ub ligase) on OMM and poly-ubiquitination of outer membranes proteins such as the voltage-dependent anion channel (VDAC), TOM or mitofusins (MFNs)[151,152]. Parkin-mediated poly-ubiquitination results in cytosolic factors recruitment at the mitochondrial membrane, required

for the initiation of mitophagy. These include p62, histone deacetylase 6 (HDAC6) or valosin-containing protein (VCP), also known as p97 in mammals. The function of this ATPase enzyme present in all eukaryotes (and archaebacteria) is to segregate protein molecules from large cellular structures such as protein assemblies, organelle membranes and chromatin, and thus facilitates the degradation of released polypeptides by the multi-subunit protease proteasome. p62, in turn, recruits LC3-BII to allow engulfment of depolarized mitochondria in autophagosomes leading to their lysosomal degradation[147,152].

Parkin-independent pathway of mitophagy includes BNIP3 and NIX regulation for mitochondria turnover (Figure 10). BNIP3, along with NIX, is a protein of the BH3-only family involved in cell death and activation of autophagy. BNIP3 is a gene commonly expressed coding for a cytosolic monomer which can form a stable homodimer under stressful conditions such as hypoxia[153]. This enables its integration in OMM by its transmembrane domain (TM) and its phosphorylation close to its LIR region, facilitating the interaction between BNIP3 and LC3B-II and then, mitochondrial engulfment in autophagosomal membranes[149]. NIX shared more than 50 % homology with BNIP3, also interacts with LC3B-II and mediates similarly parkin-independent mitophagy in response to hypoxia[154].

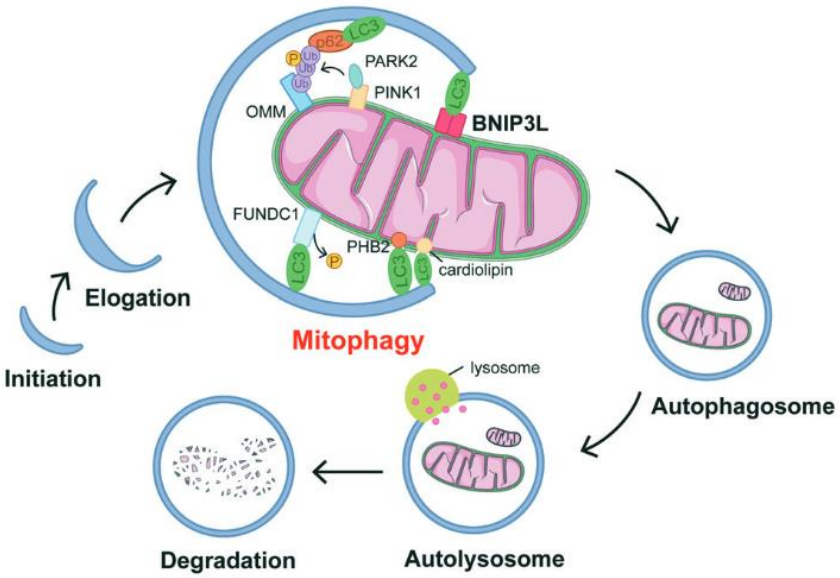

Figure 10: Schematic representation of mitophagy. *Mitochondrial degradation can take place by a parkin-dependent mitophagy, in which PINK recruits parkin, which in turn ubiquitinates OMM leading to p62 binding. The parkin-independent mitophagy requires adapters such as BNIP3 or NIX that interact like p62 with LC3B-II, allowing mitochondria to be surrounded by phagophore membranes and subsequently degraded.*[154]

c) Lysophagy

As mentioned in the Introduction (section D.2.b), lysosomes are the main proteolytic compartments of mammalian cells. They are involved in recycling intracellular but also extracellular macromolecules[155]. Lysosomal membranes are very sensitive to damages induced by ROS or pro-apoptotic Bcl-2 family members[156] which may lead to an increase in lysosomal membrane permeability (LMP), leaking of luminal content and dysfunction of the organelle[157].

Leaking lysosomes release protons and hydrolases in the cytoplasm in which residual activities might lead to lysosomal cell death[157,158].

Several quality control mechanisms may occur in response to LMP to prevent cell death. The repair of lysosomal membranes by endosomal sorting complex required for transport (ESCRT), the sequestration and degradation of damaged organelle by lysophagy or regeneration of the lysosome pool by lysosomal biogenesis (Figure 11)[159]. Lysophagy is activated when the lysosomal membrane is ruptured. Galectin-3 (Gal3) is thus able to enter the permeabilised lysosomes and oligomerize to exposed glycans at the inner leaflet of the membrane. Gal3 is recognized by the tripartite motif protein Tripartite Motif-Containing 16 (TRIM16), which binds elements involved in the autophagic response such as ATG16L1, ULK1 and Beclin1[157,159–161]. Ubiquitination by TRIM16 is a prerequisite for lysophagy. In fact, it mediates the recruitment of autophagic machinery such as p62 and the initiation complex ULK1, enabling the formation of the phagophore and the engulfment in autophagosomal membranes delivered to lysosomes for degradation. Other adapters such as F-box protein 27 (FBXO27), Gal8 or Gal9 directly recognise glycans and recruit the autophagy machinery as well. However, the Gal3-mediated lysophagy remains the most studied pathway[157,159].

Lysosomal biogenesis is required when lysosomes pool become limited or in other cases such as cell proliferation. Lysosome regeneration may occur through lysosome-related organelles such as autophagosomes, endosomes or phagosomes. In addition, lysosomal biogenesis is transcriptionally regulated by TFEB and TFE3[162,163].

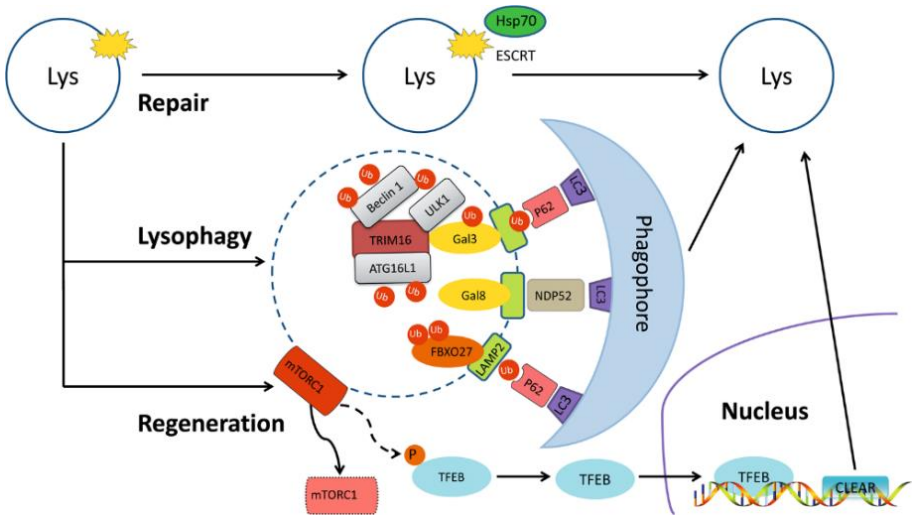

Figure 11: Schematic representation of lysosomal quality control*. The lysosome quality control system operates along 3 axes: lysosomal repair, lysophagy and lysosomal regeneration/biogenesis. The lysosomal membrane can be repaired by the chaperone protein Hsp70 in the ESCRT pathway. In lysophagy, the lysosome is eliminated after its recognition by galectins or by FBXO27 binding to glycans exposed after the lysosomal membrane is permeabilized. After polyubiquitination and recruitment of the autophagy initiation machinery, the damaged organelle is surrounded by phagophore membranes, sequestered in the autophagosome and delivered to the lysosome for degradation. Finally, lysosomal biogenesis is regulated by transcriptional factors TFEB and TFE3 that coordinate the expression of CLEAR gene complex.* [163,164]

d) ER-phagy

The ER is involved in protein synthesis (essentially plasma membrane and secreted proteins), folding, processing and transport (Rough ER: RER) but also in lipid metabolism (Smooth ER: SER) and calcium homeostasis[165,166]. To maintain its function and integrity, ER is also dynamic and undergoes remodelling and turnover. In addition, stressful conditions such as the accumulation of mis- or un-folded proteins or ceramides, may lead to ER stress[167].

In response to ER stress, intracellular signalling pathways may be activated to cope with the stress including the unfolded protein response (UPR) and their degradation in the UPS, called ER associated degradation (ERAD), as well as ER-phagy[168–170]. ER-phagy is known to be a back-up system for degradation of ER-components when ERAD is inefficient (or not enough sufficient) upon stress[171]. In physiological conditions, this process ensures the modulation of ER size, functions and content to maintain homeostasis (Figure 12)[168,172,173].

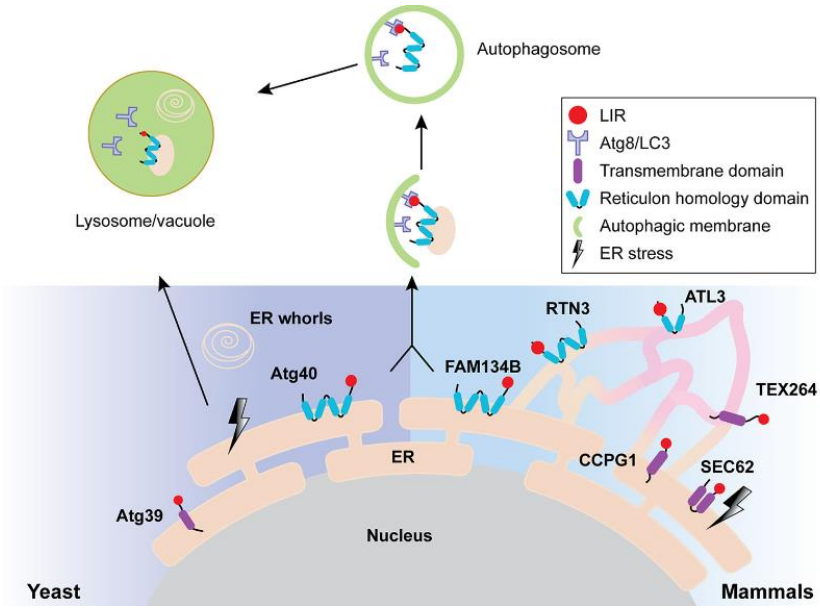

***Figure 12*: Schematic representation of ER-phagy in mammalian cells and in** *yeast. Autophagic degradation of the ER occurs through recognition of ER adapters such as FAM134B, RTN3, ATL3, CCPG1, TEX264 and SEC62 in mammalian cells or Atg39 and Atg40 in yeast. This enables recognition and binding to LC3B-II via its LIR domain. The autophagosomal membranes then surround the ER fragment to be digested in the lysosome.*[174]

ER-phagy encompasses the ER fragmentation and the degradation of ER parts by the autophagy-lysosomal system. ER-phagy requires adaptors which are ER-resident transmembrane proteins or proteins anchored in the membrane allowing the selective engulfment of ER in autophagosomes. These adaptors include: FAM134B, RTN3L, CCPG1, SEC62, TEX264 and ATL4. These possess a LIR region and are either localized in the ER tubules (CCPG1, ATL3, RTN3) or sheets (FAM134B, CCPG1, SEC62 and TEX264) [170,171,175]. The reticulophagy regulator 1 (RETREG1/FAM134B) is involved in ER-sheet fragmentation and degradation by autophagy under nutrient starvation. Its reticulon homology domain (RHD) enables the curvature of the membrane and its fission to release ER fragments to lysosomal degradation[176]. FAM134B has been showed to trigger procollagen lysosomal degradation when interacting with the membrane ER chaperone calnexin[177]. Cell cycle progression 1 (CCPG1) along with reticulon 3 (TNL3) and atlastin GTPase 3 (ATL3) are located in ER tubules and mediate ER budding and delivery to autophagy-lysosome machinery [170,171]. In addition, CCPG1

may act as an intermediate between UPR and ER-phagy because it facilitates misfolded and aggregated proteins degradation[171,178]. The preprotein translocation factor Sec62 an ER resident component of a translocation machinery controlling protein import in ER. In fact, Sec62 also acts as an ER-phagy adaptor as it allows ER clearance during ER stress to relief from this stress, through a process called "recovER-phagy"[178,179]. ER-phagy is regulated by different signals and mechanisms.

First, there are pleiotropic signals such as nutrient deprivation that inhibit mTORC1, activate AMPK, and thus initiate the autophagic pathway[173,180,181]. Second, ER-phagy is modulated by post-translational modifications including phosphorylation, arginylation or UFMylation[182,183]. UFMylation is a modification in which Ub-Fold Modifier-1 (UFM-1) is attached to lysine residues to regulate some biological processes (Figure 13). UFM1 precursor (proUFM1) is initially cleaved by UFM1-specific cysteine proteases (UFSP1 and UFSP2) and forms a mature UFM1 protein. Then, the E1 Ub-activating enzyme 5 (UBA5) binds UFM1 which is transferred to E2 UFM1-conjugase 1 (UFC1). UFM1-ligase 1 (UFL1), a E3 ligase complex localised in the ER, then conjugates UFM1 on the target protein[182–186]. ER-localised UFMylation of targeted proteins acts as an activator signal for ER-phagy[182,184,186]. Third, as previously mentioned, ER-phagy may be regulated by different cell stresses[173]. UPR activation seems to positively regulate ER-phagy but the mechanisms behind this regulation remain poorly understood[168,172,173]. However, several pieces of evidence suggest that there is a link between UPR pathway, ER stress and ER-phagy leading to what is called ER stress-mediated autophagy[172]. In addition, literature suggests that ER-phagy is regulated by ER signals including alterations of the redox and calcium homeostasis, or pathogen replication or invasion[173].

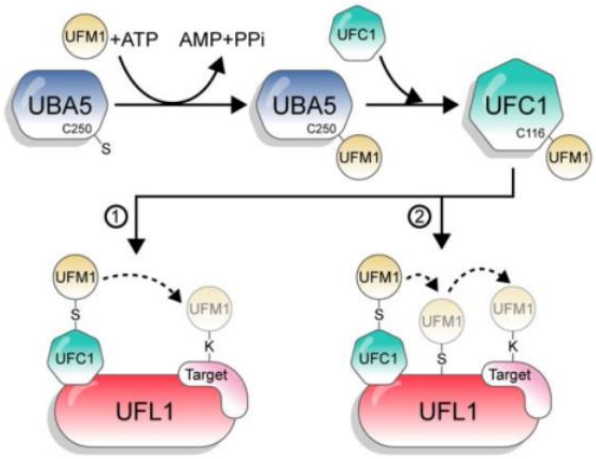

Figure 13: UFMylation of ER-localised substrates initiates ER-phagy*. Pre-UFM1 is cleaved by UFSP in a mature form, UFM1. UBA5 activates UFM1 and transfers it to UFC1. Then, UFM1 is conjugated with the substrate on UFL1.*[185]

e) Aggrephagy

Maintaining protein homeostasis requires good and efficient quality control systems. Under certain conditions, such as oxidative stress, ER stress or lipid stress, proteins can become misfolded or unfolded and form aggregates[187]. Their accumulation is deleterious and can lead to cell death[188]. As we have seen, in response to ER stress conditions, pathways are activated to eliminate damaged proteins from ER: UPR and ERAD[188]. In addition, cytosolic proteins may

also be damaged by oxidative stress and need to be degraded. So far, three systems of protein quality control take place: chaperone-mediated refolding, proteasomal degradation (described in the Introduction section D.1.), and when UPR and UPS are unable to repair or degrade dysfunctional proteins, selective autophagic degradation of protein aggregates[187]. Indeed, when proteins failed to be correctly folded or degraded, they generates abnormal local hydrophobic interactions, causing aberrant chemical interactions such as dislocated hydrogen bonds or linkages with the wrong proteins resulting in protein aggregation (Figure 13)[187].

Protein aggregates or aggresome assemble after transport to the microtubule-organizing centre (MTOC) with the help of histone deacetylase 6 (HDAC6), which has a high affinity for ubiquitinated proteins. The latter enables deacetylation of α-tubulin leading to protein aggregates motility to MTOC on microtubules. Aggresomes are insoluble and metabolically stable structures containing Ub-tagged aggregated proteins encircled by a cage-like structure composed of vimentin (VIM) and keratin allowing their stability [187,189]. Even if the UPS is vulnerable to aggregation-prone proteins, together with aggrephagy both pathways are interacting through ubiquitination and p62 and works cooperatively and complementarily[187]. Aggrephagy targets K63-linked polyubiquitinylated proteins aggregates and recruits neighbour of BRCA1 gene (NBR1) and p62 to allow phagophore formation and autophagic degradation of protein substrates after fusion with lysosomes[187,189].

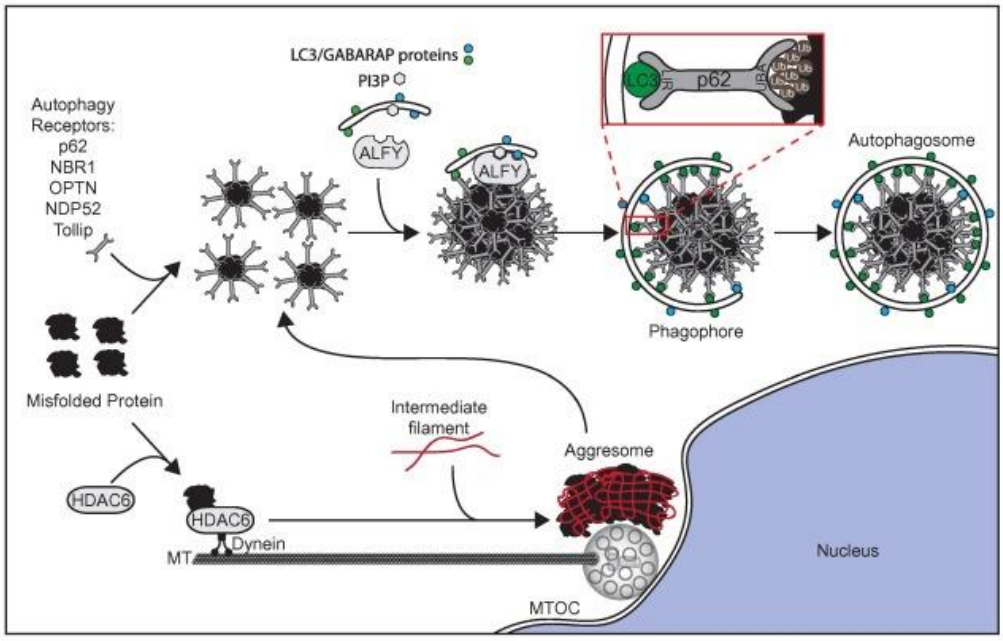

Figure 14: Schematic view of aggrephagy*. Ubiquitin-mediated recognition of the aggregates by autophagy receptors (i.e. p62) and recruitment of the autophagic machinery through LC3B-II binding before being degraded in lysosomes. In parallel, proteins aggregate with the help of HDAC6 in larger structures, aggresomes, located in MTOC.*[190]

II. AIM OF THE MASTER THESIS

In the field of obesity and lipid metabolism, it is more and more accepted that this abnormal lipid overaccumulation in PTECs, called lipotoxicity, triggers injuries and contributes to CKD development[14,191]. Lipotoxicity is a phenotype associated with mitochondrial damages, oxidative stress, ER stress, as well as autophagic alterations in PTECs[63,108]. Besides, preliminary data from our group revealed that PA-induced lipotoxicity mediates lysosomal alkalinisation and loss of degradative function, driving the accumulation of autophagosomes in mPTECs. Although these changes in autophagic flux are increasingly being studied, the type(s) of autophagy which is/are affected by lipotoxicity in mPTECs remain(s) unknown. Consequently, a better understanding of which cellular components are targeted by autophagy under lipotoxic conditions is needed to better identify how lipid stress affect mPTECs.

In this regard, the first aim of this master thesis was **to determine the content of accumulated autophagosomes in a model of lipotoxicity in mPTECs.** PTECs display a high reabsorption capacity through receptor-mediated endocytosis, which thus relies on effective autophagic and lysosomal functions[192]. As the effect of lipotoxicity on mPTECs phenotype is poorly understood, the second aim of this work was **to provide further information on the effects of PA on the physiologic features and the differentiation behaviour of these cells**.

III. MATERIAL AND METHODS

A. Mouse proximal tubular epithelial cell culture

1. Cell isolation

Murine proximal tubular epithelial cells (mPTEC) were isolated from 4- or 6-week old male wild type C57Bl6/J mice. Mice were euthanized by cervix dislocation, nephrectomy was quickly performed after, and kidneys were kept in ice-cold dissection buffered solution (DS). The buffer is composed of Hanks Balanced Salt Solution (HBSS) : 0.35 g/L of $NaHCO_3$, 1.0 g/L of glucose (Gibco, USA), 15 mM of 4-(2-hydroxyethyl)-1-piperazineethanesulfonic acid (HEPES) buffer solution; pH 7.4, 10 mM of D-glucose (Carl Roth, Germany), 5 mM of glycine (Carl Roth, Germany), 1 mM of alanine (Sigma, USA), 5 µM of NaOH (Carl Roth, Germany) and 8.8 mM of mannitol (Carl Roth, Germany). Kidneys were decapsulated and the cortex was separated from the medulla. Cortex was cut into 1 mm^3 pieces and kept in a petri dish (Greiner Bio-one, Germany) containing 7 ml of ice-cold DS during the dissection. The pieces of cortex were then transferred in a glass potter. A volume of 7 mL of 0.01 % collagenase II (Worthington, USA) solution diluted in SoyBean Trypsin Inhibitor (SBTI) (Sigma, USA) solution composed of 0.096 µg SBTI/mL of DS was added to the potter glass. The suspension was incubated at 37°C for 35 min under strong agitation (330 rotation per minute (rpm)) on a rotor plate (Innova™ 400; New Brunswick Scientific™, USA). Then, the suspension was vortexed and filtered on a 250 µm filter (Pierce™ tissue Strainers) (ThermoFisher, USA) to discard non-digested tissue aggregates. The filtrate was transferred on an 80 µm filter (Nylon Net) (MERCK, France) to keep proximal tubules. Tubules were next recovered by reversing the filter and flushing it with 30 mL of warm SBTI solution; pH 7.4, containing 1 % Bovine Serum Albumin (BSA) (Sigma, USA). The cell suspension was then centrifugated at room temperature (RT) for 5 min at 300 g (Centrifuge 5804 R; Eppendorf, Germany). Cell pellet was next resuspended in 13 mL of culture medium. Finally, 2 mL of the cell suspension were added in each well of a 6-well culture plate (Corning Incorporated, USA) previously coated for 30 min with a fibronectin (R&D system, USA) solution (15 µg/mL) diluted in 15 mM of HEPES (Gibco, USA); pH 7.5. Cells were kept in an incubator (HERAcell 240; Heraeus, Germany) at 37°C in a humid atmosphere containing 5 % CO_2.

The seeding medium is made of DMEM/F12 (Dulbecco's Modified Eagles Medium/Nutrient Mixture F12, Gibco, USA) containing 5 % HIFBS (Heat-Inactivated Fetal Bovine Serum) (Gibco, USA), 15 mM of HEPES, 0.55 mM of sodium-pyruvate (Gibco, USA), 1 % of non-essential amino-acids (Gibco, USA) 5 µM of NaOH, a kit Renal Epithelial cells Growth Medium (REGM ™ SingleQuot) containing 50 nM of hydrocortisone, 5 µg/mL of insulin, 5 µg/mL of transferrin, hEGF (human epidermal growth factor), 0.1 % of gentamycin and ampicillin, 5 µg/mL of triiodothyronine, 5 µg/mL of epinephrine. Two days after the cell seeding, the medium was discarded and replaced by another medium with the same composition as the previous one, except that it contained 2.5 % of HIFBS (instead of 5 %). The cell culture media was then changed every other day. mPTECs were used when their confluency reached 100 % at day 7 after seeding or passed when their confluency reached only 80 % at day 5-6.

2. Cell passage

mPTECs cultured in 6-well plates were passed when their confluence reached 80 %. Cells were rinsed with 2 mL/well of sterile Phosphate Buffered Saline (PBS) (Dutscher, France); pH 7.4. A volume of 330 µL/well of trypsin-ethylenediaminetetraacetic acid (EDTA) (Lonza, USA) was added and cells were incubated for a maximum of 10 min at 37°C. When

cells were detached, trypsin was inhibited by the addition of 1 mL/well of cell culture media containing 2.5 % HIFBS. Cells were then collected in a 50 mL falcon tube (Corning Incorporated, USA). The cell suspension was centrifuged for 5 min at 300 g (Centrifuge 5702, Eppendorf, Germany). Cell pellet was resuspended in 25 mL of warm (37°C) DMEM/F12 media containing 2.5 % HIFBS. Finally, 2 mL/well of cell suspension were added in each well of 6-well culture plates previously coated with fibronectin as described above.

B. RT-qPCR

1. Cell treatment

For the analyses of gene expression by RT-qPCR, mPTECs were seeded in 6-well cell culture plates at a density of 40 % with 2 mL/well of DMEM/F12 cell culture media containing 2.5 % HIFBS. When cells reached 100 % confluency, they were incubated for 24 h with 300 µM of PA (Sigma, USA) or 300 µM BSA diluted in fresh and warm (37°C) DMEM/F12 cell culture media containing 2.5 % of HIFBS.

2. RNA extraction

At the end of the different incubations, total RNA was extracted from treated mPTECs with the RNA extraction kit ReliaPrep^{TM} Cell RNA Miniprep System (Promega, USA). Briefly, cultured mPTECs were rinsed once with 1 mL/well of PBS (pH 7.4) and 100 µL/well of lysis buffer containing 20 % of thioglycerol were added. Cells were scratched and lysates were transferred in microtubes (Eppendorf, Germany). A volume corresponding to 35 µL of isopropanol (Merck, France) was added and samples were vortexed. These solutions were then transferred in the ReliaPrep™ Minicolumns.

Total RNA was extracted according to the manufacturer's recommendations. To do so, columns were centrifuged for 30 s at 12 000 g to discard the filtrate. Columns were next rinsed once with 500 µL of RNA Wash Solution (RWA) and centrifuged for 30 s at 12 000g. Then, 30 µL of a solution of DNAse containing 80 % of Yellow Core Buffer, 9 mM of magnesium chloride and 10 % of DNAse were added to the columns and incubated for 15 min. A volume of 200 µL of Column Wash Solution (CWE) was added to each column. Afterwards, the samples were centrifuged for 15 s at 12 000 g and the filtrates were discarded. Then, the columns were rinsed twice with RWA: first with 500 µL followed by a centrifugation of 15 s at 12 000 g, and then with 300 µL followed by a centrifugation of 2 min at 12 000 g. Finally, columns were placed in new microtubes (Eppendorf, Germany) and RNA was eluted with 15 µL of RNAse-free water (ThermoFisher, USA). Samples were centrifuged again for 1 min at 12 000 g and RNA samples were kept on ice. RNA concentrations were assessed by measuring the absorbance at 260 nm with a NanoDrop 1000 Spectrophotometer (ThermoFischer Scientific, United States). In addition, two ratios of absorbance were measured to assess the RNA purity and putative contamination with proteins and/or salts. Ratios of absorbance at 260 nm and 280 nm assess contaminants for proteins while ratios of absorbance at 260 nm and 230 nm evaluate salt contamination. the purity of nucleic acids. Expected 260/230 values ranged generally between 2.0 and 2.2, while a 260/280 ratio at 1.8 and 2.0 are acceptable for DNA and RNA respectively[193]. Finally, samples were stored at -80°C until further analyses.

3. Retro-transcription (RT)

The retro-transcription was performed using the RevertAid H Minus First Strand cDNA Synthesis kit (ThermoFisher, USA) according to the manufacturer's recommendations. Based on results of RNA concentrations, RNA samples were diluted in microtubes with RNAse-free water to reach 3 µg of RNA in 11 µL per condition. Then, 1 µL of random hexamers (0.2 µg/µL) was added in each microtube and samples were heated for 5 min at 65°C in a C1000 Touch Thermal Cycler (BioRad, USA). To do so, a volume of 4 µL of a buffer solution containing 1 µL of ribolock inhibitor at 20 U/µL, 2 µL of dNTPs (10 mM stock solution) and 1 µL of Enzyme RevertAid at 200 Unit/µL was added to each microtube. In parallel, a negative control was prepared, in which the enzyme was replaced by 1 µl of RNAse-free water in an extra sample. Samples were heated for 5 min at 65°C for primer binding. A volume of 180 µL of RNAse-free water was finally added to the cDNA samples.

4. Primers

The primers used in this work are listed in Table 1. Lyophilized primers were resuspended in a volume of RNAse-free water to reach a 100 µM concentration. Primers were next diluted in RNAse-free water to obtain a 2.4 µM concentration and stored at -20°C until RT-qPCR analysis.

5. qPCR

A RT-qPCR was performed by adding 10 µL of Takyon^{TM} ROX SYBRR Master Mix (Eurogentec, Germany)/well in 96-well plates (Eurogentec, Germany), 2.5 µL/well of 2.4 µM forward primer and 2.5 µL/well of 2.4 µM corresponding reverse primer (Table 1). Then, 5 µL of the cDNA sample were added to each well. The 96-well plates were sealed and spun down (Centrifuge PK131R) (ALC, UAE) for a few seconds. The qPCR was performed in a Light Cycler equipment (Carl Roch, Germany) with the following programme: 5 min at 25°C followed by 60 min at 42°C and finally 5 min at 70°C. Results were calculated in fold changes for genes expressed in cells of the experimental condition and the control cells according to the formula ($2^{-\Delta\Delta Ct}$) and normalised for the Ct measured for the value of expression of the β-actin, used as housekeeping/reference gene.

Table 1. Forward and reverse primers used for the qPCR analyses.

FAM134B-2a	Forward	GAAAGAGGGCAGGCTCTAGG
	Reverse	ATGACAGCCCCCTGCTAAAA
SEC62-2	Forward	AGCGGGAACGGGAATGATTT
	Reverse	AGTCCCCCAGCTAGTCAGAT
SEC62-1	Forward	AGCGGGAACGGGAATGATTT
	Reverse	GGGATTTCCTAAGCTCTCCATCT
ATL3-2	Forward	CTCGGTTTCTCCCCAAGTCCA
	Reverse	CATCACCTGCTCCTCTCGATG
CCPG-1	Forward	GAAGCGGCAACTGAAAAGAC
	Reverse	GAACAAACCCTTCTGGTGGA
UFL1	Forward	GTTGACATTTCGCCTCTGCT
	Reverse	TCACCACAACCGTGTCACTA
AQP-1	Forward	CCGAGACTTAGGTGGCTCAG
	Reverse	ATGCGGTCTGTAAAGTCGCT

Cadherin 16	Forward	CCAGCTCCCTCTGAACTCAC
	Reverse	CCCATGGTCATCCCATAAAG
CD44	Forward	GTACGGAGTCAAATACCAACC
	Reverse	CAGCCATCCTGGTGGTTGTC
Cubulin	Forward	TTCCTTCTGGAGTGGTTTGC
	Reverse	CCTGTCACCATATACCCTCCAC
Desmoplakin	Forward	GTGATTCTGCAAGAGGCTGC
	Reverse	GCCAGTCTTAGCTCCTCTTCC
Ebp41L5	Forward	ACGCTGCAAATGAAAGCCAG
	Reverse	GCAAATCAACGCTTAGGGGC
E-cadherin	Forward	GGCTTCAGTTCCGAGGTCTACA
	Reverse	TCCAGAGGCTGTGTCACTTTCA
FoxM1	Forward	AAGGCAAAGACAGGAGAGCT
	Reverse	AGGGCTCCTCAACCTTAACC
Lipocalin-2	Forward	CTACAACCAGTTCGCCATGG
	Reverse	ACACTCACCACCCATTCAGT
Megalin	Forward	TCACCAGTGCCTCTGTGAAG
	Reverse	AGATAATGGAGGCCGCACT
Slc3A1	Forward	ACTCAGGTGGGAATGCATGA
	Reverse	CGGCTTCCTGGATAAATGGC
Slc5A2	Forward	TTGGGCATCACCATGATTTA
	Reverse	GCTCCCAGGTATTTGTCGAA
Sox9	Forward	CAAGAACAAGCCACACGTCA
	Reverse	GTGGTCTTTCTTGTGCTGCA
Vimentin	Forward	AATGCTTCTCTGGCACGTCT
	Reverse	AGTGAGGTCAGGCTTGGAAA
β-actin	Forward	CTAAGGCCAACCGTGAAAAG
	Reverse	ACCAGAGGCATACAGGGACA

C. Western blotting analyses

1. Cell treatment

For the analyses of protein abundance (FAM134B, UFL1 and β-actin) by western blot (WB) done in the attempt to validate proteomic data, mPTEC were seeded at 40 % of density in 6-well culture plates previously coated for 30 min with a fibronectin solution (15 µg/mL) diluted in 15 mM of HEPES; pH 7.5. When cells reached 100 % confluency after X days, they were incubated with 300 µM PA or 300 µM BSA for 24 h with or without 2 nM Bafilomycin A1 (Baf A1) (Sigma, USA) during the last 6 hours of the incubation. Compounds were diluted in warm (37 °C) cell culture media containing 2.5 % HIFBS.

2. Clear cell lysate preparation

Samples were kept on ice during the whole procedure. At the end of the treatment, cell monolayers were rinsed once with 1 mL/well of PBS (pH 7.4). Cells were scratched in 200 µL/well of lysis buffer containing : 20 mM Tris-HCl (pH 7.5), 150 mM NaCl, 1 mM Na_2EDTA (ethylenediaminetetraacetic acid), 1 mM EGTA (ethylene glycol-bis(β-aminoethyl ether)-N,N,N′,N′-tetraacetic acid), 1 % Triton, 2.5 mM sodium pyrophosphate, 1 mM β-

glycerophosphate, 1 mM Na_3VO_4, 1 µg/ml leupeptin) (Cell Signaling Technology, The Netherlands) containing 1 % of Halt Protease and Phosphatase Inhibitor Cocktail (ThermoFisher, USA) diluted in milliQwater. Then, cell lysates were transferred in microtubes and centrifuged (Centrifuge 5415 R; Eppendorf, Germany) for 10 min at 14 000 rpm at 4°C. Supernatants containing proteins were collected and stored at -80°C for further analysis.

3. Protein assay

The protein concentrations of the different samples were determined by BCA (bicinchoninic acid) protein assay (Pierce Chemical, USA). For each protein assay, a standard curve was done by using serial dilutions of a BSA stock solution (2000 µg /mL) to obtain different concentrations: 1000 µg/mL, 500 µg/mL, 250 µg/mL, 125 µg/mL, 67.5 µg/mL and 37.25 µg/mL. Then, 10 µL of each dilution were added (in duplicate) in a 96-well plate (Greiner Bio-One, Germany). For the samples, they were diluted 10 times and 10 µL/well were added to the 96-well plate, also in duplicate. Then, 200 µL of BCA working reagent containing solution A and solution B (1:50) were added. The samples were then incubated for 30 min at 37°C and absorbances were read at 562 nm in a spectrophotometer xMark (BioRad, USA). The protein concentrations were determined based on the equation obtained for the standard curve reporting the absorbance according to the known protein concentration of the standard ($y= ax+b$).

4. Wester blotting using NuPAGE (PolyAcrylamide Gel Electrophoresis).

A quantity of 20 µg of proteins was diluted in milliQwater to reach a volume of 22.5 µL and 7.5 µL of NuPAGE blue loading (ThermoFisher, USA) containing 5 % of dithiothreitol (DTT) (ThermoFisher, USA) were added. Then, samples were warmed 10 min at 70°C. The NuPAGE tank was prepared by adding the 4-12 % Bis-Tris NuPAGE gels (ThermoFisher, USA). In parallel, 800 mL of running buffer solution containing 50 mM of 2-(N-morpholino)-ethanesulfonic acid (MES) (ThermoFisher, USA) diluted in milliQwater were added to the tank. The center part between gels was filled with 200 mL buffer solution containing 0.25 % of antioxidant (NP0005) (ThermoFisher, USA). The first well of the gel was filled with 1 µL of Color Prestained Protein Standard Broad Range (10 – 250 kDa) Ladder (New England Biolabs, USA). A volume of 30 µL of cell lysate proteins was added in the different wells of the gel. Proteins were separated/resolved by a migration of 40 min at 200 volts. Then, proteins in the gels were transferred to a PolyVinylidene DiFluoride (PVDF) membrane (Merck, France) previously activated in 100 % methanol (Sigma, USA) for 1 min. Proteins were transferred for 2 h at 100 volts in a transfer buffer (25 mM Tris, 192 mM glycine; pH 8.3) containing 5 % of methanol diluted in milliQwater. Membranes were next blocked with Intercept TBS (tris buffer saline) Blocking Buffer (Li-Cor Biosciences, USA) for 1 h. Then, membranes were incubated with primary and secondary antibodies (see conditions in Table 2). After each incubation, membranes were rinsed three times for 5 min with Intercept Blocking Buffer TBS. Membranes were then scanned with the Amersham™ Typhoon™ equipment. Intensities of the fluorescence signals were quantified by FiJi-ImageJ processing program and normalized for the intensities obtained for the immunodetection of the β-actin, used as a loading control.

Table 2. Antibodies and conditions used for the WB analyses.

Target/protein of interest	Primary antibodies, dilutions and incubation conditions	Secondary antibodies, dilutions and incubation conditions
FAM134B (65 kDa)	Polyclonal, Rabbit IgG 1:1000, 16 h at 4°C (Sigma, USA)	Goat anti-rabbit 800 1:10 000, 1h at RT (LI-COR, USA)
UFL1 (80 kDa)	Polyclonal, Rabbit IgG 1:1000, 16 h at 4°C (Novus Biological, USA)	
β-actin (42 kDa)	Monoclonal, Mouse 1:5000, 30 min at RT (Cell Signaling Technology, USA)	Goat anti-mouse 700 1:10 000, 1h at RT (LI-COR, USA)

D. Immunofluorescence and confocal observations

1. Cell treatment

Mitophagy: For the visualisation of proteins (OXPHOS, LC3 and LAMP1) by immunofluorescence and confocal microscopy observations, mPTEC were seeded in 24-well plates at 40 % of density on previously coated sterile glass coverslip (VWR, USA) with fibronectin (R&D system, USA). When cells reached 100 % confluency, they were incubated for 24 h with 300 µM PA or 300 µM BSA diluted in pre-warmed (37°C) cell culture media. A positive control was done in which mitochondrial uncoupling was induced by 10 µM of FCCP (2-(N-morpholino)-ethanesulfonic acid, MedChemExpress, USA)[194] diluted in warm cell culture media. Cells were incubated during 24 h and lysosomal acidification was inhibited by adding 1 nM of Baf A1 during the last 6 h of incubation.

Lipophagy: For the visualisation of proteins (PLIN2 (perilipin-2), LC3 and LAMP1) by immunofluorescence, mPTEC were seeded in 24-well plates at 40 % of density on previously coated coverslips with fibronectin. When cells reached 100 % confluency, they were treated for 24 h with 300 µM PA or 300 µM BSA diluted in warm media. A positive control was included and consisted of cells incubated for 24 h with 300 µM of oleic acid (OA), diluted in pre-warmed (37°C) cell culture media along with starvation with HBSS containing 1 nM of Baf A1 for the last 6 h (described in[195]).

Lysophagy: For the visualisation of proteins (GAL3 (galectin-3) and LC3) by immunofluorescence and confocal microscopy observations, mPTEC were seeded in 24-well plates at 40 % of density on previously coated coverslips with fibronectin. When cells reached 100 % confluency, they were treated for 24 h with 300 µM PA or 300 µM BSA diluted in pre-warmed (37°C) cell culture media. A positive control including 1 mM of LLOMe (L-Leucyl-L-Leucine methyl ester hydrobromide, Sigma, USA), diluted in cell culture media was added during last 1 h.

Aggrephagy: For the visualisation of proteins (Ub (ubiquitin), p62 and LAMP1) by immunofluorescence and confocal microscopy observations, mPTEC were seeded in 24-well plates at 40 % of density on previously coated coverslips with fibronectin. When cells reached

100 % confluency, they were incubated for either 6 or 24 h with 300 µM PA or 300 µM BSA diluted in pre-warmed (37°C) cell culture media. A positive control including cells exposed to10 µM of MG132 (N-Benzyloxycarbonyl-L-leucyl-L-leucyl-L-leucinal) and 1 nM of Baf A1 diluted in cell culture media and starvation during the last 6 h of the incubation period.

2. Cell fixation

At the end of the cell treatments, cells were rinsed once with 1 mL of PBS (pH 7.4; 37 °C). For the immunostaining of PLIN2-LC3, OXPHOS-LC3 and GAL3-LC3, cells were fixed for 5 min at 4°C with 1 mL of a solution of 50 % of methanol (Carl Roth, Germany) and 50 % of acetone (Carl Roth, Germany). For immunostaining of PLIN2-LAMP1, OXPHOS-LAMP1, Ub-LAMP1 and Ub-p62, cells were fixed for 10 min at RT with 1 mL of a solution of 4 % PFA (paraformaldehyde) under chemical hood. Cells were then rinsed 3 times with 1 mL of PBS at room temperature.

3. Permeabilization and blocking

For the immunostaining of Ub-p62, an additional step of permeabilization was performed by adding 1 mL of 1 % of Triton-X 100 (Carl Roth, Germany) diluted in PBS during 10 min. Cells were then rinsed three times with 1 mL of PBS at RT.

For the other markers, the blockade and permeabilization were performed by the addition, for 30 min and under a gentle shaking, of 1 mL of PBS containing 15 mM of glycine (Carl Roth, Germany), 0.05 % of saponin (Sigma, USA), 0.5 % of BSA (Carl Roth, Germany) and 50 mM of NH_4Cl (ammonium chloride); pH 7.4.

4. Incubation with primary and secondary antibodies

At the end of the permeabilization and blocking step, cells were rinsed twice with 1 ml of blocking buffer and incubated with 30 µL of primary antibodies (see conditions in Table 3), for 16 h at 4° C. At the end of the incubation, cells were rinsed twice 10 min with the 1 mL of PBS-0.5 % BSA solution under a gentle shaking. Cells were next incubated for 1 h with 30 µL of secondary antibodies (see conditions in Table 3) and 0.05 % of DAPI (4′, 6-diamidino-2-phénylindole) (Sigma, USA), a fluorescent dye for DNA. Then, cells were rinsed three times with 1 mL of the PBS-0.5 % BSA solution, twice with 1 mL of PBS and twice with 1 mL of milliQwater.

Coverslips were mounted on blades by using 8 µL of mounting Fluoromount-G (ThermoFisher, USA), cells were observed with Fixed samples were imaged with a Zeiss LSM 900 confocal laser-scanning microscope equipped with an Airyscan 2 multiplex system (Carl Zeiss, Germany) and 10 micrographs were taken per condition with an average of 10 cells per micrograph.

Table 3. Antibodies and conditions used for the immunofluorescence

Target	Primary antibodies, dilutions and incubation conditions	Secondary antibodies, dilutions and incubation conditions
GAL3	SC-23938, Monoclonal, Rat 1:100 (Santa Cruz, USA), 16h at 4°C	A-11077 Goat anti-rat AlexaFluor 568 (ThermoFisher, USA); 1:400, 1h at RT
LAMP1	1D4B-c, Monoclonal, Rat 1:100 (DSHB, USA), 16 h at 4°C	A-11006 Goat anti-rat AlexaFluor 488 (ThermoFisher, USA); 1:400, 1h at RT
LC3	L7543-200, Polyclonal, Rabbit 1:100 (Sigma, USA), 16 h at 4°C	A-11008 Goat anti-rabbit AlexaFluor 488 (ThermoFisher, USA); 1:400, 1 h at RT
OXPHOS	AB110413, Antibody cocktail, Mouse 1/200 (Abcam, UK) 16h at 4°C	A-11031 Goat anti-mouse AlexaFluor 568 (ThermoFisher, USA), 1/400, 1 h at RT
PLIN2	GP40, Polyclonal, Guinea pig 1:100 (Progen, Germany), 16 h at 4°C	A-11075 Goat anti-guinea pig AlexaFluor 568 (ThermoFisher, USA); 1:400, 1 h at RT
p62	D1Q5S, Rabbit 1:100 (Cell Signaling, USA), 16h at 4°C	A-11008 Goat anti-rabbit AlexaFluor 488 (ThermoFisher, USA), 1:400, 1h at RT
Ub	SC-166553, Monoclonal, Mouse 1:100 (Santa Cruz, USA), 16 h at 4°C	A-11031 Goat anti-mouse AlexaFluor 568 (ThermoFisher, USA), 1:400, 1h at RT

5. Quantifications

The percentages of colocalization between cell component or organelles and autophagosomes or lysosomes were calculated with the plugin JACoP of ImageJ using Manders' colocalization coefficients (MCC) M1 and M2. Manders' coefficients are used to

quantify the co-occurrence of colocalization between two stainings, meaning the fraction of pixels with positive values for both stainings. This method allows an intuitive and direct measure of co-occurrence independent of fluorescent signal proportionality and independent to the number of structures labelled by each probe[196]. Percentages of colocalization were determined on at least 10 micrographs containing an average of 10 cells per condition in 3 biological replicates (*n=3*), thus an equivalent of 100 cells. Data are expressed as the fraction of cellular component or organelle colocalizing with autophagosomes or lysosomes.

Number and size of positive spots for the staining were determined using the analyse of particles of ImageJ software on at least 10 micrographs containing an average of 10 cells per condition, in at least 3 biological replicates (*n=3-6*). A threshold of 0.1 mm² in size was applied for GAL3 staining while a threshold of 0.5 mm² was applied for Ub staining. Results are expressed as the number or the size (µm²) of positive stained structure per cell.

E. BSA-uptake assay

1. Cell treatment

For the visualisation of protein reabsorption in mPTEC by immunofluorescence and confocal observations, mPTEC were seeded in 24-well plates at 40 % of density on previously coated coverslips with fibronectin. When cells reached 100 % confluency, they were incubated for 24 h with 300 µM PA or 300 µM BSA with or without 2 nM Baf A1 diluted in pre-warmed cell culture media (37°C). After 23 h of treatment, cells were rinsed once with 1 mL of prewarmed sterile PBS and incubated for 1 h with 500 µL of BSA conjugated Alexa fluor™ 488 probe (ThermoFisher, USA) diluted in pre-warmed cell culture media. Nuclei were stained during last 5 min by the addition of 1 droplet of NucBlue™ Live Cell Stain ReadyProbes™ (ThermoFisher, USA).

2. Fixation

At the end of the cell treatments, cells were rinsed once with 1 mL of PBS (pH 7.4; 37 °C). Cells were fixed 10 min at room temperature with 1 mL of a solution of 4 % PFA under a chemical hood. Cells were then rinsed 3 times with 1 mL of PBS at room temperature.

3. Blade mounting

Coverslips were mounted on blades by using 8 µL of mounting Fluoromount-G (ThermoFisher, USA) and cells were analysed with a confocal microscope (Leica SP5, USA) and 10 micrographs were taken per condition with an average of 40 cells per micrograph. The intensity of fluorescence of the BSA-conjugated probe was quantified using the software ImageJ on an average of 400 cells per condition.

F. Statistical analyses

Graphs and statistical analyses were performed with Graphpad PRISM software. Results are presented as means ± Standard Error of the Mean (SEM), *n=3-4*. Statistically significant differences between groups were assessed by an unpaired Student's t-test for qPCR analyses and analyses in microscopy, a one-way analysis of variance (ANOVA) followed by Dunnett's post-hoc test for colocalization studies by immunofluorescence and a two-way ANOVA followed by a Tukey post-hoc test for western blot analyses and BSA-uptake assay. A *p*-value of 0.05 or lower was considered as statistically significant.

IV. RESULTS

A. Preliminary data of our group paving the biological questions of the Master thesis.

Primary culture of PTECs recapitulate PT cellular features. These cells form a monolayer of polarized epithelial cells with microvilli, basolateral invaginations and apical tight junctions when plated on collagen-coated membranes. In addition, primary culture of mPTECs shows that these cells express PT-specific proteins, brush border enzymes, endosomal and lysosomal proteins, as well as receptor-mediated endocytosis proteins such as megalin and cubilin. Besides, they display of a well-developed endocytic pathway and lysosomal system. They also have characteristics of a leaky proximal tubule epithelium with a high Na^+ transport rate. This evidence confirms the value of using primary cultures of mPTECs compared to immortalised mPTECs, which fail to recapitulate these characteristics, to study the impact of FA-mediated lipotoxicity on PTECs[75,192].

Our group previously showed that the autophagic pathway/flux could be altered in proximal tubules of obese mice[103,197]. Indeed, a strong accumulation of enlarged LAMP1-positive multivesicular inclusions (MLI), as well as the accumulation of autophagosome markers such as LC3 and p62 were observed in proximal tubules of mice model of obesity-induced CKD exposed to SFAs[103,197]. To further study autophagy in cells exposed to SFAs, we used a model of primary mPTECs in which lipotoxicity is induced by PA.

To assess the dysfunction of lysosomes and potentially a change in the pH of the organelle, during the PhD thesis of Louise Pierre, these cells were first transduced with baculovirus containing an expression of a chimeric construct encoding LC3 in reading frame with a pH-sensitive GFP and pH-insensitive RFP. Thus, the fluorescence related to undegraded autophagosomes appears "yellow" (GFP^+/RFP^+) while the fluorescence associated with autophagosomes fused to lysosomes appears "red" resulting from acidic pH (GFP^-/RFP^+)[198] (Figure 15A). In certain conditions, Baf A1 was used as a positive control as it is a specific inhibitor of the V-type H^+-ATPase and thus impairs the lysosomal degradation[199–201]. Micrographs and quantifications showed no change in the number of GFP^-/RFP^+ puncta representative of acidic compartment at 6 h or 24 h (Figure 15B and 15C). However, there was a significant increase in GFP^+/RFP^+ LC3 puncta number in cells treated with Baf A1, PA, as well as PA and Baf A1 when compared to control cells, both after 6 and 24 h (Figure 15B and 15D), suggesting non-degraded autophagosomes at neutral pH. These results show that PA-induced lipotoxicity leads to an accumulation of non-degraded autophagosomes in mPTECs already from 6 h of incubation. Beside the pH, colocalization studies revealed that the accumulating autophagosome in cells exposed to PA were positive for lysosomal markers (data not shown). Our group thus further looked the effect of PA on lysosomal function.

LysoSensor Yellow/Blue DND-160 is a dual-wavelength fluorophore used to sense pH in acidic organelles such as, but not exclusively, lysosomes[198]. A yellow fluorescence signal is representative of acidic lysosomes while blue signal represents lysosomes at neutral pH, with impaired hydrolytic enzyme activities[202]. In mPTECs treated with PA, Baf A1 or both, we could observe an increase in the blue/yellow ratio when compared to control cells. An increase in the ratio was observed in mPTECs treated for either 6 or 24 h with PA when compared to control cells (Figure 15E). These results indicate that the acidification of lysosomes is impaired in mPTECs exposed to PA. Finally, results generated by proteomic analyses suggested that genes encoding two ER-phagy markers, FAM134B and UFL-1, could be upregulated in mPTECs

treated with PA for 24 h when compared to BSA-treated cells (Figure 15F). FAM143B is a transmembrane adaptor involved in ER membranes degradation and recycling[168,170,171]. UFL1 is an actor of UFMylation, a post-translational modification acting as an activator signal for ER-phagy[182,184,186].

Based on these results that clearly indicate that undegraded autophagosomes accumulate in PA-treated cells, we wanted to characterize the content of these undegraded autophagosomes by analysing, successively, five (but mainly four) selective autophagic pathways: ER-phagy, lipophagy, mitophagy, lysophagy and aggrephagy.

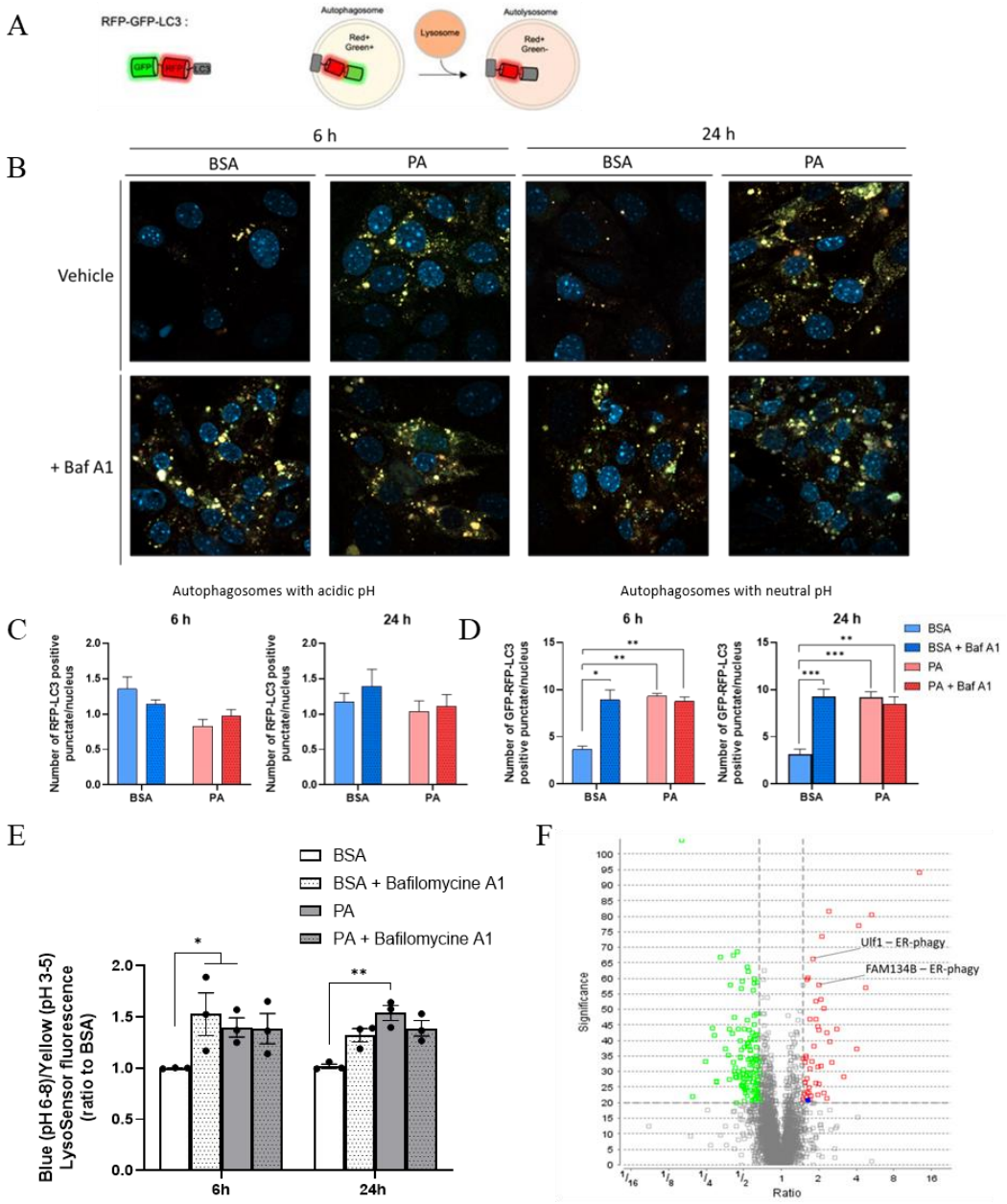

Figure 15. Data showing the effect of PA on the autophagic pathway in mPTECs. *(A) Schematic representation of the fluorescence associated with the expression of GFP-RFP-LC3 construct in autophagosomes and autolysosomes. (B) Representative micrographs and (C) quantifications of LC3-related autophagosomes at acidic pH and (D) neutral pH in mPTECs transduced with GFP-RFP-LC3 tandem system and treated with 300 µM PA (or 0.4 % BSA for control cells) during 6 or 24 h in the presence or the absence of 2 nM bafilomycin A1 added during the last 6 h. Quantifications were performed on at least 10 micrographs corresponding to 100 cells per condition. Data are presented as means ± SEM for 3 independent biological experiments (n=3) in each condition. Statistical analyses were performed by a two-way ANOVA followed by Tukey post-hoc test. * $p \leq 0.05$, ** $p \leq 0.01$, *** $p \leq 0.001$. (E) Quantification of ratio between lysosomes at neutral pH (blue) and acidic pH (yellow) in mPTECs treated with 300 µM PA or 0.4 % BSA during 6 or 24 h with or without 2 nM bafilomycin A1 added during the last 6 h. Data are presented as means ± SEM for 3 independent biological experiments (n=3) in each condition. Statistical analyses were performed by a two-way ANOVA followed by Tukey post-hoc test. * $p \leq 0.05$, ** $p \leq 0.01$. (F) Label-free quantitative analysis performed using PEAKS software in mPTECs treated with 300 µM PA or 0.4 % BSA for 24 h (n=4). BSA = Bovine Serum Albumin, PA = palmitate, Baf A1 = Bafilomycin A1.*

B. Effect of PA protein and/or mRNA abundance of ER-phagy markers

As mentioned, mass spectrometry (MS) analyses show that a 24 h-PA treatment could increase the abundance of the ER-phagy mediators FAM134B and UFL1 (Figure 15F). Based on this finding, we hypothesized that the content of PA-induced autophagosomes in mPTECs may contain ER fragments, a process named ER-phagy.

Proteomic and mass spectrometry analyses are known to generate some false positive, especially when the p-value is not adjusted, therefore we needed to confirm the MS results. The relative abundance of *RETREG1* and *UFL1* mRNA was thus analysed in mPTECs incubated either with 300 µM PA or 0.4 % BSA during 24 h (Figure 16A and 16D). These data showed no statistically significant difference in the abundance of the transcripts of these two genes between PA-treated cells and BSA-incubated control cells. While several regulation levels do exist to control gene expression between a mRNA and its corresponding protein, we next assessed their protein abundance by WB in samples prepared from mPTECs incubated with either PA or BSA in the presence or in the absence of 2 nM Baf A1 (Figure 16B and 16E) for 6 or 24 h. Quantifications showed no statistically significant difference in the abundance protein for FAM134B or ULF1 between PA-incubated and BSA-incubated mPTECs (Figure 16).

However, the engulfment of ER fragments in autophagosomes during ER-phagy requires other molecular actors and is known to be mediated and involve adaptors such as ATL-3, SEC62 or CCPG1. These adaptors mediate ER tubules fragmentation, budding and delivery to autophagy-lysosome machinery under cellular stresses[170,171,173].

Therefore, we extended our study to other markers than those identified by MS. To do so, we assessed the putative effects of PA on the relative mRNA abundance of *ATL-3*, *CCPG1* and *SEC62*. The RT-qPCR analyses performed on RNA isolated from mPTECs incubated for 24 h with either 300 µM PA or 0.4 % BSA showed no statistically significant changes in the abundance of these markers between cells incubated with PA and control cells (Figure16G).

Based on these results and the difficulties encountered in ER labelling (high background, nuclear staining and atypical labelling for ER structures in mPTECs) for the colocalization study, we did not pursue the study of ER-phagy.

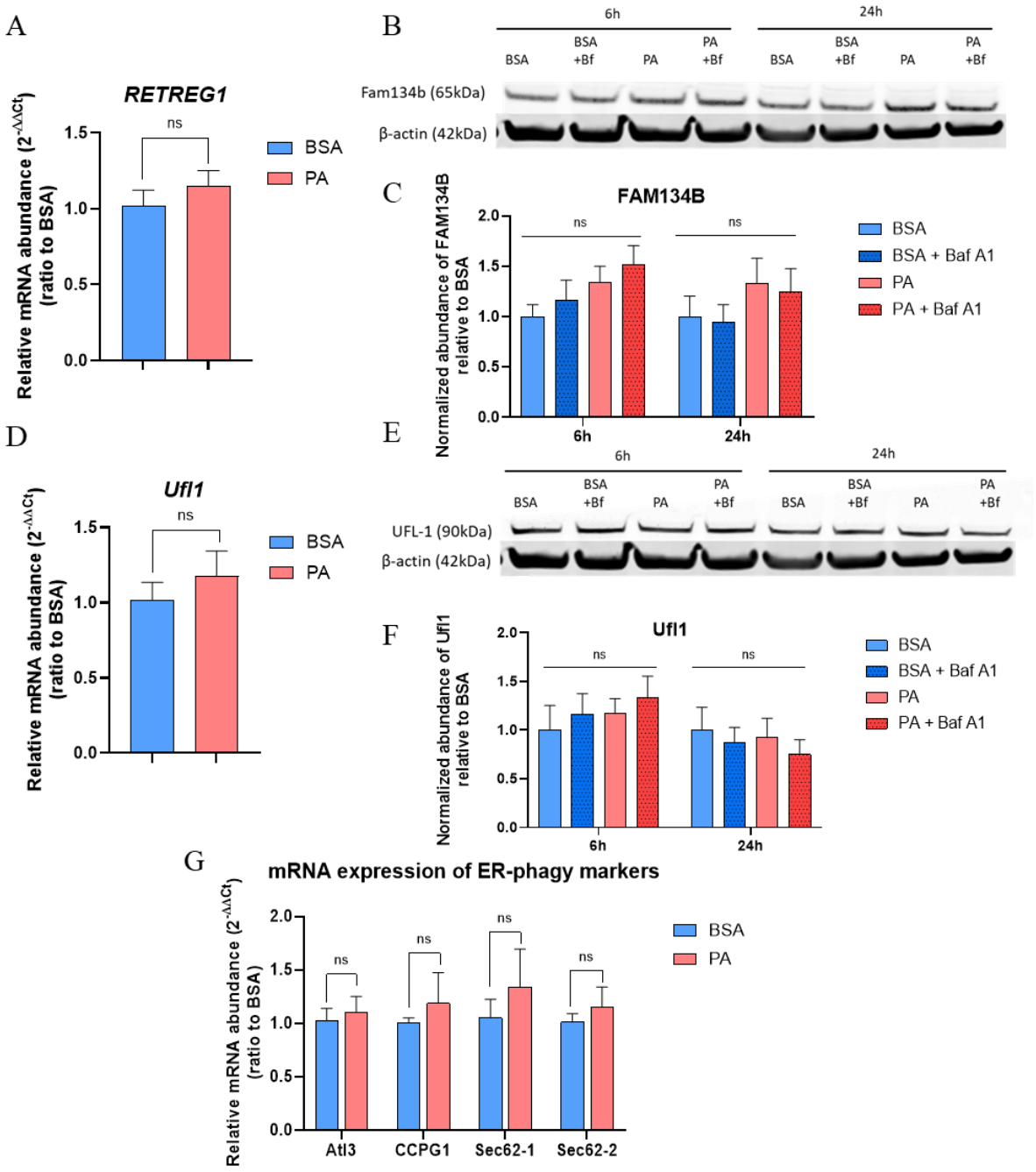

Figure 16. Effect of PA on the expression and the abundance of ER-phagy markers in mPTECs. *(A) qPCR analysis of FAM134B, (D) UFL-1 or (G) ATL3, CCPG1, SEC62-1 and SEC62-2, and β-actin in mPTEC treated with 300 µM PA (or 0.4 % BSA for control cells) during 24 h, n=4. Data are presented as means ± SEM for four independent biological experiments (n=4) in each condition. Statistical analyses were performed by an unpaired t-test. Western blot analysis and quantification of the protein abundance of (B and C) FAM134B or (E and F) Ufl1 and β-actin in mPTECs incubated with either 300 µM PA or 0.4 % BSA (control cells) for 24 h supplemented or not with 2 nM bafilomycin A1 for the last 6 h. Data are presented as means ± SEM, n=4 in each condition. Statistical analyses were performed by a two-way ANOVA followed by Tukey post-hoc test. n.s.: non statistically significant. BSA = Bovine Serum Albumin, PA = Palmitate, Baf A1 = Bafilomycin A1.*

C. Effect of PA on the colocalization between LDlets (LDs) and autophagosomes or lysosomes

Lipophagy is a process by which intracellular LDs are degraded and simple components recycled through autophagy[141,203,204]. It has been reported to be impaired in condition of lipotoxicity in hepatic cells[205]. In order to assess whether autophagosomes accumulating in cells exposed to a PA-treatment contain lipids, we studied the colocalization between PLIN2 and LC3 (a marker of autophagosomes) or LAMP1 (a marker of lysosomes) proteins in mPTECs incubated for 24 h with PA. PLIN2 is a member of the perilipin family which tightly interacts with LDs through its binding with the phospholipid membrane surrounding LDs[206,207]. A positive control was also used and consisted of cells incubated with 300 µM OA for 24 h and exposed to starvation and 2 nM Baf A1 for the last 6 h. These experimental conditions are known to induce LD formation and promote lipophagy[141,208,209].

Micrographs of cells immunostained in fluorescence for PLIN2 and LC3 or LAMP1 and observed by confocal microscopy revealed a clear accumulation of green-fluorescence signal for LC3 in PA-treated cells as well as in the positive control cells, indicating an accumulation of autophagosomes (Figure 17A). In addition, PA-treated cells displayed an accumulation of small red puncta corresponding to the immunostaining of PLIN2, while cells treated with OA revealed a strong accumulation of even larger red-structures, representing LDs. However, quantifications made using Manders' colocalization coefficients (MCC) showed no statistically significant increase in the percentages of colocalization between the marker of LDs and the autophagosome marker, no matter what the experimental condition analysed (Figure 17B).

We next assessed the colocalization between LDs and lysosomes in cells treated with BSA, PA for 24 h or with OA for the same amount of time in the presence of 2 nM of Baf A1 for the last 6 h. Micrographs presented in Figure 17C showed red fluorescence signals for PLIN2 and green fluorescence signal for LAMP1 in cells incubated in these conditions (Figure 17C). After quantification using MCC, data showed no statistically significant increase in the percentage of colocalization between PLIN2 and LAMP-1 in PA-treated cells for 24 h when compared to cells incubated with BSA (Figure 17D). As already mentioned, OA is known to trigger LD accumulation in renal epithelial cells and liver cells[63,208]. However, while the colocalization was also slightly increased in cells exposed to OA and then starved for 6 h in the presence of Baf A1, the difference was not statistically significant in our experimental conditions.

These results indicate that PA do not trigger increase in the colocalization between LD and lysosomes. However, as colocalization between LD and LC3 is not modified in PA-treated cells when compared to BSA-treated cells, we cannot conclude (neither than rule out) that the autophagosomes in PA-treated cells contain lipids.

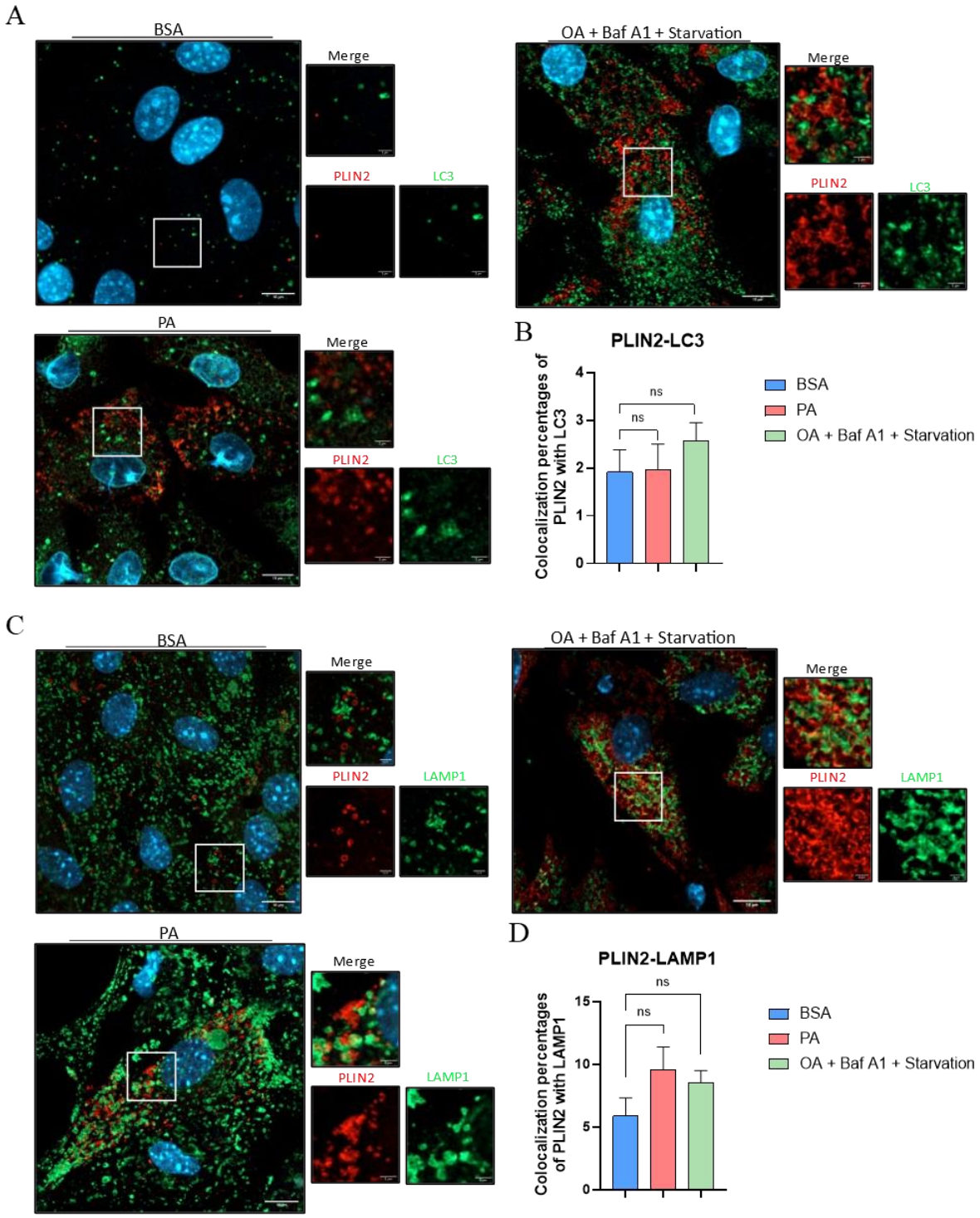

Figure 17. Effect of PA on LD colocalization with autophagosomes or lysosomes in mPTECs. *Representative micrographs of mPTECs incubated with 300 µM PA (or 0.4 % BSA for control cells) during 24 h or treated with 300 µM OA for 24 h and starved in the presence of 2 nM bafilomycin A1 for the last 6 h. Cells were fixed and immunostained for PLIN2 (a marker for LDs) and (A) LC3 or (C) LAMP1. Quantifications of colocalization percentages between PLIN2 and (B) LC3 or (D) LAMP1 in mPTECs. Quantifications were performed on at least 100 cells per condition using Manders overlap coefficients. Data are presented as means ± SEM for 3 independent biological experiments (n=3). Statistical analyses were performed by a one-way ANOVA followed by a Dunnett's post-hoc test: n.s. : non statistically significant. BSA = Bovine Serum Albumin, PA = Palmitate, OA = Oleic Acid, Baf A1 = Bafilomycin A1.*

D. Effect of PA on the colocalization between mitochondria and autophagosomes or lysosomes

Then, we continued to investigate the content of accumulated autophagosomes in mPTECs accumulating LDs by assessing the effect of PA on the putative selective degradation of mitochondria by mitophagy. Indeed, the excess of PA was reported to impair/decrease the mitochondrial membrane potential in induced-renal epithelial cells, which is a strong mitophagy signal[108]. The decrease in the mitochondrial membrane potential could be caused by electron leakage, increased mitochondrial ROS production associated with oxidative stress and respiratory chain defect[108,210].

To do so, we analysed the colocalization between OXPHOS proteins and LC3 in cells treated with BSA (control cells), 300 µM PA during 24 h or 10 µM FCCP (carbonyl cyanide-p-trifluoromethoxyphenylhydrazone) for 24 h and 2 nM Baf A1 added during the last 6 h (a condition used as a positive control). FCCP is an ionophore that acts as a mitochondrial uncoupling agent leading to the uncoupling of the oxidative phosphorylation and mitochondrial depolarization[194,211] leading to the sequestration of mitochondrial fragments in autophagosomes by mitophagy[148,194]. The addition of Baf A1 again, is used to prevent the degradation of autophagosomes[199,200].

At the end of the incubations, cells were then immunostained for LC3 and OXPHOS proteins and observed with a confocal microscope (Figure 18A). One could observe on the micrographs the accumulation of LC3 green-fluorescence signal in cells incubated with FCCP and Baf A1 while it was only observed in very few PA-treated cells. In addition, cells incubated with FCCP and Baf A1 displayed a partial fragmentation of mitochondrial network, while mitochondrial morphology appeared unchanged in PA-treated cells (Figure 18A). As expected, we observed a significant increase in the colocalization between mitochondria and autophagosomes in the cells exposed to FCCP in the presence of Baf A1 when compared to control cells while the colocalization between OXPHOS and LC3 was not significantly changed between BSA-treated control cells and PA-incubated cells (Figure 18B).

We next assessed the colocalization between mitochondria (using the immunostaining of OXPHOS proteins) and lysosomes (assessed by the immunostaining for LAMP1 lysosomal marker) in cells exposed to the different experimental conditions (Figure 18C). Results showed an increase in the percentages of colocalization between OXPHOS and LAMP1 in positive control cells when compared to BSA-treated cells (Figure 18D)[194]. However, no statistically significant change in the colocalization between these markers was observed in cells treated with PA when compared to BSA-incubated control cells (Figure 18D).

These data illustrate that colocalizations between mitochondria and autophagosomes or lysosomes are well increased in the positive controls but not in PA-treated cells. We can thus reasonably rule out the possibility that autophagosomes contain more mitochondria components in PA-incubated cells. These results suggest that mitophagy is not activated in PA-treated cells. Although PA disrupts mitochondrial membrane potential and ROS production in PTCs[108], our group showed contradictory results. PA-induced lipotoxicity does not impair oxygen consumption rates (OCRs), suggesting no alteration of FAO in mPTECs which could explain the absence of mitophagy.

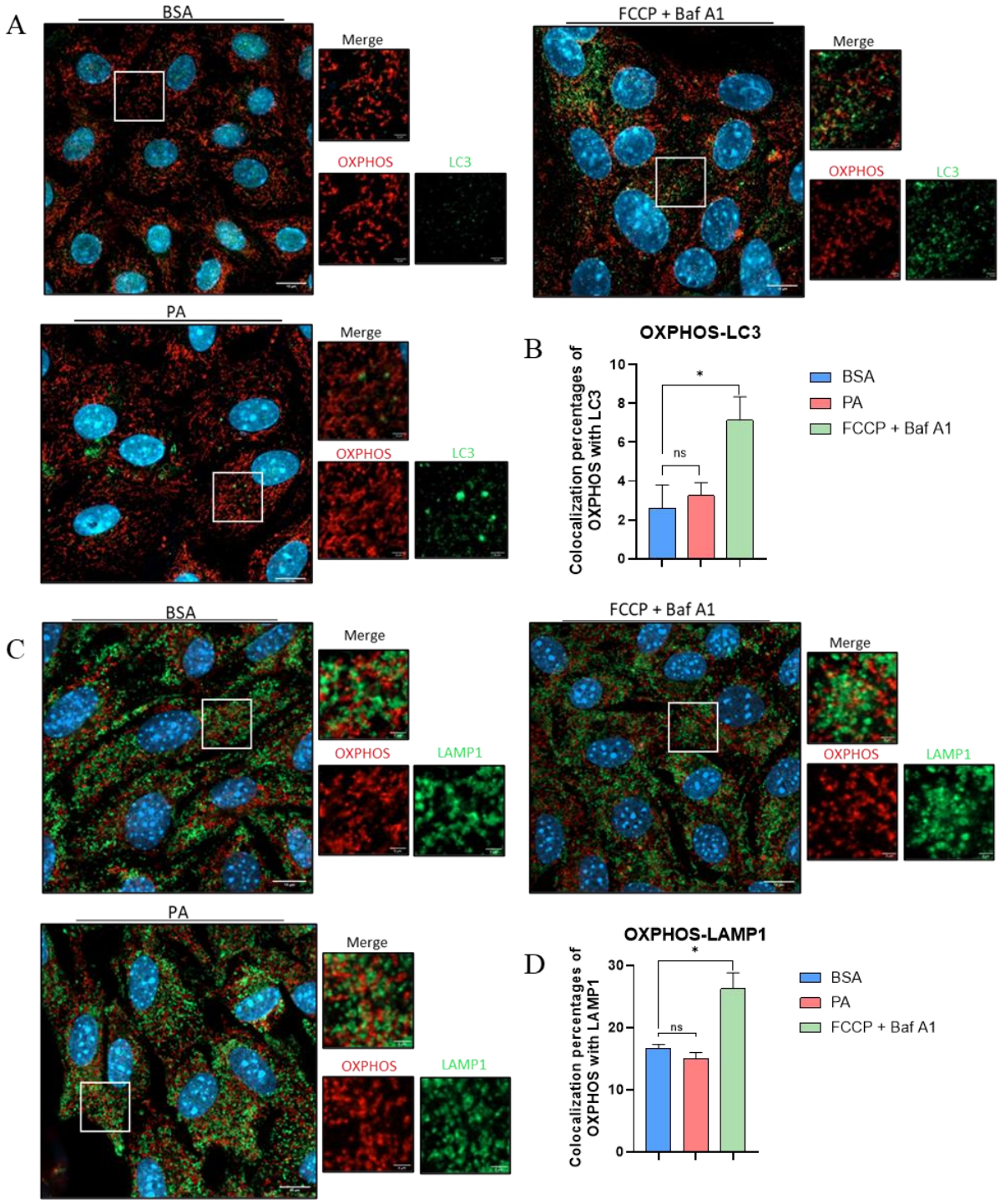

Figure 18. Effect of PA on mitochondria colocalization with autophagosomes or lysosomes in mPTECs. *Representative micrographs of mPTECs treated with 300 µM PA (or 0.4 % BSA for control cells) during 24 h or treated with 10 µM FCCP for 24 h in the presence of 2 nM bafilomycin A1 for the last 6 h. Cells were fixed and immunostained for OXPHOS proteins and (A) LC3 or (B) LAMP1. Quantifications of colocalization percentages between OXPHOS and (B) LC3 and (D) LAMP1 in mPTECs. Quantifications were performed on at least 100 cells per condition using Manders overlap coefficients. These data are presented as means ± SEM for 3 independent biological experiments (n=3). Statistical analyses were performed by a one-way ANOVA followed by a Dunnett's post-hoc test: * $p \leq 0.05$, n.s. : non statistically significant. BSA = Bovine Serum Albumin, PA = Palmitate, FCCP =carbonyl cyanide-p-trifluoromethoxyphenylhydrazone , Baf A1 = Bafilomycin A1.*

E. Effect of PA on lysosomal membrane integrity and colocalization between lysosomal markers and autophagosomes

Damaged lysosomes, meaning LMP and/or rupture, can be the target of a specific recycling pathway named lysophagy[159]. Previous results from our group showed an increase in the lysosomal mass/surface area in the cells exposed to PA, the increase expression of TFEB target genes belonging to the CLEAR (coordinated lysosomal expression and regulation) set of genes, among which several related to the biogenesis of the lysosomes (Louise Pierre, PhD thesis) and the loss of lysosomal acidification in cells treated with PA (Figure 15E). We thus hypothesised that altered lysosomes in mPTECs facing PA accumulation could be targeted to lysophagy.

We thus tested whether PA could induce a change in the lysosomal membrane permeability and lysophagy in PA-incubated cells or not. To do so, we used a monoclonal IgG antibody raised against Gal3 (galectin-3), a β-galactoside-binding cytosolic lectin that unifies and coordinates ESCRT (endosomal sorting complex required for transport) and autophagy responses to lysosomal damage used as a biomarker of damaged lysosomes[159]. Upon LMP with LLOMe (L-Leucyl-L-Leucine methyl ester hydrobromide), a dipeptide condensation product of L-leucine known to induces release of lysosomal proteases and translocation of lysosomal membrane proteins to the cytosol, for instance, intraluminal glycans and glycoconjugates are exposed to cytosol and recognized by Gal3 with a high affinity[159,161,212]. The lysotropic agent is rapidly endocytosed and converted to a toxic metabolite associated with membrane rupture in lysosomes. Once Gal3 recognized ruptured lysosomal membranes, it triggers the recruitment of core autophagy effectors and, thus lysophagy[212]. As a positive control to assess lysophagy, we thus incubated cells with 1 mM LLOMe for 1 h.

Cells were thus incubated 24 h with 300 µM of PA or 0.4 % BSA or 1 mM LLOMe for the last hour of treatment, immunostained for Gal3 and observed with a confocal laser-scanning microscope (Figure 19A). The micrographs showed the red fluorescence signal for Gal3 representative of damaged lysosomes and the green-fluorescence signal for LC3 autophagosome marker. Cells treated with LLOMe presented a strong accumulation of Gal3-positive red spots as well as an accumulation of LC3-positive fluorescent signal suggesting the accumulation of autophagosomes (Figure 19A). We also observed an increase in Gal3-positive signal (indicator of lysosomes with altered membrane permeability) in PA-treated cells (Figure 19A), the number of Gal3-positive puncta observed in PA-treated mPTECs after 24 h was significantly different than the quantification obtained for the BSA-control cells (Figure 19B). The number of Gal3 puncta was more than doubled in PA-treated cells when compared to control cells.

In addition, there was a statistically significant increase in the colocalization between the Gal3-positive damaged lysosomes and autophagosome marker in LLOMe-treated cells (Figure 19C), as observed in literature[159,212]. However, the increase in colocalization was not observed for PA-treated cells (Figure 19C).

Taken together, these results suggest that the accumulation of PA in mPTECs leads to the impairment of lysosomal membrane integrity as evidenced by a higher number of Gal3

puncta. However, we did not find that PA induces a colocalization between GAL3-positive damaged lysosomes and the autophagosome marker while both fluorescence signals colocalise in mPTECs incubated with the lysotropic peptide used as a positive control.

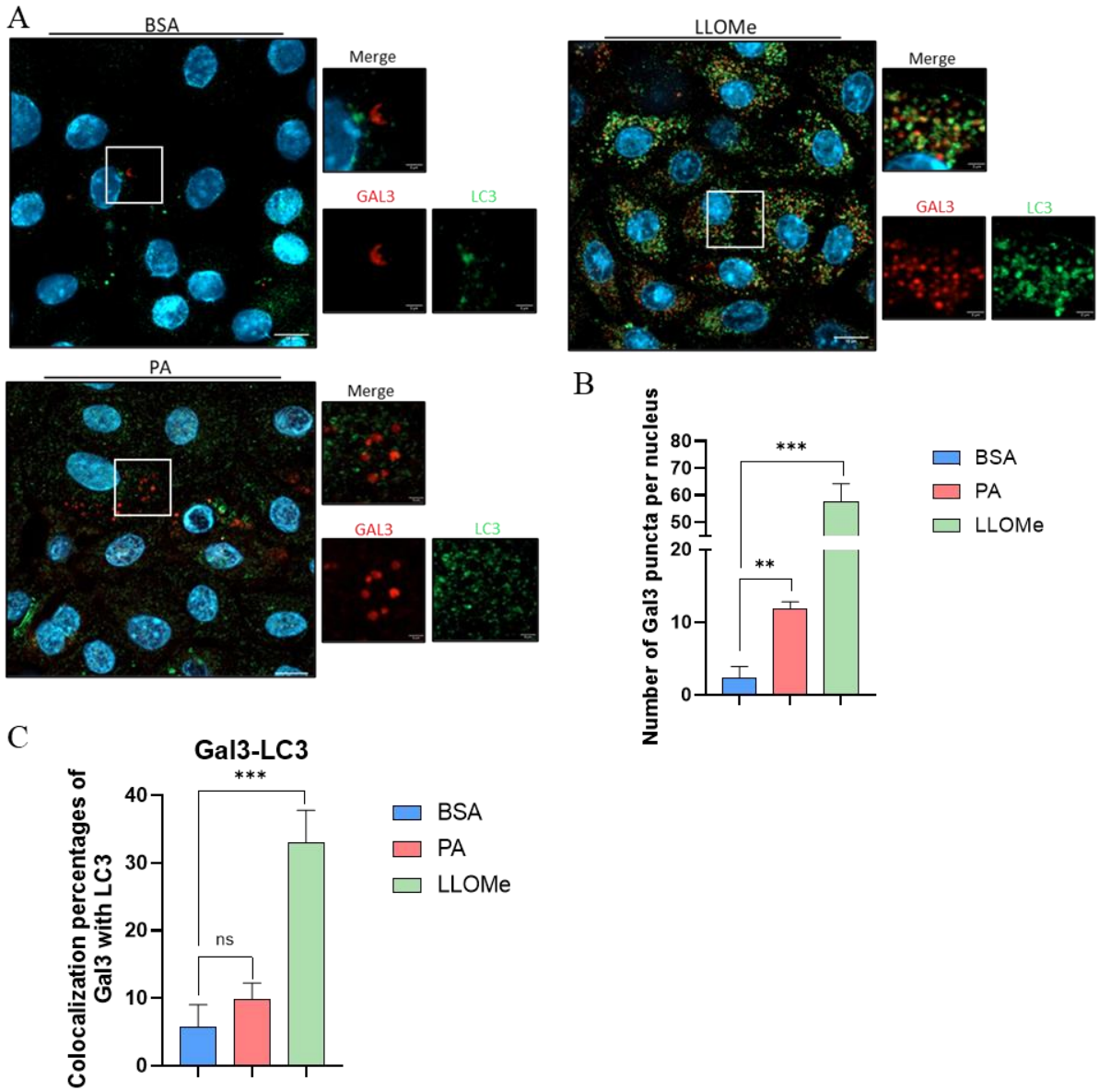

Figure 19. Effect of PA on lysosomes and colocalization with autophagosomes in mPTECs*. (A) Representative micrographs of mPTECs incubated with 300 µM PA (or 0.4 % BSA for control cells) during 24 h or treated with 1 mM LLOMe for the last hour. At the end of the incubations, cells were fixed and immunostained for Gal3 and LC3. (B) Quantifications of Gal3-positive fluorescent spots in mPTECs incubated with 300 µM PA, 0.4 % BSA during 24 h or treated with 1 mM LLOMe for 1 h. Quantifications are performed on at least 100 cells per condition using ImageJ analyze of particles. (C) Quantifications of colocalization percentages between Gal3 and LC3 in mPTECs. Quantifications were performed on at least 100 cells per condition using Manders overlap coefficients. Data are presented as means ± SEM for 3 independent biological experiments (n=3). Statistical analyses were performed by a one-way ANOVA followed by a Dunnett's post-hoc test: * $p \leq 0.05$, ** $p \leq 0.01$, n.s. : non statistically significant. BSA = Bovine Serum Albumin, PA = Palmitate, LLOMe = L-Leucyl-L-Leucine methyl ester hydrobromide.*

F. Effect of PA on protein aggregates accumulation and colocalization with autophagosomes at 6 and 24 h

As mentioned in the introduction (see section Introduction C.3.), ER stress is one of the mechanisms by which PA induces lipotoxicity along with oxidative stress, autophagic flux alterations and lysosomal dysfunction [63,108,188,213]. It has been demonstrated that saturated FAs such as PA generate ROS and alter ER membrane fluidity leading to ER stress and generation of misfolded or unfolded proteins as a result of oxidized molecules[63,108,188,213]. It is known that the inhibition of autophagic flux causes an accumulation of p62- and Ub-positive protein aggregates in kidney of mice fed with a HFD[108] and in cultured hepatocytes incubated with PA[213]. Taken together, this led us to investigate the putative effect of PA on the selective degradation pathway of protein aggregates in aggresomes, called "aggrephagy". For this purpose, colocalization percentages between protein aggregates (assessed by polyubiquitinylated proteins) and autophagosomes were calculated in mPTECs treated with 300 µM PA (or 0.4 % BSA for control cells) for 6 and 24 h and in mPTECs treated with 10 µM MG132 in the presence of 2 nM Baf A1 and starved during the last 6 h. MG132 was used as a positive control because this peptide-aldehyde is a proteasome inhibitor leading to the accumulation of misfolded or unfolded polyubiquitinylated proteins[214,215] (Figure 20).

Micrographs showed an accumulation of red spots representative of Ub-tagged protein aggregates in cells treated with PA for 6 h (Figure 20A) or 24 h (Figure 21A). We characterized the accumulation of protein aggregates by quantifying their number and measuring their size. To do so, protein aggregates were counted by using the software ImageJ and applying a threshold of 0.5 µm diameter above which all spots were scored[216–218]. The quantifications revealed a significant accumulation of Ub-positive structures in PA-incubated mPTECs as well as in positive control cells exposed to MG132-Baf A1 and starved either for 6 (Figure 20B) or 24 h (Figure 21B). Quantifications revealed a significant increase in the size of Ub aggregates) in cells incubated for 24 h (Figure 21C) with PA when compared to BSA-incubated control cells. These results confirm that PA triggers an accumulation of protein aggregates in mPTECs after 24 h. This accumulation of protein aggregates tagged with Ub was confirmed by western blotting analysis in mPTECs treated with PA for 24 h (Figure 21E, 21F). These results indicate that cell response to PA exposure is rapidly associated with mis- and/or unfolded proteins that cannot be degraded and thus accumulate in cells.

In addition, micrographs showed the colocalization between Ub-positive protein aggregates stained in red and the autophagosome marker p62 stained in green. In addition, PA-treated cells presented an accumulation of p62-green spots, some of which, did colocalize with Ub. These colocalization events were also observed in positive control mPTECs treated with MG132 while in control cells, only a few Ub-positive red spots were visible and none of them did colocalize with p62 (Figure 20A, 21A). Quantifications of these events confirmed the statistically significant increase in the colocalization between Ub-positive structures and autophagosomes in cells incubated for 6 h with PA or in positive control cells when compared to control cells exposed to BSA (Figure 20C). This was also confirmed by quantifications showing a significant increase in colocalization between protein aggregates and autophagosomes in both PA- and MG132-treated cells for 24 h (Figure 21D).

These results bring more information on the content of autophagosomes that accumulate in PA-treated cells and are in line with previous results obtained for the accumulation of non-

degraded autophagosomes and the alteration of lysosomal acidification. In addition, it shows that these features are early events of lipotoxicity as they occur in cells exposed to PA as soon as for a 6 h-incubation period (Figure 15C, 15D and 15E).

In conclusion, these data suggest that PA-induced lipotoxicity might result in protein aggregation and accumulation in the cytoplasm. In addition, the inhibition of the autophagic flux in response to PA exposure is correlated to an increase in Ub-positive structures sequestered in autophagosomes. Taken together, this led us to conclude that protein clearing could be impaired and accumulated in autophagosomes that contain protein aggregates in mPTECs suffering from PA-induced lipotoxicity.

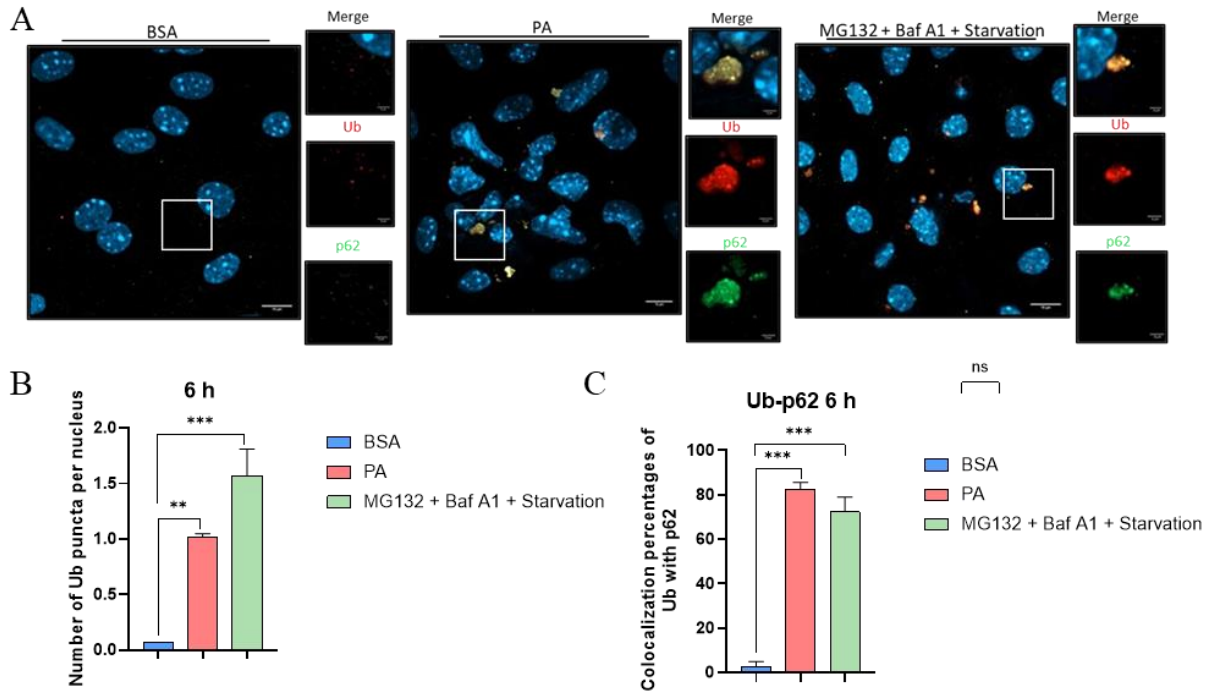

Figure 20. Effect of PA on the colocalization of protein aggregates and autophagosomes in mPTECs at 6 h. (A) *Representative micrographs of mPTECs incubated with 300 µM PA (or 0.4 % BSA for control cells) during (A) 6 or starved for 6 h in the presence of 10 µM MG132 and 2 nM bafilomycin A1. At the end of the incubations, cells were fixed and immunostained with an IgG monoclonal antibody raised against ubiquitin (Ub) and IgG antibody directed against p62. (B) Quantifications of Ub-positive puncta in mPTECs after 6 h of PA or BSA treatment. Quantifications were performed on at least 100 cells per condition using ImageJ analysis. (C) Quantifications of colocalization percentages between Ub and p62 in mPTEC after 6 h of treatment with PA or BSA. Quantifications were performed on at least 100 cells per condition using Manders overlap coefficients. Data are presented as means ± SEM for 6 independent biological experiments (n=6). Statistical analyses were performed by a one-way ANOVA followed by a Dunnett's post-hoc test: ** $p \leq 0.01$, *** $p \leq 0.001$. BSA = Bovine Serum Albumin, PA = Palmitate, MG132 = N-Benzyloxycarbonyl-L-leucyl-L-leucyl-L-leucinal, Baf A1 = Bafilomycin A1.*

G. Effect of PA on protein aggregates accumulation and colocalization with lysosomes at 24 h

We next assessed the colocalization between Ub-positive aggregates and lysosomes in cells exposed to 300 µM PA or 0.4 % BSA for 6 h or 24 h and immunostained with an IgG antibody raised against Ub and an IgG antibody raised against LAMP1. Micrographs showed an accumulation of red spots in PA-treated cells after 24 h (Figure 21G).

In addition, we found that all Ub-positive red spots were surrounded by LAMP1 green fluorescence signals immunostaining representative of lysosomes (or acidic compartments) in each condition (Figure 21A). Besides, quantifications showed no statistically significant difference in colocalization between cells incubated 24 h with PA and control cells. This is the reason why we assessed the number of Ub puncta engulfed in LAMP1-positive structures representing lysosomes. The number of Ub puncta in LAMP1 structures was significantly increased in PA-treated cells after 24 h of treatment compared to control cells (Figure 21H). This confirms that Ub aggregates are target to the autophagic pathway and accumulate in lysosomes which degradative function is impaired by PA (as seen in Figure 15B, 15C and 15D).

Physiologically, when the degradation capacity of the proteasome is insufficient, proteins tend to form protein aggregates. This, most likely, explains the presence of some aggregates in control cells as well. It could also explain the absence of statistical differences in colocalization between LAMP-1 and the Ub fluorescent signals. Let’s also add that lysosomal immunostaining for LAMP1 targets a lysosomal membrane marker and therefore it is expected that it does not allow perfect colocalization with the internal/luminal content of the organelle.

In conclusion, these results suggest that PA could be responsible for the disruption of the autophagic flux and causes the sequestration of protein aggregates in the lysosomes. Indeed, the set of data shows a significant increase in the size of the protein aggregates sequestered in the organelle. This phenotype also confirms the lysosomal dysfunction observed before in terms of alteration of lysosomal pH and increased LMP as described in section Results A and E, respectively.

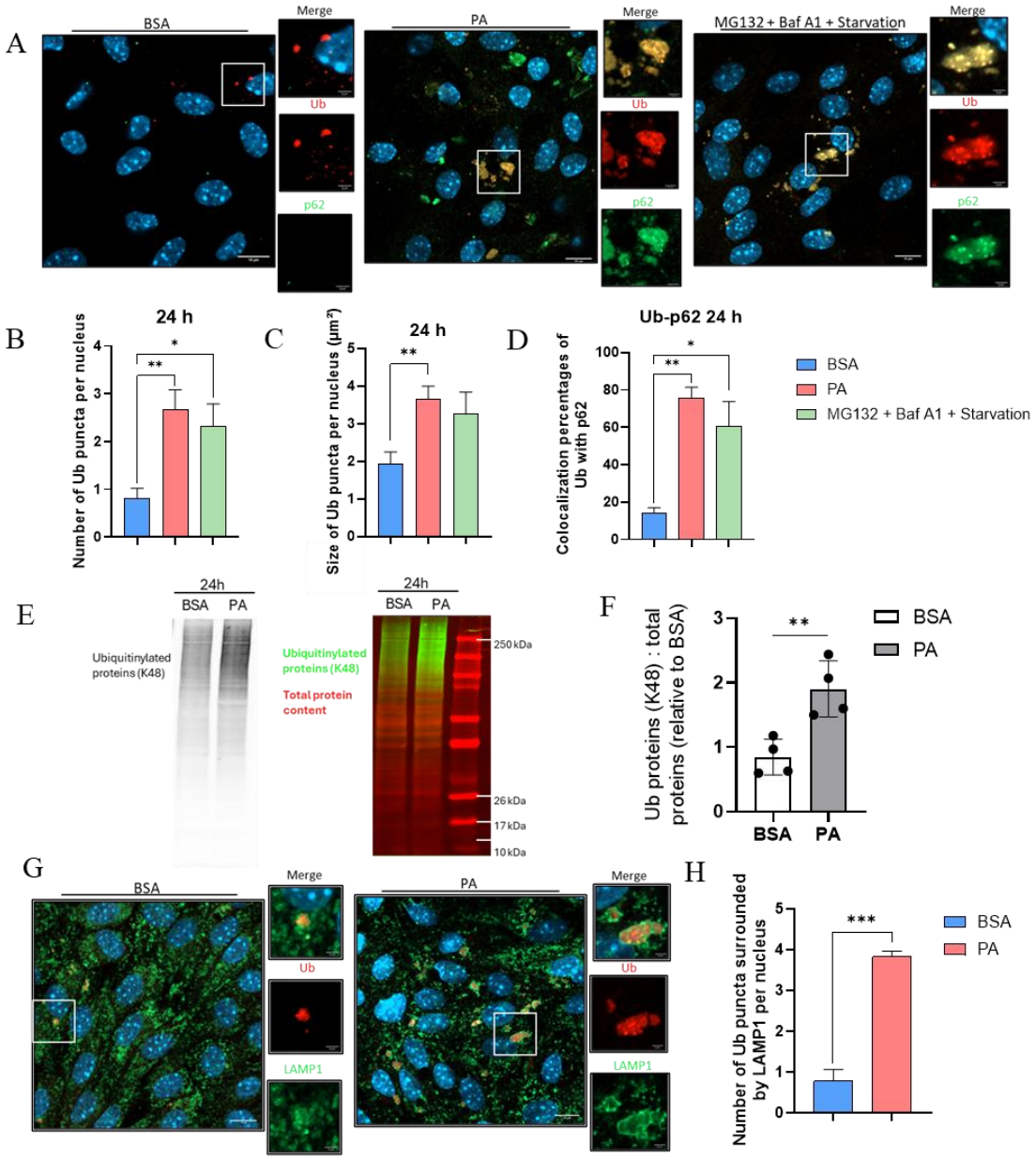

Figure 21. Effect of PA on the colocalization of protein aggregates and autophagosomes or lysosomes in mPTECs at 24 h. *(A) Representative micrographs of mPTEC incubated with 300 µM PA (or 0.4 % BSA for control cells) 24 h or starved for 6 h in the presence of 10 µM MG132 and 2 nM bafilomycin A1. At the end of the incubations, cells were fixed and immunostained with antibodies raised against ubiquitin (Ub) and p62. (B) Quantifications of Ub-positive puncta in mPTECs after 6 h of PA or BSA treatment. (C) Quantifications of the size of Ub-positive spots (µm²) in mPTEC after 24 h of a PA- or BSA-treatment. Quantifications were performed on at least 100 cells per condition using ImageJ. (D) Quantifications of colocalization percentages between Ub and p62 in mPTECs after 24 h of a treatment with PA or BSA. Quantifications were performed on at least 100 cells per condition using Manders overlap coefficients. (E) Representative western blot of ubiquitinylated proteins (grey in the left, green in the right) and total protein content (red in right) in mPTECs treated with 300 µM PA or 0.4% BSA. (F) Quantitative densitometry analysis of ubiquitinylated proteins normalized by total protein content. (G) Representative micrographs of mPTEC incubated with 300 µM PA (or 0.4 % BSA for control cells) 24 h, fixed and immunostained for antibodies raised against Ub and LAMP1. (H) Quantifications of number of Ub puncta surrounded by LAMP1 per nucleus. Quantification of the number of Ub puncta surrounded by LAMP1 staining on 30 cells per group. Data are presented as means ± SEM for (D, F) 3 or (B, C, H) 6 independent biological experiments (n=3-6). Statistical analyses were performed by an unpaired t-test: * $p \leq 0.05$, ** $p \leq 0.01$. BSA = Bovine Serum Albumin, PA = Palmitate, MG132 = N-Benzyloxycarbonyl-L-leucyl-L-leucyl-L-leucinal, Baf A1 = Bafilomycin A1.*

H. Effect of PA-induced lipotoxicity on mPTECs physiologic features

As described in the introduction (see section Introduction B.2.a.), PTECs display a high capacity of secretion and reabsorption and, especially, protein reabsorption through receptor-mediated endocytosis[71,192]. Ligands such as low molecular proteins, plasma proteins or drugs are thus reabsorbed through specific receptors such as megalin or cubilin[79]. Then, ligands are internalized in the endolysosomal system to be recycled[80]. How this pathway is affected in response to obesity and cell fat accumulation remains to be determined. These considerations led us investigate the putative effect of PA-induced lipotoxicity on mPTECs reabsorption of proteins by receptor-mediated endocytosis and differentiation.

First, we assessed the effect of PA on mPTECs reabsorption of proteins through receptor-mediated endocytosis by a BSA uptake assay using BSA-Alexa Fluor™ 488 conjugate. Based on the importance of lysosomal homeostasis for this process, we also included Baf A1 to determine whether an alteration of lysosomal pH (and thus function by affecting the autophagic flux) itself may alter the protein reabsorption.

Cells were thus incubated with 300 µM PA or 0.4 % BSA during last 6 h or 24 h supplemented or not with Baf A1 for last 6 h, and then incubated last hour with BSA-Alexa Fluor™ 488 probe and observed with a confocal microscope (Figure 22). Micrographs showed the accumulation of green fluorescence punctuates corresponding to BSA internalisation in control cells incubated with BSA-conjugated to Alexa Fluor™ 488. On the contrary, cells treated with PA and/or Baf A1 displayed a lower BSA-associated fluorescence signal after 6 or 24 h of incubation (Figure 22A). Quantifications confirmed the statistically significant decrease in BSA-conjugated uptake in cells treated with PA and/or Baf A1 at both 6 or 24 h of treatment (Figure 22B and 22C). These data suggest that protein reabsorption is altered in mPTECs exposed to PA-induced lipotoxicity. In addition, the absence of difference after addition of Baf A1 confirms the involvement of lysosomal dysfunctions in the disruption of the endocytic pathway in PA-treated mPTECs.

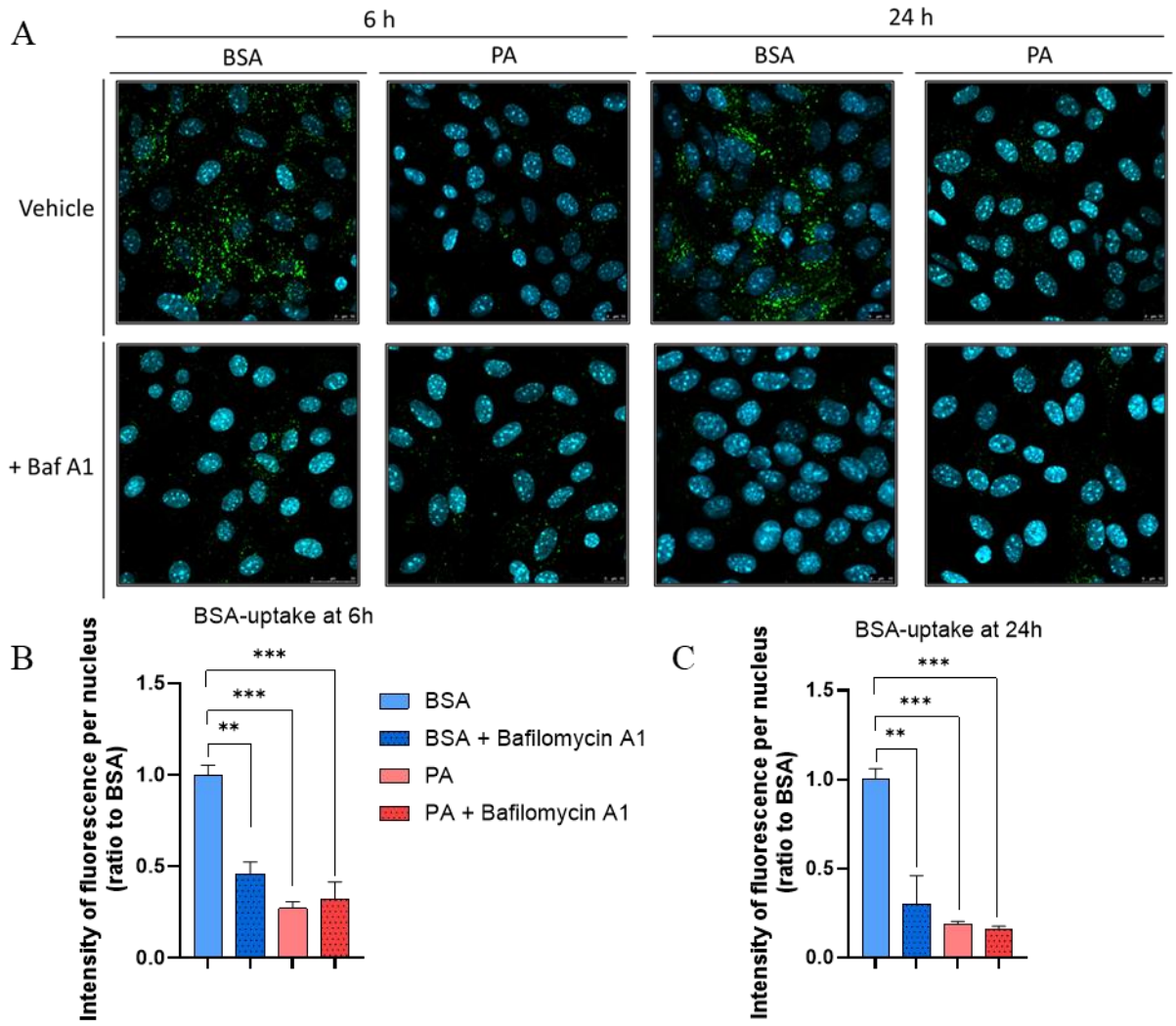

Figure 22. Effect of PA on mPTEC biological features. *(A) Representative micrographs of mPTEC treated with 300 µM PA (or 0.4 % BSA for control cells) for 6 or 24 h supplemented or not with 2 nM bafilomycin A1 during the last 6 h. Cells were incubated with BSA-conjugated Alexo Fluor™ 488, fixed and observed by confocal microscopy (Leica TCSSP5 II). Quantifications of BSA- fluorescent probe signals in mPTECs after (B) 6 or (C) 24 h of PA or BSA treatment. Quantifications were performed on at least 400 cells per condition. Data are presented as means ± SEM for three independent biological experiments (n=3). Statistical analyses were performed by a two-way ANOVA followed by Tukey post-hoc test: ** $p \leq 0.01$, *** $p \leq 0.001$. BSA = Bovine Serum Albumin, PA = Palmitate, Baf A1 = Bafilomycin A1.*

I. Study of the effect of PA on mPTEC differentiation markers

Eventually, to deeper characterize the effect of PA on the biology of mPTECs, we studied, by RT-qPCR, the effect of PA on the relative abundance of mRNA of several differentiation markers: *Lrp2*, *CUBN*, *AQP1*, *SLC3A1*, *SLC5A2*, *E-CDH*, *CDH16*, *DSP* and *EBP41L5* and dedifferentiation markers *FOXM1*, *SOX9*, *VIM*, *CD44* and *LCN2* in mPTECs (Table 4). Results indicated no statistically significant difference in the abundance of mRNA of these differentiation and dedifferentiation gene markers in mPTECs incubated with PA for only 6 h (Figure 23A and 23B). On the contrary, these data, presented in Figure 23, revealed a

significant decrease in the relative abundance of transcripts for several differentiation markers such as *Lrp2*, *AQP1*, *SLC5A2*, *CDH16* and *EPB41L5* in cells incubated for 24 h with PA when compared to the abundance of these mRNAs in BSA-treated control cells (Figure 23C). In addition, the dedifferentiation markers such as *FOXM1*, *SOX9*, *VIM* and *CD44* were downregulated in exposed to PA for 24 h (Figure 23D).

Taken together, these results show that PA-induced lipotoxicity in mPTECs disrupts biological and physiological features of these cells when they are incubated with the SFA for 24 h but not for the shorter incubation time tested (6 h). This suggest that PA disrupts the endocytic pathway which participates to PTECs dedifferentiation, before gene expression of markers is affected.

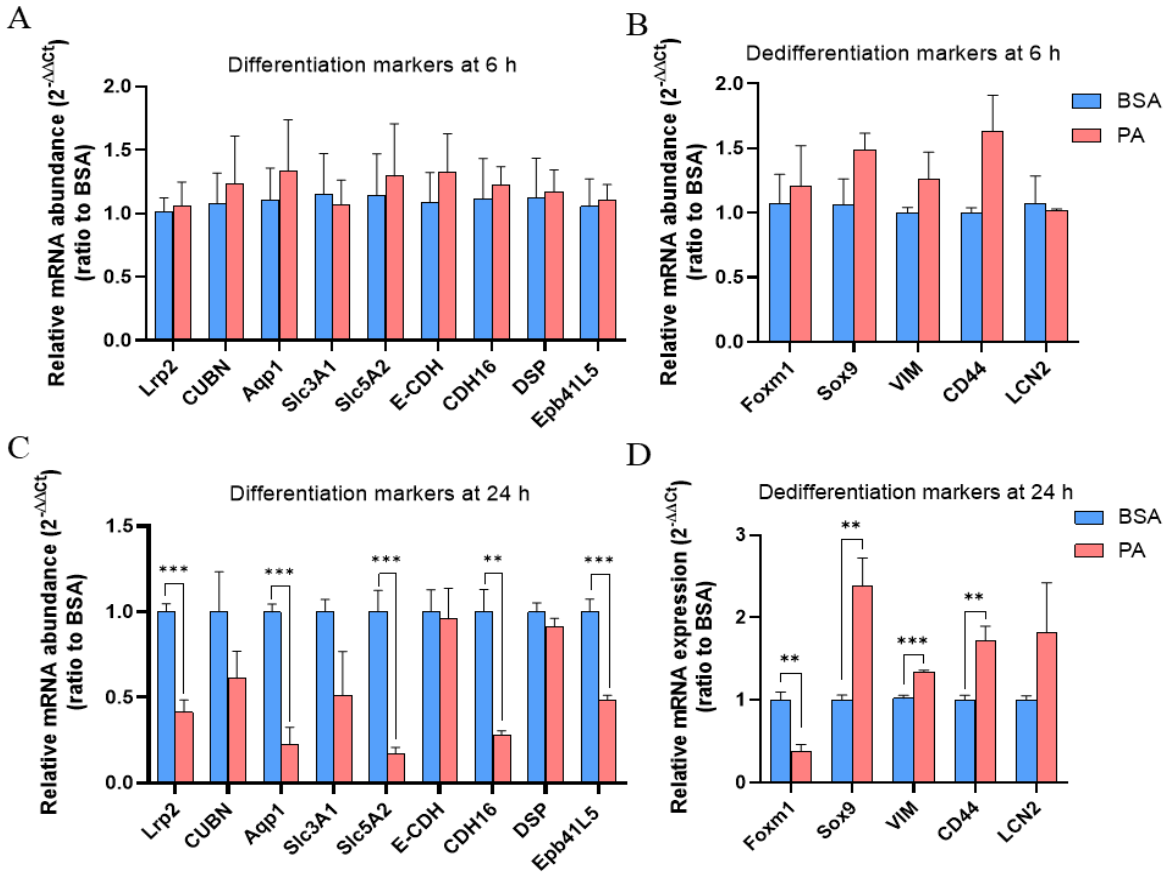

Figure 23. Effect of PA on mPTEC differentiation and dedifferentiation markers. *Relative abundance of mRNA (determined by RT-qPCR analyses) for differentiation markers such as Lrp2, CUBN, AQP1, SLC3A1, SLC5A2, E-CDH, CDH16, DSP and EBP41L5 in mPTECs treated with 300 µM PA (or 0.4 % BSA for control cells) during (A) 6 or (C) 24 h. (D) Relative abundance of mRNA (determined by RT-qPCR analyses) for dedifferentiation markers such as FOXM1, SOX9, VIM, CD44 and LCN2 in mPTECs treated with 300 µM PA or incubated with 0.4 % BSA during (B) 6 or (D) 24 h. Data are presented as means ± SEM for 4 independent biological experiments (n=4). Statistical analyses were performed by an unpaired t-test. * $p \leq 0.05$, ** $p \leq 0.01$, *** $p \leq 0.001$. BSA = Bovine Serum Albumin, PA = Palmitate, Baf A1 = Bafilomycin A1.*

Table 4. Differentiation and dedifferentiation markers and their main biological function in PTECs.

Gene symbol	Protein encoded	Biological function
Slc3A1	Amino acid transporter 1	Heavy chain subunits of the heteromeric amino acid transporter (HAT) expressed at the apical side of PTECs, facilitate biogenesis and trafficking of functional transporter heteromers[219].
AQP1	Aquaporine-1	Principal water channel in PTECs, recently showed to drive epithelial cell migration in proximal tubules[220].
CDH16	Cadherin-16	Transmembrane protein involved in cell-cell interaction, cell compaction, cell differenciation and cell migration in proximal tubules[221].
CD44	Cluster of differenciation 44	Transmembrane glycoprotein involved in receptor-médiated endocytosis of hyaluronan which regulates cell–cell adhesion, migration, proliferation, differentiation[222].
CUBN	Cubilin	Membrane glycoprotein involved in protein-mediated endocytosis in PTECs[223].
DSP	Desmoplakin	Critical component of desmosome structures which ensure cell-cell adhesion in epithelia such as proximal tubular epithelium[224].
E-CDH	E-cadherin	Transmembrane protein driving Ca2+-dependent cell-cell adhesion in renal epithelium[225].
Epb41L5	Erythrocyte Membrane Protein Band 4.1 Like 5	Podocyte-specific regulator of integrin adhesion formation and maintenance of glomerular filtration barrier[226].
Foxm1	Forkhead box M1	Transcription factor driving dedifferenciated proximal tubular epithelial cells proliferation after acrute injury[227].
LCN2	Lipocalin-1	Adipocytokine responsible of the transport of small hydrophobic molecules and the control of tubular cells proliferation, involved in the devlopment of CKD[228].
Lrp2	Megalin/low density lipoprotein receptor-related protein 2	Multiligand endocytic receptor involved in the maintenance of the endocytic pathway in PTECs[229].
Slc5A2	Sodium-glucose co-transporter 2	Receptor that mediates the endocytosis of glucose across the apical membrane of PTECs[230].
Sox9	SRY-box transcription factor 9	Transcription factor involved in kidney development through cell proliferation and multilineage differentiation[231].
VIM	Vimentin	Tubular injury marker[232].

V. DISCUSSION

Obesity is a complex, multifactorial disease that is soaring around the world[4]. Although it can be explained by different factors (genetics including SNPs (single nucleotide polymorphisms), epigenetics, changes in microbiota, …), obesity mainly results from an imbalance between caloric intake and energy expenditure[4]. In obesity, the major tissue that changes in abundance and mass is WAT. In addition, WAT dysfunction such as organelle stress, hypertrophy and modifications in the expression of gene encoding adipokines leads to FFA release in the bloodstream and abnormal accumulation of lipids in non-adipose tissues such as liver or kidneys[233,234], defined as lipotoxicity[14,15,191].

Kidney cells and more particularly PTECs are very sensitive to lipotoxicity due to their high energy needs to fulfill their functions of secretion and reabsorption of ions, vitamins, glucose, amino acids and low-molecular weight proteins[71]. It has previously been shown that PTEC lipotoxicity contributes to the development of obesity-induced kidney disease[84,101,110,235]. In addition, evidence accumulates regarding the fact that tubular injuries are at the origin of the CKD development in the context of metabolic injuries[236,237].

Several studies have shown that PTEC lipotoxicity is associated with mitochondrial alterations, production of ROS leading to oxidative stress, autophagic and lysosomal alterations as well as LD accumulation and lipid metabolism dysregulation[45,63,84,108,110]. These events globally contribute to PTECs dysfunction characterized by alterations of the brush border and loss of polarity[191]. In this regard, it is of particular interest to better understand how lipotoxicity, notably PA-mediated lipotoxicity, impairs the autophagy-lysosomal degradation system. Our group has previously demonstrated that non-degraded autophagosomes accumulate in mPTECs challenged with PA (Figure 15A-D). This accumulation has been explained by an inhibition of lysosomal degradation due to impaired acidification (Figure 15E). However, the content of these accumulated autophagosomes remained unknown at the beginning of the Master thesis. In this regard, the present work aimed to determine whether a selective autophagic pathway is dysregulated in mPTECs exposed to PA. In addition, knowing that lysosomal homeostasis is key for PTECs physiology as endolysosomal system is essential for the reabsorption process, we also aimed to determine the effects and consequences of lipotoxicity on the phenotype of mPTECs as well as the contribution to the lysosomal dysfunction.

A previous proteomic analysis generated in the laboratory URBC by Louise Pierre (PhD student, unpublished data) on mPTECs incubated with PA for 24 h showed that the abundance of two ER-phagy markers, FAM134B and UFL1, were upregulated (Figure 15F). This result suggested that the content of autophagosomes might derive from the specific degradation of ER fragments. This was our first/initial (but wrong) hypothesis at the beginning of this Master thesis.

A. ER-markers

We thus first tried to validate the proteomic results by assessing the abundance of FAM134B, an ER-phagy adaptor involved in ER sheet degradation. We did not find any difference in the mRNA nor in the protein abundance for this marker in cells incubated for 6 or 24 h with PA- in the presence or in the absence of Baf A1 when compared to the abundance found in BSA-treated control cells (Figure 16A-C). Comparable mRNA abundances between

BSA- and PA-treated cells were also obtained for other adaptors described in ER-phagy such as *ATL3*, *CCPG1* and *SEC62* (Figure 16G).

In addition, the abundance of Ufl1mRNA or protein, a molecular actor involved in UFMylation (a post-translational modification known to activate ER-phagy), was not different between PA-treated and BSA-incubated cells. In addition, UFMylation did not appear to be modified at an earlier time point (6 h) (Figure 16D-F). To sum up, in our experimental conditions, there was no change in transcriptional activity or protein translation, stability or degradation of these genes in mPTEC response to lipotoxicity. As the results did not confirm the proteomic data (at least for the two markers), we conclude that it is unlikely that UFMylation and ER-phagy are involved in the accumulation of autophagosomes in mPTECs incubated with PA.

These results could be surprising as evidence showed that PA and HFD could induce ER stress. Indeed, in immortalized mouse podocytes, a 300 µM PA-treatment of 24 h increases the abundance of ER stress markers such as BIP and CHOP-10 as well as the phosphorylation of PERK and IP3R[238]. However, it is another cell type that might have a different response/sensitivity. In immortalized human PTEC cell lines (HK2), the abundance of BIP and CHOP-10 is also increased after an incubation of 24 h with 800 µM PA[239]. As ER stress is known to trigger UPR activation, PA-induced ER stress has been demonstrated to activate the UPR pathways to cope with the stress generated by such a high PA concentration in HK2 cells[235] and H7h hepatic cells[72]. Additionally, other adaptative pathways may occur upon ER stress including ER-phagy. However, the effect of PA on ER-phagy is still poorly investigated. A study shows that PA-treatment does not affect basal ER-phagy levels in hypothalamic cells[241].

Altogether, these findings suggest that saturated FAs impair ER homeostasis. UPR pathways may be investigated in our model of PA-induced lipotoxicity in mPTECs. To do so, measurements of ER stress markers such as ATF4, CHOP-10 or BIP by RT-qPCR may be realised. In addition, activation of ER sensors may be assessed by measuring IRE1α and PERK phosphorylation or ATF6α cleavage in mPTECs treated or not with PA[242,242]. However, the effect of PA on ER-phagy is unclear from now. Another explanation could be that ER-phagy has been discovered relatively recently and that results are difficult to interpret. In this regard, our results do not support or refute the involvement of ER-phagy in autophagic dysfunctions induced by PA in mPTECs. To solve this question, colocalization studies between ER proteins involved in ER-phagy and autophagosomal and lysosomal markers (WIPI2 and LAMP1, respectively) should be done. We tried this approach but encountered some difficulties for the labelling of ER with antibodies raised against calnexin (see Annex 1). The staining remains blurred and nuclear with a high background signal. In view of these elements, we decided not to investigate this pathway any further until we can achieve good staining conditions.

We thus next pursued our approach by investigating the putative effect of PA in mPTECs on other selective autophagic pathways, and first on lipophagy.

B. Lipophagy

It is now well accepted that lipophagy is as essential as lipolysis when FFAs are required as energy fuels by some tissues during starvation periods[142]. As previously mentioned, lipotoxicity triggered by FAs overaccumulation has been reported to provoke LD accumulation in PTECs[243]. In this regard, we next wondered whether the obstruction/inhibition of autophagic flux observed in mPTECs exposed to PA could target the accumulating LDs.

Even if an increase of LDs was observed on micrographs in PA-treated cells after 24 h (Figure 17A-D), our data did not show any significant difference between BSA- and PA-treated cells in term of colocalization between LDs (assessed by the immunostaining of PLIN2) and autophagosomes (assessed by the immunostaining of LC3) nor lysosomes (with LAMP1 used as a molecular marker). This implies that LDs that accumulate in PA-exposed mPTECs might not be directed towards autophagic degradation.

Now, we would also like to discuss the fact that findings regarding the activation of lipophagy by FA accumulation are conflicting and controversial in the literature. While this pathway seems to be activated in hypothalamic cells[244], it is not the case in cultured β-cells[245]. In addition, PA-treatment and HFD have been reported to provoke the inhibition of lipophagy in hepatocytes[246,247].

Our data should thus be considered with caution. In fact, the methodology that we used was associated with some limitations that we are aware of. First, the quantification method was most likely not optimal. As seen on micrographs (Figure 17A), there were more spots of colocalization between PLIN2 and LC3 or LAMP1 in the positive control than in BSA-treated cells (negative control). However, quantifications showed no statistically significant difference in colocalization percentages between PA-treated cells and BSA-incubated cells. Indeed, this quantification method takes in to account the percentage of each of the two signals in each condition. Therefore, the proportional increase in colocalization with an increase in signal percentage explains the apparent discrepancy in colocalization between the two controls while micrographs showed the opposite. To overcome this limitation, we should rather use the number of events for PLIN2 signal colocalizing with LC3 or LAMP1 without any normalization for total PLIN2 staining. Second, the positive control did not show expected results as demonstrated in hepatocytes[195], so no real conclusion can be drawn from this analysis and experiments. Although PLIN2 is a good LD marker that attests the lipophagy activity[245] it is also shown that degradation of PLIN2 by CMA is required for the initiation of lipophagy[205]. Therefore, the degradation of PLIN2 on LDs to initiate recognition and engulfment in the autophagosome could explain the absence of colocalization differences between our experimental conditions (and thus the absence of effect in the positive control).

PLIN2 degradation by CMA could be monitored by colocalization studies between PLIN2 and LAMP1 or co-immunoprecipitation of PLIN2 with CMA actors (such as Hsp70)[144]. However, to assess whether PA-induced autophagosome accumulation contains LD portions while overcoming the limitation linked to PLIN2, autophagic and lysosomal markers may be assessed in LDs after their co-immunoprecipitation (through ATGL)[248]. In the same line, LDs may be stained by BODIPY for colocalization studies with autophagosomal or lysosomal markers. Finally, the experimental conditions related to the positive control could be changed. Indeed, since this treatment was not performed in mPTECs but in hepatic cells[195], the incubation time and/or OA concentration could/should be optimized as well as the starvation conditions.

Although quantifications showed similar colocalization percentages between PA-treated cells and cells used as positive controls, we can see that LDs colocalized with autophagosomes and lysosomes in the cells exposed to OA, Baf A1 and starvation and used as positive controls. This observation was not found in PA-treated cells. This suggests that it is unlikely that PA triggers/activates lysophagy in mPTECs, even if this statement needs to be confirmed by additional assays as discussed above. In the screen of the different selective autophagy potentially induced in PA-treated cells, we next focused our attention on mitophagy as lipid burden triggers mitochondrial alterations as decrease of mitochondrial membrane potential[249].

C. Mitophagy

We have seen in the introduction that mitophagy allows the maintenance of cell homeostasis as it degrades damaged (detected by a drop in the inner membrane potential) or superfluous mitochondria[147]. As previously mentioned, PTECs form a significant amount of ATP (95 %) by the mitochondrial FAO to ensure their transport functions[250,251]. It has been shown that an excess of SFA can cause mitochondrial damages in rat hepatoma cells[252] or renal cells[253]. Oxidative stress and decrease in/reduction of mitochondrial membrane potential are two key stimuli triggering mitophagy[251,253], so this pathway seemed of great interest to be studied in PA-treated mPTECs.

The analysis of the mitochondrial morphology revealed that the morphology of the organelle (resulting from the balance between fusion and fission events) was not changed in mPTECs incubated with 300 µM of PA for 24 h when compared to cells exposed to 0.4 % BSA (Figure 18A, 18C). Furthermore, the percentages of colocalization between mitochondria and autophagosomes or lysosomes were also comparable between BSA- and PA-treated cells. However, cells incubated with the mitochondrial uncoupler FCCP and Baf A1, known to trigger mitochondria fragmentation[194], displayed, as expected, higher colocalization percentages between mitochondria and autophagosomes and lysosomes indicative of an increased mitophagy (Figure 18B, 18D). This allows us to exclude the possibility that the autophagosomes accumulating in PA-treated mPTECs contain mitochondria fragments.

Let's mention however, that the group of Yamamoto reported that both HFD and PA trigger mitochondrial alterations and a PINK1/Parkin-dependent mitophagy in mice and human immortalized PTECs, respectively[108]. However, to date, these contradictions between the above-mentioned study and our results remain unresolved.

We next continued our research by analysing lysophagy known to degrade damaged lysosomes[157].

D. Lysophagy

When lysosomes are damaged, lysosomal quality control pathways may occur, enabling them to be repaired via the ESCRT pathway, regenerated by lysosomal biogenesis or degraded by lysophagy[157,159]. The sensing of LMP is a strong initiator of lysophagy. Gal-3, -8 or -9 recognize glycans of permeabilized lysosomes that are exposed to the cytosol and are used as markers of permeabilized lysosomes[157]. However, to the best of our knowledge, no evidence of

activation of lysophagy in cells exposed or facing lipotoxicity can be found in the literature. We therefore questioned whether the inhibition of autophagic flux in PA-exposed cells and subsequent loss of lysosomal acidification could be associated with activation of the lysophagic pathway or not[157,158].

When mPTECs were incubated with PA for 24 h, they displayed a significant increase in Gal3 puncta indicating an increase in permeabilized lysosomes in these conditions when compared to BSA-treated cells (Figure 19A, 19B). A positive control composed of cells incubated with the lysomotropic reagent LLOMe for 1 h was also included and in this condition, we observed a higher amount of Gal3 puncta, as expected[159]. These results suggest that PA induces LMP which is in line with the disruption of the proton gradient and reduced acidity in PA-treated cells (Figure 15B-E). Since the end of the experimental work, free-enzyme activity of lysosomal hydrolases has been assessed[156] (Louise Pierre, PhD thesis) and the results confirm a stronger release of these enzymes in the cytosol of PA-exposed cells when compared to BSA-incubated cells.

In parallel, we observed that the colocalization percentages between Gal3-positive lysosomes and autophagosomes (LC3) were comparable between BSA- and PA-treated cells after 24 h of treatment while this percentage was significantly higher in positive control cells exposed to FCCP and Baf A1 (Figure 19C). These results suggest that there is no clear evidence of lysophagy in PA-treated mPTECs and that permeabilized lysosomes do not seemed to be degraded.

As lysophagy does not appear to target permeabilized lysosomes in PA-exposed cells and that no cell death has been observed in response to lipid stress in mPTECs in our experimental conditions (results not shown), mPTECs could undergo other pathways of lysosomal quality control. Indeed, the ESCRT pathway catalyses lysosomal membrane budding and dissociation to damaged membranes and recovery[155,159,254]. The involvement of the ESCRT pathway in the repair of damaged lysosomes under lipotoxicity in mPTECs could be studied by Co-IP or immunofluorescence analyses between components of the ESCRT complex and lysosomal factors. Besides, lysosomal biogenesis may by studied as it could restore/maintain the lysosomal pool. Results from our groups indicated that mPTECs incubated 24 h with 300 µM displayed an increase in LAMP1 mRNA and protein abundance as well as an increase in the nuclear translocation of TFEB (Louise Pierre, PhD thesis). This suggests that the biogenesis of lysosomes could be stimulated in PA-exposed mPTECs. However, those newly formed lysosomes seem not functional as previous results showed an impaired acidification of the organelle at that time point (Figure 15E). In addition, the underlying mechanisms leading to LMP in PA-treated cells may be further investigated by studying different stress that may trigger lysosomal dysfunction such as lipid peroxidation by ROS[255], modulation of lipid membrane composition[256] or impaired lysosomal calcium homeostasis[257].

Altogether, these elements suggest that even if lysosomes are permeabilized secondary to lipid stress, it remains unlikely that accumulated autophagosomes contain damaged lysosomes. We thus moved on to another selective pathway targeting protein aggregates: aggrephagy[258].

E. Aggrephagy

We have seen that SFA-induced lipotoxicity causes ER stress and oxidative stress[188,259,260]. When the UPS pathway and the proteasome are overwhelmed, misfolded or unfolded proteins become aggregated, preventing the UPS pathway from degrading them. The autophagic pathway is then activated to eliminate these protein aggregates[111].

In this work, we reported that PA-treated cells, either after 6 or 24 h of incubation, displayed a strong accumulation of Ub puncta (Figure 20A, B and 21A, B), as well as an increase in their size (Figure 21 A, C), suggesting a significant accumulation of protein aggregates[261]. We also observed a strong accumulation of Ub-positive spots in the positive control as expected[214,215]. These data were confirmed by western blotting analysis showing a significant increase in polyubiquitinated proteins in PA-treated mPTECs incubated with the FA for 24 h (Figure 21 E, F). These results are consistent with the accumulation of Ub aggregates observed in PTs of HFD-fed mice by Yamamoto's group[108]. Therefore, we hypothesised that Ub-tagged protein aggregates accumulate and could be targeted to autophagic degradation in PA-incubated mPTECs.

We also showed that these aggregates are targeted to the autophagic degradation as Ub colocalized with autophagosomal marker p62 (Figure 20A, C and 21A, D) even at higher rates in PA-treated cells then in cells incubated with MG132, Baf A1 and starved used as positive control cells. Again, it already happens after 6 h of the cell incubation with PA, meaning that specific recognition of aggregates through aggrephagy is an early event of lipotoxicity. We confirmed this data by showing that there was a significant increase in Ub-puncta surrounded by LAMP1 in mPTECs incubated for 24 h with PA (Figure 21G, H). These results clearly indicate that protein aggregates are found in the autophagolysosomes of mPTECs exposed to PA in which their degradation is inhibited.

The underlying mechanism of protein aggregate accumulation in PA-treated cells remains unknown and should be investigated. Aggrephagy is activated when the UPS pathway and the proteasome are overwhelmed[189]. Proteasome inhibition in response to excessive lipid stress could thus possibly account for the accumulation of ubiquitinated proteins in PA-treated mPTECs. Alteration of proteasomal activity leading to the accumulation of Ub-positive protein aggregates has also been observed in hepatic cells of obese mice[262] and a downregulation of CP and RP proteasomal subunits has been reported in PA-treated podocytes[263]. To assess the relevance of this mechanisms in our experimental conditions, proteasomal activity will be assessed by measuring the activity of catalytic subunit enzymes and the mRNA and protein abundances of proteasomal subunits. Moreover, the content of protein aggregates in PA-treated cells could be analysed by mass spectrometry after their isolation to determine whether a particular pathway is affected by ubiquitylation or not.

F. Differentiation and physiologic features

At the end, to assess the potential phenotypical changes of mPTECs induced by PA exposure, we were interested to determine whether the lysosomal alterations characterised in PA-incubated mPTECs may alter their differentiation phenotype and physiologic features such as endocytic reabsorption. To date, the effects of lipotoxicity on PTECs have been poorly studied.

Then we expected to provide more data on the effect of lipid stress on PTECs behavior. Indeed, it has recently been shown that protein endocytosis is altered *in vitro* in mPTECs and *in vivo* in a mouse model of cystinosis, a lysosomal storage disease. In addition, the same group demonstrates that PTECs experienced a decrease of differentiating states leading to defective receptor-mediated endocytosis and tubular proteinuria[264].

Our results showed that PA-induced lipotoxicity altered receptor-mediated endocytosis as indicated by a decrease in the BSA reabsorption by PA-treated cells, an effect observed as soon as 6 h (Figure 22). The Bafilomycin A1 showed the same effect as PA, suggesting that this defective endocytosis might be the result of lysosomal pH modification (Figure 22).

This strong reduction of endocytic function suggests an epithelial dedifferentiation and epithelial to mesenchymal transition (EMT). This event is defined as the trans-differentiation of epithelial cells into motile mesenchymal cells[265]. EMT is characterized by loss of junctions, apicobasal polarity, cytoskeleton reorganization and changes in signalling pathways and gene expression[265]. To confirm EMT occurrence in PA-treated mPTECs, we addressed the expression of diverse epithelial and mesenchymal markers. The transcript abundances of *Lrp2*, *AQP1* and *SLC5A2* (actors involved in trafficking), as well as *CDH16* and *EPB41L5* (actors involved in cell junctions) were significantly decreased in cells treated with PA after 24 h (Figure 23C). This data reveals a loss of epithelial features as observed in another model of PTECs in which lysosomal function is genetically impaired and receptor-mediated endocytosis is defective[264]. One hypothesis that can be derived from these results is that cells respond to lysosomal dysfunction by decreasing the expression of endocytosis receptors, thereby avoiding a burden on the endocytic pathway. In addition, the expression of mesenchymal markers *SOX9, VIM* and *CD44* were significantly increased in cells incubated with PA for 24 h (Figure 23D). The mRNA abundances of all these genes were not significantly changed after 6 h of PA-treatment. This suggests that lipotoxicity modifies gene expression after changes in the endocytic receptor abundance that is already impaired in cells exposed to PA for only 6 h. What can be deduced from these analyses is that lipotoxicity first affects endocytic receptors function as shown by BSA-uptake assay. Then, mPTECs might protect from long-term lipotoxicity by promoting expression of mesenchymal markers.

Our results are in line with studies carried out on cystinosin and renal Fanconi syndrome (RFS)[266]. Indeed, it has been shown in mPTECs of RFS transgenic mouse model that lysosomal dysfunctions (enlarged lysosomes, defective proteolysis and impaired lysosomal acidification) are associated with increased cell proliferation, loss of apical expression of endocytic receptors and impaired endocytosis[266]. In addition, lipotoxicity is associated with loss of lysosomal function due to impaired acidification in mPTECs[108], the latter results in dedifferentiation and loss of reabsorption capacity of mPTECs[266]. The hypothesis built upon these findings is that mPTECs, in response to lipid stress, dedifferentiates as a protective mechanism.

When experiencing EMT, injured renal tubular epithelial cells may *in vivo* secrete pro-inflammatory mediators leading to tubular fibrosis[267,268]. Indeed, those observations are consistent with the tubulointerstitial inflammatory environment observed in kidney fibrosis and obesity-associated CKD. In addition, lipid-induced ROS production results in DNA damages and G2/M cell cycle arrest associated with senescence and EMT in TECs. EMT may be initiated by different pathways after an injury such as Sonic Hedgehog (SHH) Signaling or Wnt/β-Catenin signaling to protect from apoptosis[267,269]. In addition, dedifferentiation of epithelial

cells increase their proliferation rate as well as expression of stem-cells markers, meaning that injured epithelial cells could proliferate to repair cellular population as shown in a mouse model of injured PTs[232]. In PA-treated cells, mesenchymal characteristics could be further investigated through immunofluorescence microscopic analysis of morphologic changes (i.e. through acquisition of α-smooth muscle actin (α-SMA)). In addition, analysis of the secretome could be done as EMT of PTECs leads to secretion of inflammatory mediators such as MCP-1[267,268].

Taken together, these observations indicate that PA-induced lipotoxicity alters endocytosis and participates to EMT in mPTECs as shown by loss of epithelial markers and gain of mesenchymal ones. These modifications could be seen as protective mechanisms by which mPTECs adapt to lipid stress.

VI.CONCLUSION

The link between lipotoxicity and changes in the autophagic flux has been demonstrated several times both in obese animal models and patients as well as on *in vitro* models. Although the effect of lipotoxicity in PTECs is increasingly being studied, little is known about the underlying mechanisms of autophagic flux alterations. Our research group previously demonstrated that PA-induced lipotoxicity results in lysosomal acidification impairment which inhibit the degradation of autophagosomes leading to their accumulation in PA-treated cells. However, unknowns remain. In this regard, the present work first aimed to identify the content of accumulated autophagosomes. We therefore provided information on the structure(s) damaged in mPTECs under conditions of lipotoxicity. This question was addressed by studying bulk autophagy and selective autophagy in a murine model of PTECs in which lipotoxicity was induced by a PA-treatment. In addition, the potential effects of lipotoxicity on mPTECs phenotype are still poorly studied and limited information is currently available. Thus, secondly, this work aimed to assess the effects of lipotoxicity on PTEC fate/destiny.

In the present work, we identified (by Mass Spectrometry) an increase in two ER-phagy markers, but results could not be confirmed by targeted approaches. We therefore moved towards other selective autophagy pathways such as lipophagy and mitophagy, particularly for their link with the presence of LDs and oxidative stress. However, no cause-effect relationship could be established between lipotoxicity and these two selective autophagy pathways. Since lysosomes are defective in cells exposed to PA, we investigated lysosomal membrane integrity and lysophagy. We have shown that PA-induced lipotoxicity induces LMP, but there is no evidence that these permeabilised lysosomes are directed towards lysophagy. We also found that protein aggregates accumulate in PA-treated cells which colocalized with autophagic markers and are finally found in lysosomes where their degradation is inhibited likely because of lysosomal alkalinization. Finally, we showed that PTECs undergo a fate change and dedifferentiate in response to lipotoxicity. Indeed, PA-treated cells displayed altered receptor-mediated protein endocytosis and changes in their expression profile with an upregulation of mesenchymal markers while epithelial ones were downregulated. This EMT can be seen as a tool for cells to protect themselves from lipid stress (Figure 24).

Several perspectives emerged from this work. First, it would be interesting to understand how proteins are no longer degraded and aggregate. Moreover, the content of accumulated protein aggregates should be analysed to determine whether a particular protein is affected or if protein homeostasis in general is disrupted. This would provide information on the potential disruption of the two degradation pathways, the proteasome and the autophagy-lysosome pathway. In addition, the mechanisms driving lysosomal increase in membrane permeability are still poorly understood and may be further studied. Finally, the contribution of lysosomal dysfunction to alterations of endocytosis and phenotypic changes in PTECs could be explored.

This work has provided further insights on how lipotoxicity does alter the homeostasis of mPTECs. Our group previously identified lysosomal alkalinization as the first event leading to the inhibition of autophagosome degradation. In this work, we showed that autophagosomes contained Ub-tagged proteins aggregates. In addition, we identified LMP as a feature of lysosomal dysfunction.

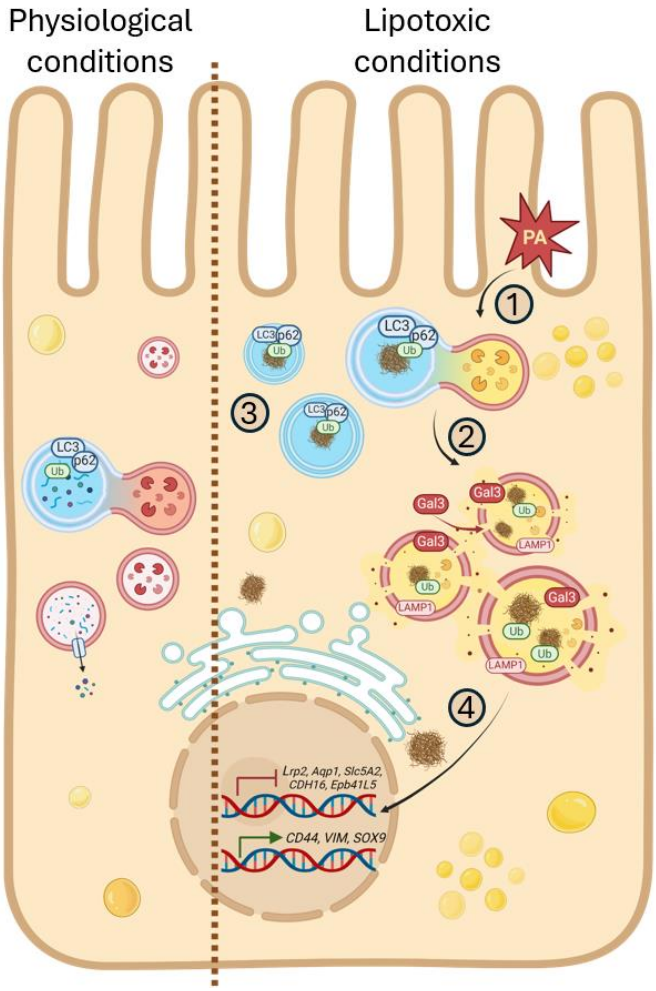

Figure 24: ***Schematic representation of the main findings of this work***. *1) mPTECs treated for 24 h with 300 µM PA display an accumulation of undegraded autophagosomes. While fusion between autophagosomes and lysosomes is maintained in these conditions, lysosomal degradation is impaired due to lysosomal lumen alkalinisation. 2) In addition, increasing Gal3 staining indicate an accumulation of permeabilised lysosomes in PA-treated mPTECs after 24 h of treatment. Indeed, lysosomal membrane rupture may account for increasing lysosomal pH and accumulation of undegraded autophagosomes and their content. 3) Further investigations show that Ub-tagged protein aggregates accumulate in undegraded autophagosomes and altered lysosomes as soon as 6 h of treatment with 300 µM of PA. 4) Finally, lysosomal dysfunctions are involved in mPTECs dedifferentiation. Indeed, while epithelial markers are downregulated in 24 h PA-treated mPTECs, mesenchymal markers such as CD44, SOX9 and VIM are upregulated suggesting the dedifferentiation of mPTECs under lipid stress. Illustration created with BioRender.com.*

VII. ANNEX

A

Calnexin antibody Enzo ADI-SPA-860
mPTECs

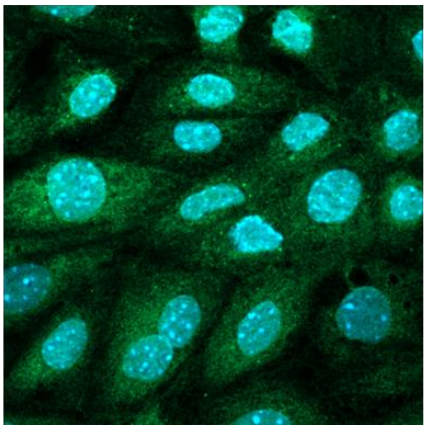

B

Calnexin Antibody (10427-2-AP)
HepG2

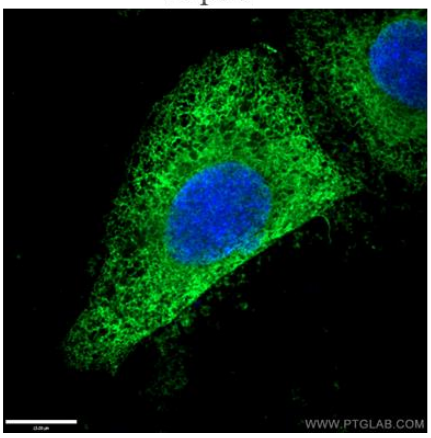

Annex: *Comparison between calnexin staining with (A) anti-calnexin (enzo ADI-SPA-860) at dilution 1:50 in mPTECs fixed with for 10 min at RT with 1 mL of a solution of 4 % PFA and permeabilised with 1 mL of PBS containing 15 mM of glycine, 0.05 % of saponin, 0.5 % of BSA and 50 mM of NH_4Cl (ammonium chloride); pH 7.4, and anti-calnexin 10427-2-AP at dilution 1:50 in fixed HepG2 with 10% PFA.*

VIII. BIBLIOGRAPHY

1. Chooi YC, Ding C, Magkos F. The epidemiology of obesity. *Metabolism*. 2019;92:6-10. doi:10.1016/j.metabol.2018.09.005

2. World Health Organization. Regional Office for Europe. *WHO European Regional Obesity Report 2022*. World Health Organization. Regional Office for Europe; 2022. Accessed August 5, 2023. https://apps.who.int/iris/handle/10665/353747

3. Heindel JJ, Alvarez JA, Atlas E, et al. Obesogens and Obesity: State-of-the-Science and Future Directions Summary from a Healthy Environment and Endocrine Disruptors Strategies Workshop. *Am J Clin Nutr*. 2023;118(1):329-337. doi:10.1016/j.ajcnut.2023.05.024

4. Hruby A, Hu FB. The Epidemiology of Obesity: A Big Picture. *PharmacoEconomics*. 2015;33(7):673-689. doi:10.1007/s40273-014-0243-x

5. Boutari C, Mantzoros CS. A 2022 update on the epidemiology of obesity and a call to action: as its twin COVID-19 pandemic appears to be receding, the obesity and dysmetabolism pandemic continues to rage on. *Metabolism*. 2022;133:155217. doi:10.1016/j.metabol.2022.155217

6. Hampl SE, Hassink SG, Skinner AC, et al. Clinical Practice Guideline for the Evaluation and Treatment of Children and Adolescents With Obesity. *Pediatrics*. 2023;151(2):e2022060640. doi:10.1542/peds.2022-060640

7. Blüher M. Obesity: global epidemiology and pathogenesis. *Nat Rev Endocrinol*. 2019;15(5):288-298. doi:10.1038/s41574-019-0176-8

8. Hill JO, Wyatt HR, Peters JC. The Importance of Energy Balance. *Eur Endocrinol*. 2013;9(2):111-115. doi:10.17925/EE.2013.09.02.111

9. Silver HJ, Welch EB, Avison MJ, Niswender KD. Imaging body composition in obesity and weight loss: challenges and opportunities. *Diabetes Metab Syndr Obes Targets Ther*. 2010;3:337-347. doi:10.2147/DMSOTT.S9454

10. Declèves AE, Sharma K. Obesity and kidney disease: differential effects of obesity on adipose tissue and kidney inflammation and fibrosis. *Curr Opin Nephrol Hypertens*. 2015;24(1):28-36. doi:10.1097/MNH.0000000000000087

11. Fahed G, Aoun L, Bou Zerdan M, et al. Metabolic Syndrome: Updates on Pathophysiology and Management in 2021. *Int J Mol Sci*. 2022;23(2):786. doi:10.3390/ijms23020786

12. Ghaben AL, Scherer PE. Adipogenesis and metabolic health. *Nat Rev Mol Cell Biol*. 2019;20(4):242-258. doi:10.1038/s41580-018-0093-z

13. Goossens GH. The Metabolic Phenotype in Obesity: Fat Mass, Body Fat Distribution, and Adipose Tissue Function. *Obes Facts*. 2017;10(3):207-215. doi:10.1159/000471488

14. Longo M, Zatterale F, Naderi J, et al. Adipose Tissue Dysfunction as Determinant of Obesity-Associated Metabolic Complications. *Int J Mol Sci*. 2019;20(9):2358. doi:10.3390/ijms20092358

15. Lakkis JI, Weir MR. Obesity and Kidney Disease. *Prog Cardiovasc Dis*. 2018;61(2):157-167. doi:10.1016/j.pcad.2018.07.005

16. Grosso G, Laudisio D, Frias-Toral E, et al. Anti-Inflammatory Nutrients and Obesity-Associated Metabolic-Inflammation: State of the Art and Future Direction. *Nutrients*. 2022;14(6):1137. doi:10.3390/nu14061137

17. Chouchani ET, Kajimura S. Metabolic adaptation and maladaptation in adipose tissue. *Nat Metab*. 2019;1(2):189-200. doi:10.1038/s42255-018-0021-8

18. Richard AJ, White U, Elks CM, Stephens JM. Adipose Tissue: Physiology to Metabolic Dysfunction. In: Feingold KR, Anawalt B, Blackman MR, et al., eds. *Endotext*. MDText.com, Inc.; 2000. Accessed August 9, 2023. http://www.ncbi.nlm.nih.gov/books/NBK555602/

19. Yang Loureiro Z, Solivan-Rivera J, Corvera S. Adipocyte Heterogeneity Underlying Adipose Tissue Functions. *Endocrinology*. 2022;163(1):bqab138. doi:10.1210/endocr/bqab138

20. Koenen M, Hill MA, Cohen P, Sowers JR. Obesity, Adipose Tissue and Vascular Dysfunction. *Circ Res*. 2021;128(7):951-968. doi:10.1161/CIRCRESAHA.121.318093

21. Fernández-Verdejo R, Marlatt KL, Ravussin E, Galgani JE. Contribution of brown adipose tissue to human energy metabolism. *Mol Aspects Med*. 2019;68:82-89. doi:10.1016/j.mam.2019.07.003

22. Pilkington AC, Paz HA, Wankhade UD. Beige Adipose Tissue Identification and Marker Specificity—Overview. *Front Endocrinol*. 2021;12. doi:10.3389/fendo.2021.599134

23. Barbatelli G, Murano I, Madsen L, et al. The emergence of cold-induced brown adipocytes in mouse white fat depots is determined predominantly by white to brown adipocyte transdifferentiation. *Am J Physiol Endocrinol Metab*. 2010;298(6):E1244-1253. doi:10.1152/ajpendo.00600.2009

24. Zhu Q, Scherer PE. Immunologic and endocrine functions of adipose tissue: implications for kidney disease. *Nat Rev Nephrol*. 2018;14(2):105-120. doi:10.1038/nrneph.2017.157

25. Lafontan M. Historical perspectives in fat cell biology: the fat cell as a model for the investigation of hormonal and metabolic pathways. *Am J Physiol Cell Physiol*. 2012;302(2):C327-359. doi:10.1152/ajpcell.00168.2011

26. Wronska A, Kmiec Z. Structural and biochemical characteristics of various white adipose tissue depots. *Acta Physiol*. 2012;205(2):194-208. doi:10.1111/j.1748-1716.2012.02409.x

27. Althaher AR. An Overview of Hormone-Sensitive Lipase (HSL). *Sci World J*. 2022;2022:1964684. doi:10.1155/2022/1964684

28. Bays HE, González-Campoy JM, Bray GA, et al. Pathogenic potential of adipose tissue and metabolic consequences of adipocyte hypertrophy and increased visceral adiposity. *Expert Rev Cardiovasc Ther*. 2008;6(3):343-368. doi:10.1586/14779072.6.3.343

29. Scherer PE. The many secret lives of adipocytes: implications for diabetes. *Diabetologia*. 2019;62(2):223-232. doi:10.1007/s00125-018-4777-x

30. Kershaw EE, Flier JS. Adipose Tissue as an Endocrine Organ. *J Clin Endocrinol Metab*. 2004;89(6):2548-2556. doi:10.1210/jc.2004-0395

31. Ouchi N, Parker JL, Lugus JJ, Walsh K. Adipokines in inflammation and metabolic disease. *Nat Rev Immunol*. 2011;11(2):85-97. doi:10.1038/nri2921

32. Tripathi D, Kant S, Pandey S, Ehtesham NZ. Resistin in metabolism, inflammation, and disease. *FEBS J*. 2020;287(15):3141-3149. doi:10.1111/febs.15322

33. Cox AR, Chernis N, Masschelin PM, Hartig SM. Immune Cells Gate White Adipose Tissue Expansion. *Endocrinology*. 2019;160(7):1645-1658. doi:10.1210/en.2019-00266

34. Lumeng CN, Bodzin JL, Saltiel AR. Obesity induces a phenotypic switch in adipose tissue macrophage polarization. *J Clin Invest*. 2007;117(1):175-184. doi:10.1172/JCI29881

35. Gustafson B, Hammarstedt A, Hedjazifar S, et al. BMP4 and BMP Antagonists Regulate Human White and Beige Adipogenesis. *Diabetes*. 2015;64(5):1670-1681. doi:10.2337/db14-1127

36. Karczewski J, Śledzińska E, Baturo A, et al. Obesity and inflammation. *Eur Cytokine Netw*. 2018;29(3):83-94. doi:10.1684/ecn.2018.0415

37. Ferrante Jr AW. Obesity-induced inflammation: a metabolic dialogue in the language of inflammation. *J Intern Med*. 2007;262(4):408-414. doi:10.1111/j.1365-2796.2007.01852.x

38. Ellulu MS, Patimah I, Khaza'ai H, Rahmat A, Abed Y. Obesity and inflammation: the linking mechanism and the complications. *Arch Med Sci*. 2017;13(4):851-863. doi:10.5114/aoms.2016.58928

39. Serra D, Mera P, Malandrino MI, Mir JF, Herrero L. Mitochondrial Fatty Acid Oxidation in Obesity. *Antioxid Redox Signal*. 2013;19(3):269-284. doi:10.1089/ars.2012.4875

40. Guilherme A, Virbasius JV, Puri V, Czech MP. Adipocyte dysfunctions linking obesity to insulin resistance and type 2 diabetes. *Nat Rev Mol Cell Biol*. 2008;9(5):367-377. doi:10.1038/nrm2391

41. Klop B, Elte JWF, Castro Cabezas M. Dyslipidemia in Obesity: Mechanisms and Potential Targets. *Nutrients*. 2013;5(4):1218-1240. doi:10.3390/nu5041218

42. Lopaschuk GD. Fatty Acid Oxidation and Its Relation with Insulin Resistance and Associated Disorders. *Ann Nutr Metab*. 2016;68 Suppl 3:15-20. doi:10.1159/000448357

43. Unger RH, Orci L. Lipotoxic diseases of nonadipose tissues in obesity. *Int J Obes*. 2000;24(4):S28-S32. doi:10.1038/sj.ijo.0801498

44. Rada P, González-Rodríguez Á, García-Monzón C, Valverde ÁM. Understanding lipotoxicity in NAFLD pathogenesis: is CD36 a key driver? *Cell Death Dis*. 2020;11(9):1-15. doi:10.1038/s41419-020-03003-w

45. Castro BBA, Foresto-Neto O, Saraiva-Camara NO, Sanders-Pinheiro H. Renal lipotoxicity: Insights from experimental models. *Clin Exp Pharmacol Physiol*. 2021;48(12):1579-1588. doi:10.1111/1440-1681.13556

46. Kusminski CM, Bickel PE, Scherer PE. Targeting adipose tissue in the treatment of obesity-associated diabetes. *Nat Rev Drug Discov*. 2016;15(9):639-660. doi:10.1038/nrd.2016.75

47. Rowland I, Gibson G, Heinken A, et al. Gut microbiota functions: metabolism of nutrients and other food components. *Eur J Nutr*. 2018;57(1):1-24. doi:10.1007/s00394-017-1445-8

48. German JB. Food Processing and Lipid Oxidation. In: Jackson LS, Knize MG, Morgan JN, eds. *Impact of Processing on Food Safety*. Advances in Experimental Medicine and Biology. Springer US; 1999:23-50. doi:10.1007/978-1-4615-4853-9_3

49. Natesan V, Kim SJ. Lipid Metabolism, Disorders and Therapeutic Drugs – Review. *Biomol Ther*. 2021;29(6):596-604. doi:10.4062/biomolther.2021.122

50. Gunstone FD, Norris FA. *Lipids in Foods: Chemistry, Biochemistry and Technology*. Elsevier; 2013.

51. Sampath H, Ntambi JM. Polyunsaturated fatty acid regulation of gene expression. *Nutr Rev*. 2004;62(9):333-339. doi:10.1301/nr.2004.sept.333-339

52. Rustan A, Drevon C. Fatty Acids: Structures and Properties. In: ; 2005. doi:10.1038/npg.els.0003894

53. Forman BM, Chen J, Evans RM. Hypolipidemic drugs, polyunsaturated fatty acids, and eicosanoids are ligands for peroxisome proliferator-activated receptors α and δ. *Proc Natl Acad Sci*. 1997;94(9):4312-4317. doi:10.1073/pnas.94.9.4312

54. Muszbek L, Rácz E, Laposata M. Posttranslational modification of proteins with fatty acids in platelets. *Prostaglandins Leukot Essent Fatty Acids*. 1997;57(4-5):359-366. doi:10.1016/s0952-3278(97)90411-7

55. Chen B, Sun Y, Niu J, Jarugumilli GK, Wu X. Protein lipidation in cell signaling and diseases: function, regulation and therapeutic opportunities. *Cell Chem Biol*. 2018;25(7):817-831. doi:10.1016/j.chembiol.2018.05.003

56. Nakamura MT, Nara TY. Essential fatty acid synthesis and its regulation in mammals. *Prostaglandins Leukot Essent Fatty Acids*. 2003;68(2):145-150. doi:10.1016/S0952-3278(02)00264-8

57. Wrzosek M, Zawadzka Z, Sawicka A, Bobrowska-Korczak B, Białek A. Impact of Fatty Acids on Obesity-Associated Diseases and Radical Weight Reduction. *Obes Surg*. 2022;32(2):428-440. doi:10.1007/s11695-021-05789-w

58. Zhou H, Urso C, Jadeja V. Saturated Fatty Acids in Obesity-Associated Inflammation. *J Inflamm Res*. 2020;13:1-14. doi:10.2147/JIR.S229691

59. Nelson DL, Cox MM. Lehninger - Principles of Biochemistry.

60. Guillou H, Zadravec D, Martin PGP, Jacobsson A. The key roles of elongases and desaturases in mammalian fatty acid metabolism: Insights from transgenic mice. *Prog Lipid Res*. 2010;49(2):186-199. doi:10.1016/j.plipres.2009.12.002

61. Carta G, Murru E, Banni S, Manca C. Palmitic Acid: Physiological Role, Metabolism and Nutritional Implications. *Front Physiol*. 2017;8. Accessed April 4, 2023. https://www.frontiersin.org/articles/10.3389/fphys.2017.00902

62. Murru E, Manca C, Carta G, Banni S. Impact of Dietary Palmitic Acid on Lipid Metabolism. *Front Nutr*. 2022;9. Accessed September 5, 2023. https://www.frontiersin.org/articles/10.3389/fnut.2022.861664

63. Pérez-Martí A, Ramakrishnan S, Li J, et al. Reducing lipid bilayer stress by monounsaturated fatty acids protects renal proximal tubules in diabetes. *eLife*. 2022;11:e74391. doi:10.7554/eLife.74391

64. Boden G. Obesity and Free Fatty Acids. *Endocrinol Metab Clin North Am*. 2008;37(3):635-646. doi:10.1016/j.ecl.2008.06.007

65. Tutunchi H, Ostadrahimi A, Saghafi-Asl M. The Effects of Diets Enriched in Monounsaturated Oleic Acid on the Management and Prevention of Obesity: a Systematic Review of Human Intervention Studies. *Adv Nutr Bethesda Md*. 2020;11(4):864-877. doi:10.1093/advances/nmaa013

66. Pardo V, González-Rodríguez Á, Muntané J, Kozma SC, Valverde ÁM. Role of hepatocyte S6K1 in palmitic acid-induced endoplasmic reticulum stress, lipotoxicity, insulin resistance and in oleic acid-induced protection. *Food Chem Toxicol Int J Publ Br Ind Biol Res Assoc*. 2015;80:298-309. doi:10.1016/j.fct.2015.03.029

67. Harwood JL. Fatty Acid Metabolism. *Annu Rev Plant Physiol Plant Mol Biol*. 1988;39(1):101-138. doi:10.1146/annurev.pp.39.060188.000533

68. Murray IV, Paolini MA. Histology, Kidney and Glomerulus. In: *StatPearls*. StatPearls Publishing; 2023. Accessed August 19, 2023. http://www.ncbi.nlm.nih.gov/books/NBK554544/

69. Ogobuiro I, Tuma F. Physiology, Renal. In: *StatPearls*. StatPearls Publishing; 2023. Accessed August 21, 2023. http://www.ncbi.nlm.nih.gov/books/NBK538339/

70. Radi ZA. Kidney Pathophysiology, Toxicology, and Drug-Induced Injury in Drug Development. *Int J Toxicol*. 2019;38(3):215-227. doi:10.1177/1091581819831701

71. Gueutin V, Deray G, Isnard-Bagnis C. Physiologie rénale. *Bull Cancer (Paris)*. 2012;99(3):237-249. doi:10.1684/bdc.2011.1482

72. Mihevc M, Petreski T, Maver U, Bevc S. Renal proximal tubular epithelial cells: review of isolation, characterization, and culturing techniques. *Mol Biol Rep*. 2020;47(12):9865-9882. doi:10.1007/s11033-020-05977-4

73. Massa F. The crucial roles played by HNF1β during kidney development. Published online November 14, 2012.

74. Oxburgh L. Kidney Nephron Determination. *Annu Rev Cell Dev Biol*. 2018;34:427-450. doi:10.1146/annurev-cellbio-100616-060647

75. Terryn S, Jouret F, Vandenabeele F, et al. A primary culture of mouse proximal tubular cells, established on collagen-coated membranes. *Am J Physiol-Ren Physiol*. 2007;293(2):F476-F485. doi:10.1152/ajprenal.00363.2006

76. Denker BM, Sabath E. The biology of epithelial cell tight junctions in the kidney. *J Am Soc Nephrol JASN*. 2011;22(4):622-625. doi:10.1681/ASN.2010090922

77. Zhuo JL, Li XC. Proximal nephron. *Compr Physiol*. 2013;3(3):1079-1123. doi:10.1002/cphy.c110061

78. Christensen EI, Kristoffersen IB, Grann B, Thomsen JS, Andreasen A, Nielsen R. A well-developed endolysosomal system reflects protein reabsorption in segment 1 and 2 of rat proximal tubules. *Kidney Int*. 2021;99(4):841-853. doi:10.1016/j.kint.2020.11.015

79. Christensen EI, Birn H, Storm T, Weyer K, Nielsen R. Endocytic Receptors in the Renal Proximal Tubule. *Physiology*. 2012;27(4):223-236. doi:10.1152/physiol.00022.2012

80. Christensen EI, Gburek J. Protein reabsorption in renal proximal tubule-function and dysfunction in kidney pathophysiology. *Pediatr Nephrol Berl Ger*. 2004;19(7):714-721. doi:10.1007/s00467-004-1494-0

81. Eshbach ML, Weisz OA. Receptor-Mediated Endocytosis in the Proximal Tubule. *Annu Rev Physiol*. 2017;79:425-448. doi:10.1146/annurev-physiol-022516-034234

82. Christensen EI, Birn H. Tubular handling of albumin—degradation or salvation? *Nat Rev Nephrol*. 2013;9(12):700-702. doi:10.1038/nrneph.2013.212

83. Bhargava P, Schnellmann RG. Mitochondrial energetics in the kidney. *Nat Rev Nephrol*. 2017;13(10):629-646. doi:10.1038/nrneph.2017.107

84. Bobulescu IA. Renal lipid metabolism and lipotoxicity. *Curr Opin Nephrol Hypertens*. 2010;19(4):393-402. doi:10.1097/MNH.0b013e32833aa4ac

85. Pei K, Gui T, Li C, et al. Recent Progress on Lipid Intake and Chronic Kidney Disease. *BioMed Res Int*. 2020;2020:3680397. doi:10.1155/2020/3680397

86. Gai Z, Wang T, Visentin M, Kullak-Ublick GA, Fu X, Wang Z. Lipid Accumulation and Chronic Kidney Disease. *Nutrients*. 2019;11(4):722. doi:10.3390/nu11040722

87. Merritt JL, MacLeod E, Jurecka A, Hainline B. Clinical manifestations and management of fatty acid oxidation disorders. *Rev Endocr Metab Disord*. 2020;21(4):479-493. doi:10.1007/s11154-020-09568-3

88. Talley JT, Mohiuddin SS. Biochemistry, Fatty Acid Oxidation. In: *StatPearls*. StatPearls Publishing; 2024. Accessed June 19, 2024. http://www.ncbi.nlm.nih.gov/books/NBK556002/

89. Houten SM, Violante S, Ventura FV, Wanders RJA. The Biochemistry and Physiology of Mitochondrial Fatty Acid β-Oxidation and Its Genetic Disorders. *Annu Rev Physiol*. 2016;78(Volume 78, 2016):23-44. doi:10.1146/annurev-physiol-021115-105045

90. Deshpande OA, Mohiuddin SS. Biochemistry, Oxidative Phosphorylation. In: *StatPearls*. StatPearls Publishing; 2024. Accessed June 19, 2024. http://www.ncbi.nlm.nih.gov/books/NBK553192/

91. Kang HM, Ahn SH, Choi P, et al. Defective fatty acid oxidation in renal tubular epithelial cells has a key role in kidney fibrosis development. *Nat Med*. 2015;21(1):37-46. doi:10.1038/nm.3762

92. Votruba S, Zeddun S, Schoeller D. Validation of deuterium labeled fatty acids for the measurement of dietary fat oxidation: A method for measuring fat-oxidation in free-living subjects. *Int J Obes Relat Metab Disord J Int Assoc Study Obes*. 2001;25:1240-1245. doi:10.1038/sj.ijo.0801672

93. Rampanelli E, Ochodnicky P, Vissers JP, et al. Excessive dietary lipid intake provokes an acquired form of lysosomal lipid storage disease in the kidney. *J Pathol*. 2018;246(4):470-484. doi:10.1002/path.5150

94. Herman-Edelstein M, Scherzer P, Tobar A, Levi M, Gafter U. Altered renal lipid metabolism and renal lipid accumulation in human diabetic nephropathy. *J Lipid Res*. 2014;55(3):561-572. doi:10.1194/jlr.P040501

95. Abbate M, Zoja C, Remuzzi G. How Does Proteinuria Cause Progressive Renal Damage? *J Am Soc Nephrol*. 2006;17(11):2974. doi:10.1681/ASN.2006040377

96. Moorhead JF, El-Nahas M, Chan MK, Varghese Z. LIPID NEPHROTOXICITY IN CHRONIC PROGRESSIVE GLOMERULAR AND TUBULO-INTERSTITIAL DISEASE. *The Lancet*. 1982;320(8311):1309-1311. doi:10.1016/S0140-6736(82)91513-6

97. Chen TK, Knicely DH, Grams ME. Chronic Kidney Disease Diagnosis and Management: A Review. *JAMA*. 2019;322(13):1294-1304. doi:10.1001/jama.2019.14745

98. Jha V, Garcia-Garcia G, Iseki K, et al. Chronic kidney disease: global dimension and perspectives. *The Lancet*. 2013;382(9888):260-272. doi:10.1016/S0140-6736(13)60687-X

99. Stasi A, Cosola C, Caggiano G, et al. Obesity-Related Chronic Kidney Disease: Principal Mechanisms and New Approaches in Nutritional Management. *Front Nutr*. 2022;9:925619. doi:10.3389/fnut.2022.925619

100. Briffa JF, McAinch AJ, Poronnik P, Hryciw DH. Adipokines as a link between obesity and chronic kidney disease. *Am J Physiol-Ren Physiol*. 2013;305(12):F1629-F1636. doi:10.1152/ajprenal.00263.2013

101. Schelling JR. The Contribution of Lipotoxicity to Diabetic Kidney Disease. *Cells*. 2022;11(20):3236. doi:10.3390/cells11203236

102. Romagnani P, Remuzzi G, Glassock R, et al. Chronic kidney disease. *Nat Rev Dis Primer*. 2017;3(1):1-24. doi:10.1038/nrdp.2017.88

103. Declèves AE, Zolkipli Z, Satriano J, et al. Regulation of lipid accumulation by AMP-activated kinase [corrected] in high fat diet-induced kidney injury. *Kidney Int*. 2014;85(3):611-623. doi:10.1038/ki.2013.462

104. Declèves AE, Sharma K, Satriano J. Beneficial Effects of AMP-Activated Protein Kinase Agonists in Kidney Ischemia-Reperfusion: Autophagy and Cellular Stress Markers. *Nephron Exp Nephrol*. Published online December 6, 2014. doi:10.1159/000368932

105. Cobbs A, Chen X, Zhang Y, et al. Saturated fatty acid stimulates production of extracellular vesicles by renal tubular epithelial cells. *Mol Cell Biochem*. 2019;458(1-2):113-124. doi:10.1007/s11010-019-03535-6

106. Soumura M, Kume S, Isshiki K, et al. Oleate and eicosapentaenoic acid attenuate palmitate-induced inflammation and apoptosis in renal proximal tubular cell. *Biochem Biophys Res Commun*. 2010;402(2):265-271. doi:10.1016/j.bbrc.2010.10.012

107. Engin AB, Engin A, eds. *Obesity and Lipotoxicity*. Vol 960. Springer International Publishing; 2017. doi:10.1007/978-3-319-48382-5

108. Yamamoto T, Takabatake Y, Takahashi A, et al. High-Fat Diet-Induced Lysosomal Dysfunction and Impaired Autophagic Flux Contribute to Lipotoxicity in the Kidney. *J Am Soc Nephrol JASN*. 2017;28(5):1534-1551. doi:10.1681/ASN.2016070731

109. Mihai S, Codrici E, Popescu ID, et al. Inflammation-Related Mechanisms in Chronic Kidney Disease Prediction, Progression, and Outcome. *J Immunol Res*. 2018;2018:2180373. doi:10.1155/2018/2180373

110. Escasany E, Izquierdo-Lahuerta A, Medina-Gomez G. Underlying Mechanisms of Renal Lipotoxicity in Obesity. *Nephron*. 2019;143(1):28-32. doi:10.1159/000494694

111. Dikic I. Proteasomal and Autophagic Degradation Systems. *Annu Rev Biochem*. 2017;86(Volume 86, 2017):193-224. doi:10.1146/annurev-biochem-061516-044908

112. Eskelinen EL, Saftig P. Autophagy: A lysosomal degradation pathway with a central role in health and disease. *Biochim Biophys Acta BBA - Mol Cell Res*. 2009;1793(4):664-673. doi:10.1016/j.bbamcr.2008.07.014

113. Kwon YT, Ciechanover A. The Ubiquitin Code in the Ubiquitin-Proteasome System and Autophagy. *Trends Biochem Sci*. 2017;42(11):873-886. doi:10.1016/j.tibs.2017.09.002

114. Zou T, Lin Z. The Involvement of Ubiquitination Machinery in Cell Cycle Regulation and Cancer Progression. *Int J Mol Sci*. 2021;22:5754. doi:10.3390/ijms22115754

115. Glick D, Barth S, Macleod KF. Autophagy: cellular and molecular mechanisms. *J Pathol*. 2010;221(1):3-12. doi:10.1002/path.2697

116. Bauckman KA, Owusu-Boaitey N, Mysorekar IU. Selective Autophagy: Xenophagy. *Methods San Diego Calif*. 2015;75:120-127. doi:10.1016/j.ymeth.2014.12.005

117. Klionsky DJ, Cuervo AM, Dunn Jr William A, Levine B, van der Klei IJ, Seglen PO. How Shall I Eat Thee? *Autophagy*. 2007;3(5):413-416. doi:10.4161/auto.4377

118. Gewirtz DA. Autophagy and senescence. *Autophagy*. 2013;9(5):808-812. doi:10.4161/auto.23922

119. Zaffagnini G, Martens S. Mechanisms of Selective Autophagy. *J Mol Biol*. 2016;428(9Part A):1714-1724. doi:10.1016/j.jmb.2016.02.004

120. Hansen M, Rubinsztein DC, Walker DW. Autophagy as a promoter of longevity: insights from model organisms. *Nat Rev Mol Cell Biol*. 2018;19(9):579-593. doi:10.1038/s41580-018-0033-y

121. English L, Chemali M, Duron J, et al. Autophagy enhances the presentation of endogenous viral antigens on MHC class I molecules during HSV-1 infection. *Nat Immunol*. 2009;10(5):10.1038/ni.1720. doi:10.1038/ni.1720

122. Liu C, Ji L, Hu J, et al. Functional Amino Acids and Autophagy: Diverse Signal Transduction and Application. *Int J Mol Sci*. 2021;22(21):11427. doi:10.3390/ijms222111427

123. Tang C, Livingston MJ, Liu Z, Dong Z. Autophagy in kidney homeostasis and disease. *Nat Rev Nephrol*. 2020;16(9):489-508. doi:10.1038/s41581-020-0309-2

124. Yu L, Chen Y, Tooze SA. Autophagy pathway: Cellular and molecular mechanisms. *Autophagy*. 2018;14(2):207-215. doi:10.1080/15548627.2017.1378838

125. Ballabio A, Bonifacino JS. Lysosomes as dynamic regulators of cell and organismal homeostasis. *Nat Rev Mol Cell Biol*. 2020;21(2):101-118. doi:10.1038/s41580-019-0185-4

126. Xu H, Ren D. Lysosomal Physiology. *Annu Rev Physiol*. 2015;77(Volume 77, 2015):57-80. doi:10.1146/annurev-physiol-021014-071649

127. Periyasamy-Thandavan S, Jiang M, Schoenlein P, Dong Z. Autophagy: molecular machinery, regulation, and implications for renal pathophysiology. *Am J Physiol-Ren Physiol*. 2009;297(2):F244-F256. doi:10.1152/ajprenal.00033.2009

128. Li Y, Chen Y. AMPK and Autophagy. In: Qin ZH, ed. *Autophagy: Biology and Diseases*. Vol 1206. Advances in Experimental Medicine and Biology. Springer Singapore; 2019:85-108. doi:10.1007/978-981-15-0602-4_4

129. Park S, Scheffler TL, Rossie SS, Gerrard DE. AMPK activity is regulated by calcium-mediated protein phosphatase 2A activity. *Cell Calcium*. 2013;53(3):217-223. doi:10.1016/j.ceca.2012.12.001

130. Kim I, He YY. Targeting the AMP-Activated Protein Kinase for Cancer Prevention and Therapy. *Front Oncol*. 2013;3. Accessed June 11, 2023. https://www.frontiersin.org/articles/10.3389/fonc.2013.00175

131. Kim J, Yang G, Kim Y, Kim J, Ha J. AMPK activators: mechanisms of action and physiological activities. *Exp Mol Med*. 2016;48(4):e224-e224. doi:10.1038/emm.2016.16

132. Janzen NR, Whitfield J, Hoffman NJ. Interactive Roles for AMPK and Glycogen from Cellular Energy Sensing to Exercise Metabolism. *Int J Mol Sci*. 2018;19(11). doi:10.3390/ijms19113344

133. Bolster DR, Crozier SJ, Kimball SR, Jefferson LS. AMP-activated protein kinase suppresses protein synthesis in rat skeletal muscle through down-regulated mammalian target of rapamycin (mTOR) signaling. *J Biol Chem*. 2002;277(27):23977-23980. doi:10.1074/jbc.C200171200

134. Martina JA, Chen Y, Gucek M, Puertollano R. MTORC1 functions as a transcriptional regulator of autophagy by preventing nuclear transport of TFEB. *Autophagy*. 2012;8(6):903-914. doi:10.4161/auto.19653

135. Li M, Wang Z, Wang P, Li H, Yang L. TFEB: A Emerging Regulator in Lipid Homeostasis for Atherosclerosis. *Front Physiol*. 2021;12. doi:10.3389/fphys.2021.639920

136. Pohl C, Dikic I. Cellular quality control by the ubiquitin-proteasome system and autophagy. *Science*. 2019;366(6467):818-822. doi:10.1126/science.aax3769

137. Yoo YD, Mun SR, Ji CH, et al. N-terminal arginylation generates a bimodal degron that modulates autophagic proteolysis. *Proc Natl Acad Sci U S A*. 2018;115(12):E2716-E2724. doi:10.1073/pnas.1719110115

138. Senft D, Ronai ZA. UPR, autophagy and mitochondria crosstalk underlies the ER stress response. *Trends Biochem Sci*. 2015;40(3):141-148. doi:10.1016/j.tibs.2015.01.002

139. Ji CH, Kwon YT. Crosstalk and Interplay between the Ubiquitin-Proteasome System and Autophagy. *Mol Cells*. 2017;40(7):441-449. doi:10.14348/molcells.2017.0115

140. Cybulsky AV. Endoplasmic reticulum stress, the unfolded protein response and autophagy in kidney diseases. *Nat Rev Nephrol*. 2017;13(11):681-696. doi:10.1038/nrneph.2017.129

141. Schulze RJ, Sathyanarayan A, Mashek DG. Breaking fat: The regulation and mechanisms of lipophagy. *Biochim Biophys Acta BBA - Mol Cell Biol Lipids*. 2017;1862(10, Part B):1178-1187. doi:10.1016/j.bbalip.2017.06.008

142. Singh R, Cuervo AM. Lipophagy: Connecting Autophagy and Lipid Metabolism. *Int J Cell Biol*. 2012;2012:282041. doi:10.1155/2012/282041

143. Sztalryd C, Brasaemle DL. The perilipin family of lipid droplet proteins: Gatekeepers of intracellular lipolysis. *Biochim Biophys Acta*. 2017;1862(10 Pt B):1221-1232. doi:10.1016/j.bbalip.2017.07.009

144. Kaushik S, Cuervo AM. Degradation of lipid droplet-associated proteins by chaperone-mediated autophagy facilitates lipolysis. *Nat Cell Biol*. 2015;17(6):759-770. doi:10.1038/ncb3166

145. Kaushik S, Cuervo AM. AMPK-dependent phosphorylation of lipid droplet protein PLIN2 triggers its degradation by CMA. *Autophagy*. 2016;12(2):432-438. doi:10.1080/15548627.2015.1124226

146. Grabner GF, Xie H, Schweiger M, Zechner R. Lipolysis: cellular mechanisms for lipid mobilization from fat stores. *Nat Metab*. 2021;3(11):1445-1465. doi:10.1038/s42255-021-00493-6

147. Ding WX, Yin XM. Mitophagy: mechanisms, pathophysiological roles, and analysis. *Biol Chem*. 2012;393(7):547-564. doi:10.1515/hsz-2012-0119

148. Patergnani S, Pinton P. Mitophagy and Mitochondrial Balance. In: Palmeira CM, Rolo AP, eds. *Mitochondrial Regulation: Methods and Protocols*. Methods in Molecular Biology. Springer; 2015:181-194. doi:10.1007/978-1-4939-1875-1_15

149. Onishi M, Yamano K, Sato M, Matsuda N, Okamoto K. Molecular mechanisms and physiological functions of mitophagy. *EMBO J*. 2021;40(3):e104705. doi:10.15252/embj.2020104705

150. Sack MN. Mitochondrial depolarization and the role of uncoupling proteins in ischemia tolerance. *Cardiovasc Res*. 2006;72(2):210-219. doi:10.1016/j.cardiores.2006.07.010

151. Jiang X shun, Chen X mei, Hua W, et al. PINK1/Parkin mediated mitophagy ameliorates palmitic acid-induced apoptosis through reducing mitochondrial ROS production in podocytes. *Biochem Biophys Res Commun*. 2020;525(4):954-961. doi:10.1016/j.bbrc.2020.02.170

152. Jin SM, Youle RJ. PINK1- and Parkin-mediated mitophagy at a glance. *J Cell Sci*. 2012;125(4):795-799. doi:10.1242/jcs.093849

153. Chinnadurai G, Vijayalingam S, Gibson SB. BNIP3 subfamily BH3-only proteins - mitochondrial stress sensors in normal and pathological functions. *Oncogene*. 2008;27(Suppl 1):S114-S127. doi:10.1038/onc.2009.49

154. Li Y, Zheng W, Lu Y, et al. BNIP3L/NIX-mediated mitophagy: molecular mechanisms and implications for human disease. *Cell Death Dis*. 2021;13(1):1-11. doi:10.1038/s41419-021-04469-y

155. Trivedi PC, Bartlett JJ, Pulinilkunnil T. Lysosomal Biology and Function: Modern View of Cellular Debris Bin. *Cells*. 2020;9(5):1131. doi:10.3390/cells9051131

156. Wang F, Gómez-Sintes R, Boya P. Lysosomal membrane permeabilization and cell death. *Traffic*. 2018;19(12):918-931. doi:10.1111/tra.12613

157. Papadopoulos C, Kravic B, Meyer H. Repair or Lysophagy: Dealing with Damaged Lysosomes. *J Mol Biol*. 2020;432(1):231-239. doi:10.1016/j.jmb.2019.08.010

158. Yim WWY, Mizushima N. Lysosome biology in autophagy. *Cell Discov*. 2020;6(1):1-12. doi:10.1038/s41421-020-0141-7

159. Eriksson I, Wäster P, Öllinger K. Restoration of lysosomal function after damage is accompanied by recycling of lysosomal membrane proteins. *Cell Death Dis*. 2020;11(5):1-16. doi:10.1038/s41419-020-2527-8

160. Gallagher ER, Holzbaur ELF. The selective autophagy adaptor p62/SQSTM1 forms phase condensates regulated by HSP27 that facilitate the clearance of damaged lysosomes via lysophagy. *Cell Rep*. 2023;42(2):112037. doi:10.1016/j.celrep.2023.112037

161. Jia J, Claude-Taupin A, Gu Y, et al. Galectin-3 coordinates a cellular system for lysosomal repair and removal. *Dev Cell*. 2020;52(1):69-87.e8. doi:10.1016/j.devcel.2019.10.025

162. Saftig P, Klumperman J. Lysosome biogenesis and lysosomal membrane proteins: trafficking meets function. *Nat Rev Mol Cell Biol*. 2009;10(9):623-635. doi:10.1038/nrm2745

163. Yang C, Wang X. Lysosome biogenesis: Regulation and functions. *J Cell Biol*. 2021;220(6):e202102001. doi:10.1083/jcb.202102001

164. Zhu S yu, Yao R qi, Li Y xuan, et al. Lysosomal quality control of cell fate: a novel therapeutic target for human diseases. *Cell Death Dis*. 2020;11(9):1-13. doi:10.1038/s41419-020-03032-5

165. Zhang K, Kaufman RJ. From endoplasmic-reticulum stress to the inflammatory response. *Nature*. 2008;454(7203):455-462. doi:10.1038/nature07203

166. Schwarz DS, Blower MD. The endoplasmic reticulum: structure, function and response to cellular signaling. *Cell Mol Life Sci*. 2016;73:79-94. doi:10.1007/s00018-015-2052-6

167. Chong WC, Shastri MD, Eri R. Endoplasmic Reticulum Stress and Oxidative Stress: A Vicious Nexus Implicated in Bowel Disease Pathophysiology. *Int J Mol Sci*. 2017;18(4):771. doi:10.3390/ijms18040771

168. Yang M, Luo S, Wang X, et al. ER-Phagy: A New Regulator of ER Homeostasis. *Front Cell Dev Biol*. 2021;9. Accessed April 3, 2023. https://www.frontiersin.org/articles/10.3389/fcell.2021.684526

169. Han J, Kaufman RJ. The role of ER stress in lipid metabolism and lipotoxicity. *J Lipid Res*. 2016;57(8):1329-1338. doi:10.1194/jlr.R067595

170. Chino H, Mizushima N. ER-Phagy: Quality Control and Turnover of Endoplasmic Reticulum. *Trends Cell Biol*. 2020;30(5):384-398. doi:10.1016/j.tcb.2020.02.001

171. Grumati P, Dikic I, Stolz A. ER-phagy at a glance. *J Cell Sci*. 2018;131(17):jcs217364. doi:10.1242/jcs.217364

172. Song S, Tan J, Miao Y, Zhang Q. Crosstalk of ER stress-mediated autophagy and ER-phagy: Involvement of UPR and the core autophagy machinery. *J Cell Physiol*. 2018;233(5):3867-3874. doi:10.1002/jcp.26137

173. Reggiori F, Molinari M. ER-phagy: mechanisms, regulation, and diseases connected to the lysosomal clearance of the endoplasmic reticulum. *Physiol Rev*. 2022;102(3):1393-1448. doi:10.1152/physrev.00038.2021

174. Sun Z, Brodsky JL. Protein quality control in the secretory pathway. *J Cell Biol*. 2019;218(10):3171-3187. doi:10.1083/jcb.201906047

175. Smith M, Wilkinson S. ER homeostasis and autophagy. Lane JD, Korolchuk VI, Murray JT, eds. *Essays Biochem*. 2017;61(6):625-635. doi:10.1042/EBC20170092

176. Mo J, Chen J, Zhang B. Critical roles of FAM134B in ER-phagy and diseases. *Cell Death Dis*. 2020;11(11):1-12. doi:10.1038/s41419-020-03195-1

177. Forrester A, De Leonibus C, Grumati P, et al. A selective ER-phagy exerts procollagen quality control via a Calnexin-FAM134B complex. *EMBO J*. 2019;38(2):e99847. doi:10.15252/embj.201899847

178. Smith MD, Harley ME, Kemp AJ, et al. CCPG1 Is a Non-canonical Autophagy Cargo Receptor Essential for ER-Phagy and Pancreatic ER Proteostasis. *Dev Cell*. 2018;44(2):217-232.e11. doi:10.1016/j.devcel.2017.11.024

179. Fumagalli F, Noack J, Bergmann TJ, et al. Translocon component Sec62 acts in endoplasmic reticulum turnover during stress recovery. *Nat Cell Biol*. 2016;18(11):1173-1184. doi:10.1038/ncb3423

180. Vlachaki Walker JM, Robb JL, Cruz AM, et al. AMP-activated protein kinase (AMPK) activator A-769662 increases intracellular calcium and ATP release from astrocytes in an AMPK-independent manner. *Diabetes Obes Metab*. 2017;19(7):997-1005. doi:10.1111/dom.12912

181. Li H, Min Q, Ouyang C, et al. AMPK activation prevents excess nutrient-induced hepatic lipid accumulation by inhibiting mTORC1 signaling and endoplasmic reticulum stress response. *Biochim Biophys Acta*. 2014;1842(9):1844-1854. doi:10.1016/j.bbadis.2014.07.002

182. Eldeeb MA, Zorca CE, Ragheb MA, Rashidi FB, Salah El-Din DS. Fine-tuning ER-phagy by post-translational modifications. *BioEssays News Rev Mol Cell Dev Biol*. 2021;43(2):e2000212. doi:10.1002/bies.202000212

183. Iavarone F, Di Lorenzo G, Settembre C. Regulatory events controlling ER-phagy. *Curr Opin Cell Biol*. 2022;76:102084. doi:10.1016/j.ceb.2022.102084

184. Liang JR, Lingeman E, Luong T, et al. A Genome-wide ER-Phagy Screen Highlights Key Roles of Mitochondrial Metabolism and ER-Resident UFMylation. *Cell*. 2020;180(6):1160-1177.e20. doi:10.1016/j.cell.2020.02.017

185. Banerjee S, Kumar M, Wiener R. Decrypting UFMylation: How Proteins Are Modified with UFM1. *Biomolecules*. 2020;10(10):1442. doi:10.3390/biom10101442

186. Millrine D, Peter JJ, Kulathu Y. A guide to UFMylation, an emerging posttranslational modification. *FEBS J*. n/a(n/a). doi:10.1111/febs.16730

187. Hyttinen JMT, Amadio M, Viiri J, Pascale A, Salminen A, Kaarniranta K. Clearance of misfolded and aggregated proteins by aggrephagy and implications for aggregation diseases. *Ageing Res Rev*. 2014;18:16-28. doi:10.1016/j.arr.2014.07.002

188. Ly LD, Xu S, Choi SK, et al. Oxidative stress and calcium dysregulation by palmitate in type 2 diabetes. *Exp Mol Med*. 2017;49(2):e291-e291. doi:10.1038/emm.2016.157

189. Lamark T, Johansen T. Aggrephagy: Selective Disposal of Protein Aggregates by Macroautophagy. *Int J Cell Biol*. 2012;2012:736905. doi:10.1155/2012/736905

190. Lystad AH, Simonsen A. Assays to monitor aggrephagy. *Methods*. 2015;75:112-119. doi:10.1016/j.ymeth.2014.12.019

191. Declèves AE, Sharma K. Obesity and kidney disease: differential effects of obesity on adipose tissue and kidney inflammation and fibrosis. *Curr Opin Nephrol Hypertens*. 2015;24(1):28-36. doi:10.1097/MNH.0000000000000087

192. Berquez M, Krohn P, Luciani A, Devuyst O. Receptor-Mediated Endocytosis and Differentiation in Proximal Tubule Cell Systems. *J Am Soc Nephrol JASN*. 2021;32(5):1265-1267. doi:10.1681/ASN.2021020253

193. Matlock B. Assessment of Nucleic Acid Purity.

194. Berezhnov AV, Soutar MPM, Fedotova EI, et al. Intracellular pH Modulates Autophagy and Mitophagy. *J Biol Chem*. 2016;291(16):8701-8708. doi:10.1074/jbc.M115.691774

195. Singh R, Kaushik S, Wang Y, et al. Autophagy regulates lipid metabolism. *Nature*. 2009;458(7242):1131-1135. doi:10.1038/nature07976

196. Dunn KW, Kamocka MM, McDonald JH. A practical guide to evaluating colocalization in biological microscopy. *Am J Physiol - Cell Physiol*. 2011;300(4):C723-C742. doi:10.1152/ajpcell.00462.2010

197. Juszczak F, Vlassembrouck M, Botton O, et al. Delayed Exercise Training Improves Obesity-Induced Chronic Kidney Disease by Activating AMPK Pathway in High-Fat Diet-Fed Mice. *Int J Mol Sci*. 2020;22(1):350. doi:10.3390/ijms22010350

198. Yagi M, Toshima T, Amamoto R, et al. Mitochondrial translation deficiency impairs NAD+-mediated lysosomal acidification. *EMBO J*. 2021;40(8):e105268. doi:10.15252/embj.2020105268

199. Redmann M, Benavides GA, Berryhill TF, et al. Inhibition of autophagy with bafilomycin and chloroquine decreases mitochondrial quality and bioenergetic function in primary neurons. *Redox Biol*. 2017;11:73-81. doi:10.1016/j.redox.2016.11.004

200. Klionsky DJ, Elazar Z, Seglen PO, Rubinsztein DC. Does bafilomycin A1 block the fusion of autophagosomes with lysosomes? *Autophagy*. 2008;4(7):849-850. doi:10.4161/auto.6845

201. Yoshii SR, Mizushima N. Monitoring and Measuring Autophagy. *Int J Mol Sci*. 2017;18(9):1865. doi:10.3390/ijms18091865

202. DePedro HM, Urayama P. Using LysoSensor Yellow/Blue DND-160 to sense acidic pH under high hydrostatic pressures. *Anal Biochem*. 2009;384(2):359-361. doi:10.1016/j.ab.2008.10.007

203. Minami S, Yamamoto T, Takabatake Y, et al. Lipophagy maintains energy homeostasis in the kidney proximal tubule during prolonged starvation. *Autophagy*. 2017;13(10):1629-1647. doi:10.1080/15548627.2017.1341464

204. Cui W, Sathyanarayan A, Lopresti M, Aghajan M, Chen C, Mashek DG. Lipophagy-derived fatty acids undergo extracellular efflux via lysosomal exocytosis. *Autophagy*. 2021;17(3):690-705. doi:10.1080/15548627.2020.1728097

205. Zhang T, Liu J, Shen S, Tong Q, Ma X, Lin L. SIRT3 promotes lipophagy and chaperon-mediated autophagy to protect hepatocytes against lipotoxicity. *Cell Death Differ*. 2020;27(1):329-344. doi:10.1038/s41418-019-0356-z

206. Filali-Mouncef Y, Hunter C, Roccio F, et al. The ménage à trois of autophagy, lipid droplets and liver disease. *Autophagy*. 2022;18(1):50-72. doi:10.1080/15548627.2021.1895658

207. Xu S, Lee E, Sun Z, et al. Perilipin 2 Impacts Acute Kidney Injury via Regulation of PPARα. *J Immunol Res*. 2021;2021:9972704. doi:10.1155/2021/9972704

208. Park EJ, Lee AY, Chang SH, Yu KN, Kim JH, Cho MH. Role of p53 in the cellular response following oleic acid accumulation in Chang liver cells. *Toxicol Lett*. 2014;224(1):114-120. doi:10.1016/j.toxlet.2013.09.018

209. Liu K, Czaja MJ. Regulation of lipid stores and metabolism by lipophagy. *Cell Death Differ*. 2013;20(1):3-11. doi:10.1038/cdd.2012.63

210. Mthembu SXH, Mazibuko-Mbeje SE, Silvestri S, et al. Low levels and partial exposure to palmitic acid improves mitochondrial function and the oxidative status of cultured cardiomyoblasts. *Toxicol Rep*. 2024;12:234-243. doi:10.1016/j.toxrep.2024.01.014

211. Demine S, Renard P, Arnould T. Mitochondrial Uncoupling: A Key Controller of Biological Processes in Physiology and Diseases. *Cells*. 2019;8(8):795. doi:10.3390/cells8080795

212. Maejima I, Takahashi A, Omori H, et al. Autophagy sequesters damaged lysosomes to control lysosomal biogenesis and kidney injury. *EMBO J*. 2013;32(17):2336-2347. doi:10.1038/emboj.2013.171

213. Park M, Sabetski A, Kwan Chan Y, Turdi S, Sweeney G. Palmitate Induces ER Stress and Autophagy in H9c2 Cells: Implications for Apoptosis and Adiponectin Resistance. *J Cell Physiol*. 2015;230(3):630-639. doi:10.1002/jcp.24781

214. Guo N, Peng Z. MG132, a proteasome inhibitor, induces apoptosis in tumor cells. *Asia Pac J Clin Oncol*. 2013;9(1):6-11. doi:10.1111/j.1743-7563.2012.01535.x

215. Zaarur N, Meriin AB, Gabai VL, Sherman MY. Triggering Aggresome Formation: DISSECTING AGGRESOME-TARGETING AND AGGREGATION SIGNALS IN SYNPHILIN 1. *J Biol Chem*. 2008;283(41):27575-27584. doi:10.1074/jbc.M802216200

216. Fu L, Gao Y sheng, Tousson A, et al. Nuclear Aggresomes Form by Fusion of PML-associated Aggregates. *Mol Biol Cell*. 2005;16(10):4905-4917. doi:10.1091/mbc.E05-01-0019

217. Lu M, Banetta L, Young LJ, et al. Live-cell super-resolution microscopy reveals a primary role for diffusion in polyglutamine-driven aggresome assembly. *J Biol Chem*. 2019;294(1):257-268. doi:10.1074/jbc.RA118.003500

218. Prosser SL, Tkach J, Gheiratmand L, et al. Aggresome assembly at the centrosome is driven by CP110–CEP97–CEP290 and centriolar satellites. *Nat Cell Biol*. 2022;24(4):483-496. doi:10.1038/s41556-022-00869-0

219. Xia R, Peng HF, Zhang X, Zhang HS. Comprehensive review of amino acid transporters as therapeutic targets. *Int J Biol Macromol*. 2024;260:129646. doi:10.1016/j.ijbiomac.2024.129646

220. Hara-Chikuma M, Verkman AS. Aquaporin-1 facilitates epithelial cell migration in kidney proximal tubule. *J Am Soc Nephrol JASN*. 2006;17(1):39-45. doi:10.1681/ASN.2005080846

221. Igarashi P, Shashikant CS, Thomson RB, et al. Ksp-cadherin gene promoter. II. Kidney-specific activity in transgenic mice. *Am J Physiol*. 1999;277(4):F599-610. doi:10.1152/ajprenal.1999.277.4.F599

222. Jones SG, Ito T, Phillips AO. Regulation of proximal tubular epithelial cell CD44-mediated binding and internalisation of hyaluronan. *Int J Biochem Cell Biol*. 2003;35(9):1361-1377. doi:10.1016/S1357-2725(03)00040-2

223. Christensen EI, Birn H. Megalin and cubilin: multifunctional endocytic receptors. *Nat Rev Mol Cell Biol*. 2002;3(4):258-267. doi:10.1038/nrm778

224. Xu T, Herkens L, Jia T, et al. The role of desmoglein-2 in kidney disease. *Kidney Int*. 2024;105(5):1035-1048. doi:10.1016/j.kint.2024.01.037

225. Prozialeck WC, Lamar PC, Appelt DM. Differential expression of E-cadherin, N-cadherin and beta-catenin in proximal and distal segments of the rat nephron. *BMC Physiol*. 2004;4:10. doi:10.1186/1472-6793-4-10

226. Maier JI, Rogg M, Helmstädter M, et al. EPB41L5 controls podocyte extracellular matrix assembly by adhesome-dependent force transmission. *Cell Rep*. 2021;34(12):108883. doi:10.1016/j.celrep.2021.108883

227. Chang-Panesso M, Kadyrov FF, Lalli M, et al. FOXM1 drives proximal tubule proliferation during repair from acute ischemic kidney injury. *J Clin Invest*. 129(12):5501-5517. doi:10.1172/JCI125519

228. Viau A, Karoui KE, Laouari D, et al. Lipocalin 2 is essential for chronic kidney disease progression in mice and humans. *J Clin Invest*. 2010;120(11):4065-4076. doi:10.1172/JCI42004

229. Long KR, Rbaibi Y, Bondi CD, et al. Cubilin-, megalin-, and Dab2-dependent transcription revealed by CRISPR/Cas9 knockout in kidney proximal tubule cells. *Am J Physiol Renal Physiol*. 2022;322(1):F14-F26. doi:10.1152/ajprenal.00259.2021

230. Vallon V, Platt KA, Cunard R, et al. SGLT2 Mediates Glucose Reabsorption in the Early Proximal Tubule. *J Am Soc Nephrol JASN*. 2011;22(1):104-112. doi:10.1681/ASN.2010030246

231. Kang HM, Huang S, Reidy K, Han SH, Chinga F, Susztak K. Sox9-Positive Progenitor Cells Play a Key Role in Renal Tubule Epithelial Regeneration in Mice. *Cell Rep*. 2016;14(4):861-871. doi:10.1016/j.celrep.2015.12.071

232. Kusaba T, Lalli M, Kramann R, Kobayashi A, Humphreys BD. Differentiated kidney epithelial cells repair injured proximal tubule. *Proc Natl Acad Sci*. 2014;111(4):1527-1532. doi:10.1073/pnas.1310653110

233. Prasad R, Jha RK, Keerti A. Chronic Kidney Disease: Its Relationship With Obesity. *Cureus*. 14(10):e30535. doi:10.7759/cureus.30535

234. Yang A, Mottillo EP. Adipocyte Lipolysis: from molecular mechanisms of regulation to disease and therapeutics. *Biochem J*. 2020;477(5):985-1008. doi:10.1042/BCJ20190468

235. Rinaldi A, Lazareth H, Poindessous V, et al. Impaired fatty acid metabolism perpetuates lipotoxicity along the transition to chronic kidney injury. *JCI Insight*. 7(18):e161783. doi:10.1172/jci.insight.161783

236. Christensen EI, Verroust PJ. Interstitial fibrosis: tubular hypothesis versus glomerular hypothesis. *Kidney Int*. 2008;74(10):1233-1236. doi:10.1038/ki.2008.421

237. Vallon V, Thomson SC. The tubular hypothesis of nephron filtration and diabetic kidney disease. *Nat Rev Nephrol*. 2020;16(6):317-336. doi:10.1038/s41581-020-0256-y

238. Xu S, Nam SM, Kim JH, et al. Palmitate induces ER calcium depletion and apoptosis in mouse podocytes subsequent to mitochondrial oxidative stress. *Cell Death Dis*. 2015;6(11):e1976-e1976. doi:10.1038/cddis.2015.331

239. Li C, Lin Y, Luo R, et al. Intrarenal renin-angiotensin system mediates fatty acid-induced ER stress in the kidney. *Am J Physiol-Ren Physiol*. 2016;310(5):F351-F363. doi:10.1152/ajprenal.00223.2015

240. González-Rodríguez Á, Mayoral R, Agra N, et al. Impaired autophagic flux is associated with increased endoplasmic reticulum stress during the development of NAFLD. *Cell Death Dis*. 2014;5(4):e1179-e1179. doi:10.1038/cddis.2014.162

241. Lim Y, Kim S, Kim EK. Palmitate reduces starvation-induced ER stress by inhibiting ER-phagy in hypothalamic cells. *Mol Brain*. 2021;14(1):65. doi:10.1186/s13041-021-00777-8

242. Oslowski CM, Urano F. Measuring ER stress and the unfolded protein response using mammalian tissue culture system. *Methods Enzymol*. 2011;490:71-92. doi:10.1016/B978-0-12-385114-7.00004-0

243. Eicosapentaenoic acid attenuates renal lipotoxicity by restoring autophagic flux - PMC. Accessed August 3, 2024. https://www.ncbi.nlm.nih.gov/pmc/articles/PMC8354598/

244. Park S, Oh TS, Kim S, Kim EK. Palmitate-induced autophagy liberates monounsaturated fatty acids and increases Agrp expression in hypothalamic cells. *Anim Cells Syst*. 2019;23(6):384-391. doi:10.1080/19768354.2019.1696407

245. Varshney R, Varshney R, Mishra R, Gupta S, Sircar D, Roy P. Kaempferol alleviates palmitic acid-induced lipid stores, endoplasmic reticulum stress and pancreatic β-cell dysfunction through AMPK/mTOR-mediated lipophagy. *J Nutr Biochem*. 2018;57:212-227. doi:10.1016/j.jnutbio.2018.02.017

246. Liu K, Qiu D, Liang X, et al. Lipotoxicity-induced STING1 activation stimulates MTORC1 and restricts hepatic lipophagy. *Autophagy*. 2022;18(4):860-876. doi:10.1080/15548627.2021.1961072

247. Exercise and dietary intervention ameliorate high-fat diet-induced NAFLD and liver aging by inducing lipophagy - ScienceDirect. Accessed August 3, 2024. https://www.sciencedirect.com/science/article/pii/S2213231720308405

248. Sathyanarayan A, Mashek MT, Mashek DG. ATGL Promotes Autophagy/Lipophagy via SIRT1 to Control Hepatic Lipid Droplet Catabolism. *Cell Rep*. 2017;19(1):1-9. doi:10.1016/j.celrep.2017.03.026

249. Ge M, Fontanesi F, Merscher S, Fornoni A. The Vicious Cycle of Renal Lipotoxicity and Mitochondrial Dysfunction. *Front Physiol*. 2020;11. Accessed April 4, 2023. https://www.frontiersin.org/articles/10.3389/fphys.2020.00732

250. Nsiah-Sefaa A, McKenzie M. Combined defects in oxidative phosphorylation and fatty acid β-oxidation in mitochondrial disease. *Biosci Rep*. 2016;36(2):e00313. doi:10.1042/BSR20150295

251. Tang C, Cai J, Dong Z. Mitochondrial dysfunction in obesity-related kidney disease: a novel therapeutic target. *Kidney Int*. 2016;90(5):930-933. doi:10.1016/j.kint.2016.07.045

252. Egnatchik RA, Leamy AK, Noguchi Y, Shiota M, Young JD. Palmitate-induced Activation of Mitochondrial Metabolism Promotes Oxidative Stress and Apoptosis in H4IIEC3 Rat Hepatocytes. *Metabolism*. 2014;63(2):283-295. doi:10.1016/j.metabol.2013.10.009

253. Jang HS, Noh MR, Kim J, Padanilam BJ. Defective Mitochondrial Fatty Acid Oxidation and Lipotoxicity in Kidney Diseases. *Front Med*. 2020;7. doi:10.3389/fmed.2020.00065

254. Radulovic M, Schink KO, Wenzel EM, et al. ESCRT-mediated lysosome repair precedes lysophagy and promotes cell survival. *EMBO J*. 2018;37(21):e99753. doi:10.15252/embj.201899753

255. Su LJ, Zhang JH, Gomez H, et al. Reactive Oxygen Species-Induced Lipid Peroxidation in Apoptosis, Autophagy, and Ferroptosis. *Oxid Med Cell Longev*. 2019;2019:5080843. doi:10.1155/2019/5080843

256. Serrano-Puebla A, Boya P. Lysosomal membrane permeabilization as a cell death mechanism in cancer cells. *Biochem Soc Trans*. 2018;46(2):207-215. doi:10.1042/BST20170130

257. Chen W, Motsinger MM, Li J, Bohannon KP, Hanson PI. Ca2+-sensor ALG-2 engages ESCRTs to enhance lysosomal membrane resilience to osmotic stress. *Proc Natl Acad Sci*. 2024;121(22):e2318412121. doi:10.1073/pnas.2318412121

258. Bauer B, Martens S, Ferrari L. Aggrephagy at a glance. *J Cell Sci*. 2023;136(10):jcs260888. doi:10.1242/jcs.260888

259. Kim YJ, Takahashi R. Role of Polyunsaturated Fatty Acids for Misfolding Protein Aggregations. *Ann N Y Acad Sci*. 2006;1086(1):11-20. doi:10.1196/annals.1377.021

260. Kim PK, Hailey DW, Mullen RT, Lippincott-Schwartz J. Ubiquitin signals autophagic degradation of cytosolic proteins and peroxisomes. *Proc Natl Acad Sci U S A*. 2008;105(52):20567-20574. doi:10.1073/pnas.0810611105

261. Legesse-Miller A, Raitman I, Haley E, et al. Quiescent fibroblasts are protected from proteasome inhibition–mediated toxicity. *Mol Biol Cell*. 2012;23:3566-3581. doi:10.1091/mbc.E12-03-0192

262. Otoda T, Takamura T, Misu H, et al. Proteasome Dysfunction Mediates Obesity-Induced Endoplasmic Reticulum Stress and Insulin Resistance in the Liver. *Diabetes*. 2013;62(3):811-824. doi:10.2337/db11-1652

263. Lee HS, Suh JY, Kang BC, Lee E. Lipotoxicity dysregulates the immunoproteasome in podocytes and kidneys in type 2 diabetes. *Am J Physiol Renal Physiol*. 2021;320(4):F548-F558. doi:10.1152/ajprenal.00509.2020

264. Berquez M, Chen Z, Festa BP, et al. Lysosomal cystine export regulates mTORC1 signaling to guide kidney epithelial cell fate specialization. *Nat Commun*. 2023;14(1):3994. doi:10.1038/s41467-023-39261-3

265. Lamouille S, Xu J, Derynck R. Molecular mechanisms of epithelial–mesenchymal transition. *Nat Rev Mol Cell Biol*. 2014;15(3):178-196. doi:10.1038/nrm3758

266. Luciani A, Sirac C, Terryn S, et al. Impaired Lysosomal Function Underlies Monoclonal Light Chain–Associated Renal Fanconi Syndrome. *J Am Soc Nephrol JASN*. 2016;27(7):2049-2061. doi:10.1681/ASN.2015050581

267. Seccia T, Caroccia B, Piazza M, Rossi GP. The Key Role of Epithelial to Mesenchymal Transition (EMT) in Hypertensive Kidney Disease. *Int J Mol Sci*. 2019;20(14):3567. doi:10.3390/ijms20143567

268. Sheng L, Zhuang S. New Insights Into the Role and Mechanism of Partial Epithelial-Mesenchymal Transition in Kidney Fibrosis. *Front Physiol*. 2020;11. doi:10.3389/fphys.2020.569322

269. Yuan Q, Tang B, Zhang C. Signaling pathways of chronic kidney diseases, implications for therapeutics. *Signal Transduct Target Ther*. 2022;7(1):1-27. doi:10.1038/s41392-022-01036-5